



FACULTY OF PHARMACEUTICAL SCIENCES

Ghent University

Faculty of Pharmaceutical Sciences

**DEVELOPMENT OF PROCESS ANALYTICAL AND CONTROL METHODOLOGIES
FOR PHARMACEUTICAL WET GRANULATION PROCESSES**

ANNELEEN BURGGRAEVE

Master in Chemistry

Thesis submitted to obtain the degree of Doctor in Pharmaceutical Sciences

2012

Promoter: **Prof. Dr. T. De Beer**

Laboratory of Pharmaceutical Process Analytical Technology (Ghent University)

Co-promoter: **Prof. Dr. C. Vervaet**

Laboratory of Pharmaceutical Technology (Ghent University)

The author, the promoter and the co-promoter give the authorization to consult and to copy part of this thesis for personal use only. Any other use is limited by the Laws of Copyright, especially concerning the obligation to refer to the source whenever results are cited from this thesis.

Ghent, June 15, 2012

The author

The promoter

The co-promoter

Anneleen Burggraeve

Prof. Dr. Thomas De Beer

Prof. Dr. Chris Vervaeet

ACKNOWLEDGEMENTS

About 4.5 years ago, I was introduced into the world of pharmacy. During this period, both my scientific knowledge and personal perspective developed extensively and this would not have been possible without the help of numerous people. Therefore I would like to acknowledge all those who have directly or indirectly contributed to this work.

I would like to start by thanking Prof. Dr. Willy Baeyens, for giving me the chance to start this PhD under his supervision. Upon his retirement, Prof. Dr. Thomas De Beer took on the task of promoter, and I would like to express my gratitude to him for the many opportunities and the excellent supervision he gave me. I greatly appreciate all of his advice and contributions.

I am grateful to my co-promoter, Prof. Dr. Chris Vervaeke, for the fruitful discussions and critical revisions of my work. Thanks also go to Prof. Dr. Jean Paul Remon for his interest and financial support of this project.

Special thanks go to Sofie Timmers, with whom I was privileged to share an office during the first years. I truly appreciate the many conversations we shared both on scientific and personal matters.

With the change in promoter, also came a different work environment and colleagues. Lien and Margot were the first official PAT group members, and I would like to thank them for their scientific help, friendship, support and fun moments together. In the meantime, the PAT group has expanded, and therefore thanks also go to Laurent, Tinne and Ana for creating a very pleasant working environment. I am also grateful for the help of Claudine to manage the administrative tasks.

The help and support from colleagues of the Pharmaceutical Technology lab is greatly appreciated.

I am indebted to Prof. Dr. Jouko Yliruusi for the opportunity he gave me to perform a part of the presented research work in his department at the University of Helsinki during a three months' visit. Thanks go to all the people of the department who were a great support to me in Helsinki, in particular Prof. Dr. Niklas Sandler and Prof. Dr. Jyrki Heinämäki for the excellent scientific (and non-scientific) help and supervision.

Sincere thanks go to IWT (Agentschap voor Innovatie door Wetenschap en Technologie – Vlaanderen), Ghent University and FWO (Fonds Wetenschappelijk Onderzoek – Vlaanderen) for providing the necessary funding to successfully complete this PhD project.

Further, I would like to thank some friends (Audrey, Julie, Sien, Nathalie, Jonas, Kenny and Annelien) for their interest in my work, encouragement, and many moments of pleasant distraction.

Special thanks go to my parents, who gave me the opportunity and support to study and continue this PhD. Mieke & Luc and Lieselot, thanks for the interest in my work, even without sometimes understanding what I was doing, and the endless encouragement.

I also value the interest and encouragement shown by Greet and Piet during these past years.

And finally, many thanks go to Wouter. Although we lived about 1000 km apart during the greater part of this PhD, your support, sense of perspective, humor and the fantastic moments during the trips to Norway were indispensable. Also your expertise in Microsoft Office Word was undoubtedly appreciated during these last months.

Anneleen

TABLE OF CONTENTS

LIST OF ABBREVIATIONS	1
CHAPTER 1 INTRODUCTION AND OBJECTIVES	5
CHAPTER 2 FLUIDIZED BED GRANULATION & EXTRUSION-SPHERONIZATION AS WET GRANULATION TECHNIQUES	11
2.1. Introduction	11
2.2. Fundamentals of wet granule growth	13
2.3. Fluidized bed granulation	15
2.3.1. General description of the process	15
2.3.2. Process equipment	15
2.3.3. Traditional methods of process control and endpoint detection	18
2.4. Extrusion-spheronization	21
2.4.1. General description of the process	21
2.4.2. Process equipment	22
2.4.3. Traditional methods of process control and endpoint detection	24
CHAPTER 3 PROCESS ANALYTICAL TECHNOLOGY IN FLUIDIZED BED GRANULATION & EXTRUSION-SPHERONIZATION	31
3.1. Process Analytical Technology	31
3.1.1. Introduction	31
3.1.2. The PAT Framework	33
3.2. Measurement principles of the applied process analyzers	36
3.2.1. Spatial filter velocimetry	36
3.2.2. Photometric stereo imaging	38
3.2.3. Focused beam reflectance measurement	40
3.2.4. Near infrared spectroscopy	41
3.2.5. Raman spectroscopy	43
3.3. Literature overview of the process analyzers applied in fluidized bed granulation	47
3.3.1. Near infrared spectroscopy	49

3.3.2.	Image analysis	53
3.3.3.	Focused beam reflectance measurement	54
3.3.4.	Spatial filter velocimetry	55
3.3.5.	Acoustic emission	56
3.3.6.	Raman spectroscopy	57
3.3.7.	Combining complementary process analyzers	58
3.4.	Literature overview of the process analyzers applied in extrusion-spheronization	60
CHAPTER 4 EVALUATION OF IN-LINE SPATIAL FILTER VELOCIMETRY AS PAT MONITORING TOOL FOR PARTICLE GROWTH DURING FLUID BED GRANULATION		69
4.1.	Introduction	69
4.2.	Materials and methods	72
4.2.1.	Materials	72
4.2.2.	Fluid bed granulation	72
4.2.3.	In-line measurements with spatial filter velocimetry probe	72
4.2.4.	Design of experiments	73
4.2.5.	Characterization of granules	74
4.2.6.	Data analysis	74
4.3.	Results and discussion	75
4.3.1.	Comparison between in-line SFV and off-line LD results	75
4.3.2.	DoE analysis	78
4.3.2.1.	Comparison between in-line SFV and off-line LD DoE results	78
4.3.2.2.	Explanation of the (in)significance of the DoE factors based on in-line SFV data	80
4.3.2.3.	Influence of DoE factors upon density and powder flow	83
4.3.2.4.	Assessment of granule density and flowability from in-line SFV measurements	84
4.4.	Conclusions	86
CHAPTER 5 BATCH STATISTICAL PROCESS CONTROL (BSPC) OF A FLUID BED GRANULATION PROCESS USING IN-LINE SPATIAL FILTER VELOCIMETRY AND PRODUCT TEMPERATURE MEASUREMENTS		91
5.1.	Introduction	91
5.2.	Materials and methods	93
5.2.1.	Materials	93
5.2.2.	Fluid bed granulation setup	93
5.2.3.	Characterization of granules	94

5.2.4.	Development of batch model	94
5.3.	Results and discussion	97
5.3.1.	Real-time batch progress evaluation	97
5.3.2.	Evaluation of completed batches	104
5.4.	Conclusions	106
CHAPTER 6 DEVELOPMENT OF A FLUID BED GRANULATION PROCESS CONTROL STRATEGY BASED ON REAL-TIME PROCESS AND PRODUCT MEASUREMENTS		111
6.1.	Introduction	111
6.2.	Materials and methods	115
6.2.1.	Materials	115
6.2.2.	Process description	115
6.2.3.	Collection of granule product information during processing	116
6.2.3.1.	Case study A: in-line SFV and at-line NIR spectroscopy	116
6.2.3.2.	Case study B: in-line SFV and in-line NIR spectroscopy	116
6.2.3.3.	Case study C: in-line FBRM and in-line Lighthouse NIR spectroscopy	117
6.2.4.	Characterization of granules	117
6.2.4.1.	Karl Fischer titration	117
6.2.4.2.	Density measurements	118
6.2.5.	Development of the granulation feed-forward control strategy	118
6.2.6.	Development of an NIR method to predict end product moisture content	122
6.2.6.1.	Use of conventional NIR probe (case study B)	122
6.2.6.2.	Use of Lighthouse NIR probe (case study C)	122
6.3.	Results and discussion	123
6.3.1.	Case study A: in-line SFV and at-line NIR spectroscopy	123
6.3.2.	Case study B: in-line SFV and in-line NIR spectroscopy	126
6.3.2.1.	Qualitative monitoring of the granulation process	126
6.3.2.2.	Development of the granulation feed-forward control strategy	128
6.3.2.3.	Development of an NIR method to predict end product moisture content	132
6.3.3.	Case study C: in-line FBRM and in-line Lighthouse NIR spectroscopy	133
6.3.3.1.	Development of the granulation feed-forward control strategy	133
6.3.3.2.	Development of an NIR method to predict end product moisture content	135
6.4.	Conclusions	137

CHAPTER 7 REAL-TIME IMAGE-BASED INVESTIGATION OF SPHERONIZATION AND DRYING PHENOMENA USING DIFFERENT PELLET FORMULATIONS	143
7.1. Introduction	143
7.2. Materials and methods	146
7.2.1. Materials	146
7.2.2. Methods	146
7.2.2.1. Pelletization and drying	146
7.2.2.2. Sampling	147
7.2.2.3. Photometric stereo imaging	147
7.2.2.4. Raman spectroscopy	148
7.2.2.5. Moisture analysis	148
7.3. Results and discussion	149
7.3.1. Photometric stereo imaging during spheronization	149
7.3.2. Photometric stereo imaging during pellet fluid bed drying	154
7.3.2.1. Particle size distribution	154
7.3.2.2. Surface brightness and visualization	157
7.4. Conclusions	158
SUMMARY & GENERAL CONCLUSIONS	161
FUTURE PERSPECTIVES	167
SAMENVATTING & ALGEMEEN BESLUIT	171
CURRICULUM VITAE	179

LIST OF ABBREVIATIONS

AE	acoustic emission
ANN	artificial neural network
API	active pharmaceutical ingredient
BD	bulk density
BSPC	batch statistical process control
CL	control limit
DoE	design of experiments
ECT	electrical capacitance tomography
ES	extrusion-spheronization
FBRM	focused beam reflectance measurement
FDA	Food and Drug Administration
FS3D	FlashSizer 3D
GMP	good manufacturing practice
HPMC	hydroxypropylmethylcellulose
ICH	International Conference of Harmonization
KF	Karl Fischer
LD	laser diffraction
LHP	Lighthouse Probe
MC	moisture content
MCC	microcrystalline cellulose
MCR	multivariate curve resolution
MRT	microwave resonance technology
NIR	near infrared
N-PLS	N-way partial least squares
PAT	process analytical technology
PC	principal component
PCA	principal component analysis
PID	Proportional, Integral, Derivative
PLS	partial least squares
PLSC	partial least squares component

PSD	particle size distribution
RMSEE	root mean square error of estimation
RMSEP	root mean square error of prediction
SD	standard deviation
SFV	spatial filter velocimetry
SNV	standard normal variation
TD	tapped density
TP	theophylline
TP AH	theophylline anhydrate
TP MH	theophylline monohydrate
XRPD	X-ray powder diffraction

CHAPTER 1

INTRODUCTION AND OBJECTIVES

CHAPTER 1

INTRODUCTION AND OBJECTIVES

Granulation is a general term to describe methods of size enlargement in the pharmaceutical industry. Powder particles are agglomerated into larger, permanent structures (granules) in which the original particles are identifiable [1]. Improvement of one or more powder properties (e.g., flowability, bulk density, dust formation, risk of size segregation, etc.) motivates the pharmaceutical industry to adopt granulation as a key intermediate process step in most solid dosage form production processes.

For several decades after the earliest work performed on granulation, it remained more of an art than a science with high recycle ratios [2]. Granulations were performed based on popular practice rather than on scientific strategies. The granulation behavior of new formulations was not predicted by the scientific understanding of the underlying granulation phenomena, but extensive testing was undertaken. Therefore, next to empirically based granulation knowledge, a more theoretically based knowledge on the particle wetting mechanisms was required [3].

Understanding the fundamental physical and chemical phenomena that contribute to the granulation behavior and granule properties, enables to model/predict how a material will granulate given that formulation properties, equipment type and operating conditions are adequately characterized. Empirical models, mechanistic models, or a combination of both are considered for modeling a granulation system [4].

Next to a better *understanding* of granule formation mechanisms and *modeling* of the process, adequate granulation *control* is necessary to shift from a granulation art to a granulation science [5]. The increasing production scale and production speed in combination with the good manufacturing practice (GMP) and validation requirements necessitates the development of strictly controlled granulation processes. Traditionally, pharmaceutical granulation is controlled by monitoring process parameters [6, 7]. The quality of the manufactured granules is assessed afterwards via (time-consuming) laboratory analysis of the critical quality attributes of selected samples. A more efficient way to control the granulation process consists of the *real-time* product quality assessment, supplemented with real-time process parameter adjustments correcting for undesired changes in the product properties and process progress. This entails the development of automated granulation

processes that use in-line process analytical sensors to directly measure the critical product characteristics.

The process analytical technology (PAT) concept initiated by the Food and Drug Administration (FDA) in 2004 offers a regulatory framework to encourage this continuous monitoring and control of pharmaceutical production processes [8]. Implementation of PAT should lead to the in-depth understanding and control of the manufacturing process with minimal end product testing to guarantee the quality. The ultimate goal is to create a real-time based release production environment. Implementation of PAT strategies is not restricted to the commercial manufacturing scale, but should already start during process development studies. The applied techniques will help to increase product knowledge and process understanding, which in turn can be exploited during granulation scale-up. Moreover, defining an endpoint in terms of in-line measured granule properties (instead of process parameter values), makes moving from development to full production scale more easy. Adaptation of the pharmaceutical industry towards science-based manufacturing with use of quality risk management is also driven by the increased costs involved in drug research and the diminishing R&D productivity [9]. The expiration of patents and loss of exclusivity have decreased revenues.

The current use of process parameters to determine the state and endpoint of granulation processes is often inadequate, since it does not account for changes in feed material properties or external disturbances. Moreover, product information is mainly obtained after processing for a limited number of samples, preventing in-depth knowledge and efficient control of the process. In this thesis, the application of novel process analyzers for fluidized bed granulation and extrusion-spheronization, capturing direct granule product information, was evaluated. Both granulation techniques are complex, as numerous interrelated process and formulation parameters influence granule properties. By direct monitoring of the critical granule characteristics, an in-depth understanding of the granulation process can be achieved. In addition, combining the real-time collected granule product information with appropriate data processing techniques and chemometrics enables the development of adequate process control and endpoint determination tools to consistently produce granules with the desired quality.

The first part of this thesis provides a theoretical background on the applied granulation techniques and PAT. In **Chapter 2**, the fundamentals of the mechanisms contributing to wet granule growth and the characteristics of granulation via fluidized bed and extrusion-spheronization are discussed. **Chapter 3** outlines the definition of PAT according to the FDA guideline and the measurement principles of the in this thesis applied PAT sensors. In addition, the literature on the most frequently

studied analytical process sensors for fluid bed granulation and extrusion-spheronization is discussed, with emphasis on the real-time captured granule product information and the challenges encountered during the sensors' application.

Chapters 4 – 7 provide the results of the performed experimental studies. The feasibility of spatial filter velocimetry as a potential PAT tool for the in-line particle size monitoring during a fluidized bed granulation process was critically examined in **Chapter 4**. Herewith, a design of experiments was performed, examining the influence of several process and formulation variables on the granule size. Real-time obtained sizes were compared with the results from a conventional sizing technique (laser diffraction) and a better insight into the granulation process based on the continuously collected granule size information was obtained.

Once it was demonstrated that spatial filter velocimetry enables the direct, fast and non-destructive size determination during fluid bed granulation, the technique was used for the multivariate statistical modeling and control of the process (**Chapter 5**). The presented approach uses in-line granule size measurements combined with continuous granule product temperature registrations, and allows early fault detection, hence reducing bath losses (and/or reprocessing) and improving granulation efficiency.

In **Chapter 6**, an overall control strategy for a fluid bed granulation process was proposed. Spatial filter velocimetry measurements were appended with in-line near infrared spectra collection, enabling the continuous granule size and moisture monitoring. Granule size and moisture trajectories were compared with traditionally used product and exhaust air temperature control charts, showing the advantages of implementing an advanced PAT system. In addition, a feed-forward process control method was developed, where in-line collected granulation information during the process spraying phase was used to determine the optimum drying temperature of the consecutive drying phase, guiding the process towards the desired end product bulk density. Implementation of the automated control strategy should result into the production of high quality batches at lower overall costs.

In **Chapter 7**, the application of a real-time imaging method during the final steps of the extrusion-spheronization process, namely spheronization and drying, was evaluated. The at-line collected images during the spheronization and drying of different pellet formulations contained information related to the pellet size distribution, shape and surface brightness. These parameters provided valuable insight into the formulations' spheronization and drying characteristics, showing the potential of the technique as a fast and non-destructive research tool in the development and optimization of an extrusion-spheronization process.

REFERENCES

- [1] B.J. Ennis, J.D. Litster, in: R.H. Perry, D.W. Green (Eds.), *Perry's Chemical Engineers' Handbook*, McGraw-Hill, New York, 1997.
- [2] J.D. Litster, *Powder Technology*, 130 (2003) 35-40.
- [3] S.M. Iveson, J.D. Litster, K. Hapgood, B.J. Ennis, *Powder Technology*, 117 (2001) 3-39.
- [4] I.T. Cameron, F.Y. Wang, in: A.D. Salman, M.J. Hounslow, J.P.K. Seville (Eds.), *Handbook of Powder Technology*, Elsevier, Amsterdam, 2007, p. 499-552.
- [5] S. Khatry, *Pharma Times*, 42 (2010) 14-15.
- [6] D.M. Parikh, J.A. Bonck, M. Mogavero, in: D.M. Parikh (Ed.), *Handbook of Pharmaceutical Granulation Technology*, Marcel Dekker Inc., New York, 1997, p. 227-302.
- [7] D.I. Wilson, S.L. Rough, in: A.D. Salman, M.J. Hounslow, J.P.K. Seville (Eds.), *Handbook of Powder Technology*, Elsevier, Amsterdam, 2007, p. 189-217.
- [8] Food and Drug Administration, *Guidance for Industry; PAT - A framework for innovative pharmaceutical development, manufacturing and quality assurance*, (2004)
- [9] P. Kanneganti, in: D.M. Parikh (Ed.), *Handbook of Pharmaceutical Granulation Technology - Third edition*, Informa Healthcare, New York, 2010, p. 597-616.

CHAPTER 2

FLUIDIZED BED GRANULATION & EXTRUSION-SPHERONIZATION AS WET GRANULATION TECHNIQUES

Parts of this chapter are accepted for publication (with minor revisions) in:

A. Burggraeve, T. Monteyne, J.P. Remon, C. Vervaet, T. De Beer, Process analytical tools for monitoring, understanding and control of pharmaceutical fluidized bed granulation: a review, *European Journal of Pharmaceutics and Biopharmaceutics*, accepted with minor revisions.

CHAPTER 2

FLUIDIZED BED GRANULATION & EXTRUSION-SPHERONIZATION AS WET GRANULATION TECHNIQUES

2.1. INTRODUCTION

Granulation is defined as a particle size enlargement process whereby small powder particles are gathered into larger, permanent structures in which the original particles can be distinguished [1]. Hence, granulation can be considered as the pharmaceutical opposite of milling [2]. Instead of reducing the particle size, the process aims at particle growth. Two major granulation methods are widely applied, namely *wet* and *dry* granulation [3]. As its name suggests, wet granulation involves the use of a binder liquid, which is introduced onto agitated powder particles binding these together through a combination of capillary and viscous forces [4]. During subsequent drying, the solvent is removed via evaporation and more permanent bonds are established. The granule strength is then mainly related to the solid bridges, formed by hardening of binders and the crystallization of dissolved particles. Dry granulation methods are based on the compaction of the powder mass, before it is crushed and fractionated. Hence, particle size enlargement is achieved without the use of a binder liquid, making this process particularly suitable for moisture- or heat-sensitive drugs. Compared to dry granulation processes, wet granulation offers a better control of drug content uniformity, product bulk density and compactibility [5]. However, the process is more complicated to validate and control due to the additional preparation of binder liquid and supplementary drying step. It is also more expensive with regard to labor, equipment, energy and space [6].

The use of granulation techniques in the pharmaceutical industry is driven by the improvement of one or more powder properties. These include, increased bulk density, flowability and solubility, reduced risk of size segregation and dust formation [7]. The manufactured granules are mainly tableted, or filled into capsules.

In this thesis, the application of analytical process sensors during two wet granulation techniques, namely *fluidized bed granulation* and *extrusion-spheronization*, was evaluated. Therefore, the fundamentals of the mechanisms contributing to wet granule growth and the characteristics of granulation by fluidized bed and extrusion-spheronization are discussed in this chapter.

2.2. FUNDAMENTALS OF WET GRANULE GROWTH

During wet granulation, a number of different mechanisms take place. In this work, the classification according to Iveson et al. [4] is considered, viewing the wet granulation process as a combination of three different mechanisms or sets of rate processes. These include:

- wetting and nucleation of particles
- consolidation and growth by collisions of material in the granulator
- attrition and breakage

Wetting advances the nucleation of fine powders, which is strongly influenced by the distribution of the binding fluid and the powder properties. The growth stage involves collisions between two (partially) wetted granules (i.e., coalescence) or granules and feed powder (i.e., layering) resulting in larger granules composed of several particles. During granule growth, the agglomerates are subjected to compaction forces (due to bed agitation) causing the granules to gradually consolidate. This is accompanied by a reduction in size and porosity, and forces out entrapped air and binder liquid to the particle surface. The rate of consolidation or densification depends on the properties of the feed material, such as particle size distribution, particle shape and surface roughness. The final densification level determines end product porosity and therefore granule hardness, strength and dissolution. High porosity granules are weak and friable (unwanted creation of dust during product handling), but display often an advantageous fast dissolution rate which makes granule porosity an important product property to control. The third rate process includes two phenomena. Low binding strengths in the moist agglomerates create weak *wet* granules that may *break* in the granulator, influencing the final granule size distribution. This breakage is more prominent in granulation processes displaying high shear forces. Weak *dried* granules are susceptible to *attrition* or fracture in the fluid bed granulator or during subsequent handling. The associated generation of dusty fines counteracts the objectives of granulation and should therefore be avoided.

During a fluid bed granulation process, the binder liquid addition and evaporation take place at the same time, making this a unique granulation process [8]. Hence, the three rate mechanisms occur simultaneously and the contribution of each of them to the developed agglomerates depends on granulation equipment, process settings and feed material properties. The combination of the most dominant rate processes determines the final granule size distribution, structure and porosity and therefore end product quality attributes.

According to the relative amount of liquid phase, a number of different states of the moist agglomerates are described, i.e., the *pendular*, the *funicular* and the *capillary* state (Figure 2.1) [9].

The herewith associated increasing amount of liquid phase is expressed by the liquid saturation, describing the ratio of pore volume occupied by the liquid to the total pore volume within the agglomerate. In each state, a different type of bonding is holding the particles together. In the pendular state, liquid bridges at particle contact points are holding the particles together, whereas in the capillary state all the voids are saturated with liquid and the surface liquid is drawn into the particle pores under capillary action. The intermediate funicular state is characterized by voids that are not completely filled with liquid. In addition to these three stages, a fourth one, the *droplet* state has been defined (Figure 2.1) [10]. This state is characterized by the addition of more liquid to the powder mixture than the amount required to completely fill all inter- and intra-particulate voids. Hence, the liquid completely surrounds the solid particles. If the droplet state is achieved during conventional wet granulation (i.e., fluidized bed and high shear granulation), generally too much liquid has been added and granulation will not be successful [2]. This in contrast to the process of granulation by spray-drying of a suspension, where the droplet state is an important stage of the process.

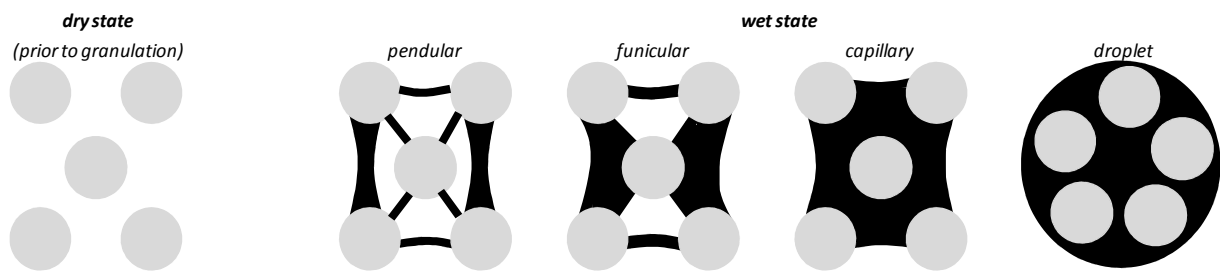


Figure 2.1. Overview of the four stages of powder wetting (liquid saturation). The solid particles are represented by grey circles and the binding liquid is colored black.

2.3. FLUIDIZED BED GRANULATION

2.3.1. General description of the process

During fluidization, solids are subjected to a gas (usually air) which converts the material from a static state to a dynamic fluid state. At certain gas velocities the gas will support the particles, allowing an up- and downward movement, suspending the material in the gas [11].

Pharmaceutical fluidized bed granulation was first described by Wurster, when he reported on the use of the air suspension technique to coat tablets [12]. This was followed by a paper describing the process of granulation and drying via the air suspension technique to prepare compressed tablets [13]. A fluid bed granulation process entails the suspension of particles in a conical shaped container by use of a (heated) air stream. The applied air velocity should allow proper particle movement in the container, but keep the material out of the filter bags (Figure 2.2). Good fluidization can be visually monitored by the free downward flow of the granules at the windows of the container. As particles move up and down in the container, a binder solution is sprayed (i.e., spraying phase). Binder liquid droplets are deposited onto the fluidized particles in the spray granulation zone. This wetting causes the formation of granules according to different mechanisms (Section 2.2). After spraying the required amount of binder liquid, further fluidization enables rapid drying of the granules in the same equipment (i.e., drying phase). Drying reduces the residual moisture of the granules to a level that ensures the stability of product active(s), and meets the requirements for downstream processing. A good granulation is achieved when particles are uniformly mixed and liquid bridges between the particles are strong and easy to dry. The size of the agglomerates usually ranges from 0.1 mm to 2.0 mm.

Compared to high shear granules, the lack of shear forces in a conventional fluidized bed results into the production of more porous and less dense granules with better dissolution and compression characteristics [14]. Generally, the fluidized bed granules exhibit a narrower size distribution, without oversized granules. The most common problems encountered during fluid bed granulation include the production of excessively coarse granules, excessive fines, poor fluidization, inconsistency of final moisture content, low yield and non-uniformity of finished product [15].

2.3.2. Process equipment

A fluidized bed granulator consists of several key components (Figure 2.2, [16, 17]). A *control panel (1)* allows operating the process and monitoring critical process variables. As generally outside air is used to fluidize the particles, an *air handling unit (2)* is essential for air filtering, heating, cooling and removal of humidity. After preconditioning the air, it is passed through the bed of solids in the

product container (3) via the *air distributor plate (4)*. The type of container and air distributor must be selected accordingly to obtain a proper product fluidization. The binder liquid is introduced onto the fluidizing particles via a *nozzle (5)* system. The two-fluid (binary) nozzle is most commonly applied in fluid bed granulation as it is able to function at very slow liquid rates and offers a controlled droplet size, independent of flow rate. With this nozzle, the binder solution (one fluid) is atomized by compressed air (other fluid). The spray pattern and angle can be modified by adjusting the position of the air cap surrounding the nozzle needle and by varying the air pressure required for atomization of binder liquid.

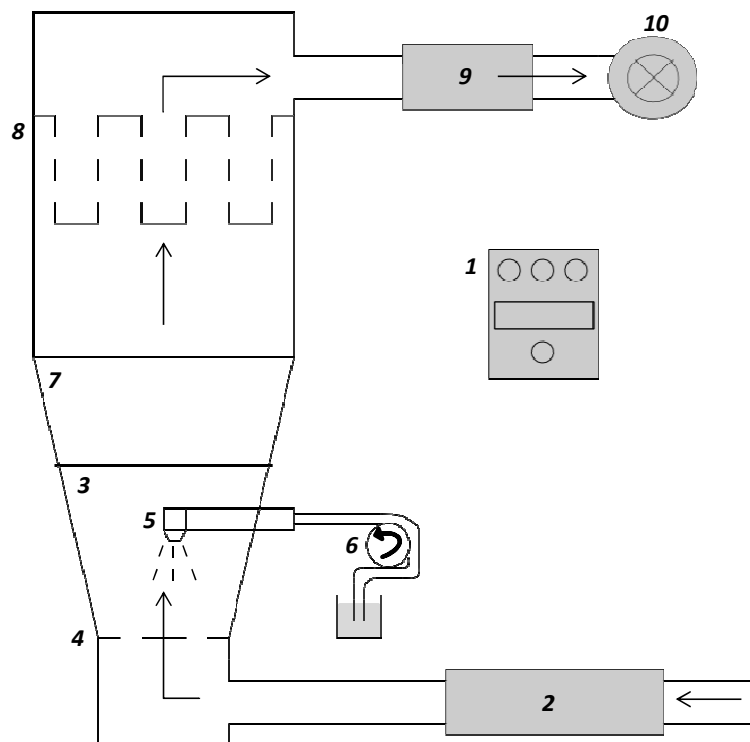


Figure 2.2. Schematic of a top-spray fluid bed granulator with assignment of its different components: (1) control panel, (2) air handling unit, (3) product container, (4) air distributor plate, (5) top-spray installed nozzle, (6) pump, (7) air expansion chamber, (8) filter bags, (9) air filter system, (10) exhaust blower. Arrows indicate the direction of the airflow.

Depending on the location of the spray nozzle, different types of fluid bed granulators are considered producing granules with varying characteristics [18]. Top-spray fluid bed granulation, with the nozzle located at the top of the chamber is the most frequently studied and used technique [19]. The binder liquid is sprayed from the top down onto the fluidized bed, counter-currently to the fluidizing air. During bottom-spray granulation, the nozzle is positioned at the base of the chamber, in the middle of the distributor plate, and liquid is sprayed in the same direction of the fluidizing air. The bottom-spray granulator can be equipped with a partition column (i.e., Wurster partition) and a specially designed distributor plate to regulate the fluidization pattern. The plate, with perforation

sizes decreasing from the centre to the outer part, enables a higher air velocity inside the Wurster partition than in the outer region creating a fountain-like movement. Introducing the spray nozzle at the side of the chamber, embedded in the powder bed during granulation, corresponds to tangential-spray granulation. This technique is also called rotary fluidized bed granulation due to the rotating disk installed at the bottom of the bed (no use of air distributor plate). This modification of the standard fluid bed granulation set-up combines the advantages of fluidized bed and high shear granulation due to the additional mechanical agitation. The rotary granulation process is marked by centrifugal, high intensity mixing and efficient fluid bed drying, yielding a product that is more spherical, denser and less porous compared to top-sprayed granules [20]. The binder liquid is peristaltic *pumped (6)* to the nozzle through a spray lance and tubing. To separate particles from the outlet air, two zones in the fluid bed equipment are used. In the *air expansion chamber (7)*, the largest particles are withdrawn as they lose their momentum. *Filter bags (8)* can be periodically shaken to reintroduce the collected fines into the fluidized bed. The air leaves the system through an *air filter system (9)*, removing the residual smaller particles from the exhaust air and a *blower (10)* or fan, keeping the system at a lower pressure than the surrounding atmosphere.

The quality attributes of the final product may be manipulated by changing process operating variables (*process engineering*) and product formulation variables (*product engineering*), which affect the underlying granulation mechanisms. Operating variables are related to the granulation equipment and can be divided into apparatus variables and process parameters. Formulation variables are defined by the choice of starting materials and binder solution (Table 2.1).

All factors influencing the wetting of the powder by the sprayed binder liquid affect the formation of liquid bonds and therefore agglomerate growth [21]. Especially in fluidized bed granulation, these wetting factors critically determine the final granule size distribution due to the relatively low shear forces present during processing. The absence of shear forces largely restricts particle densification and liquid saturation of the agglomerates, therefore reducing granule growth by coalescence. Increasing granule growth by increasing the bed moisture level is difficult, as this may result into bed collapse due to the poor fluidizing capacity of the wet mass [22]. Detailed reviews of the effects of operating and formulation variables on the quality properties of granules produced by fluid bed granulation, are available in literature [6, 8, 16, 19, 23-28]. An overview of the parameters is listed in Table 2.1, with the assumption that binder and surfactant are added in solution (not as a dry material in the powder mix) and the nozzle is installed top-spray. In addition to the individual influences of operating and formulation variables on the end product quality, the parameters' effects are also highly co-dependent. Hence, these interactions need to be understood and taken into account during optimization and particularly scale-up if one wants to achieve a desired product quality. Faure

and co-workers [29] reviewed the parameters that need controlling during wet granulation, and how this influences process control and scale-up.

Table 2.1. Overview of top-spray fluid bed granulation operating and material variables influencing granule quality attributes (*binder and surfactant are added in solution*).

Operating variables		Material variables	
apparatus variables	process variables	starting material	binder solution
<i>shape product container</i>	<i>inlet air temperature</i>	<i>particle size</i>	<i>type of solvent</i>
<i>design air distributor plate</i>	<i>inlet air velocity</i>	<i>particle size distribution</i>	<i>type of binder</i>
<i>nozzle position</i>	<i>inlet air humidity</i>	<i>particle shape</i>	<i>binder concentration</i>
<i>nozzle type</i>	<i>inlet air volume</i>	<i>moisture content</i>	<i>binder content in formulation</i>
<i>diameter of nozzle tip</i>	<i>fluid bed height</i>	<i>cohesiveness</i>	<i>binder viscosity</i>
	<i>product temperature</i>	<i>static charge</i>	<i>type of surfactant</i>
	<i>binder liquid spray rate</i>	<i>wettability</i>	<i>surfactant concentration</i>
	<i>nozzle atomization air pressure</i>	<i>stickiness</i>	
	<i>nozzle atomization air volume</i>		
	<i>exhaust air temperature</i>		
	<i>drying time</i>		

2.3.3. Traditional methods of process control and endpoint detection

During the first applications of fluidized bed granulation, precise control of the process was absent. A historical method of determining the drying endpoint consisted of feeling the expansion chamber for increasing temperature [30]. This method took considerable time to ‘fine tune’ and was purely based on intuition and empiricism. The lack of monitoring and control systems made reproducible granulation in a reliable manner difficult [18].

Control of the formulation components and the process is essential to ensure the consistent production of granules with the desired quality characteristics (i.e., granule size, size distribution, moisture content, density, flowability and friability). The quality attributes are affected by the properties of starting material (Table 2.1), therefore variations in feed material properties should be minimized. The use of an air handling unit allows filtering, heating, cooling and humidity removal of the inlet process air [8, 16]. The air dehumidification is especially important when the production unit is located in a climate with large moisture variations, as the binder liquid evaporation rate is determined by the processes of heat and mass transfer. Heat is transferred to the granules to evaporate the binder solvent, while mass is transferred as a vapor from the granules in the

surrounding gas. The capacity of the incoming air to absorb moisture (i.e., drying capacity) depends upon its temperature and relative humidity. Therefore, by controlling these parameters, a reproducible drying capacity can be achieved contributing to a controlled fluid bed granulation process.

The recording and control of critical granulation process parameters was initially carried out by a pneumatic analog control device, which uses compressed air as a signaling medium to convey information from granulator measuring instruments. The pneumatic signaling system exhibited a desired simplicity and safety, but its effectiveness was highly dependent of the operator's interpretations and actions to ensure product quality and accurate data logging. Through the development of programmable logic controllers and computers a more reliable control, batch production and data acquisition was achieved. A PID (Proportional, Integral, Derivative) controller is commonly used as a feedback control mechanism. It calculates an error value for a process variable as the difference between the measured process variable and a desired set point. The controller attempts to minimize the error by use of a corrective adjustment action. The airflow rate and temperature are typical process variables that can be adjusted by a PID controller in fluid bed granulation. The collected process sensor signals are computer-stored and can be recalled to issue a batch certificate. During the spraying period, critical data related to the inlet air humidity and temperature, product and outlet air temperature, airflow, binder spray rate, atomizing air pressure and pressure drops across the bed are collected. During drying, the inlet air temperature and humidity, product and exhaust air temperature and airflow are continuously monitored. In particular, the product and exhaust air temperature indicate the progress of drying since fluid bed drying is typically characterized by two stages of water loss [31]. The first is heat transfer limited and corresponds to the evaporation of water from the particles in the bed. It shows a linear dependency with time and the bed temperature remains constant during this phase (*evaporative cooling stage*). When surface and loosely associated water has evaporated, the remaining water diffuses to the surface of the granules before it is lost, which is greatly affected by the particle geometry. When the amount of water left to evaporate reaches a minimum value during this second stage, the exhaust air temperature will increase, approaching the inlet air temperature. Hence, drying endpoint is mainly determined by the temperature of the exhaust air [8].

Research showed that this well-established method of detecting drying endpoint via the exhaust air or product temperature, is only repeatable if the humidity level of the inlet air is controlled. By use of the temperature difference between the inlet air and fluid bed mass (ΔT), the effect of variations in process air humidity on drying endpoint detection is eliminated [32]. However, one should also take the influence of fluidization on the ΔT technique into account. Improper fluidization, even for

short periods, can be a major source of deviation for the ΔT technique, as the temperature of the granulation mass is relatively higher when fluidization is low [33]. To handle this interdependency of process parameters, multi-way models have been recognized to be useful in the monitoring of batch data. Successful batches were separated from unsuccessful ones by a PARAFAC2 method based on the monitoring of three granulation process variables (i.e., inlet air, outlet air and mass temperature) [34].

2.4. EXTRUSION-SPHERONIZATION

2.4.1. General description of the process

Extrusion-spheronization is one of several techniques to prepare pelletized dosage forms. Pellets are spherical, free-flowing granules with a narrow size distribution, typically varying between 500 μm and 1500 μm in pharmaceutical applications. Therapeutic advantages of pellets as a drug delivery system include less irritation of the gastro-intestinal tract and a lowered risk of side effects due to dose dumping [35]. By use of pellets, several active components, incompatible drugs or drugs with different release profiles may be combined in the same dosage unit. Pellets produced by extrusion-spheronization exhibit a good flowability, low friability, high hardness and reproducible packing [36]. These properties also contribute to the ease with which the pellets may be coated. Extrusion-spheronization exhibits a high process yield, and high levels of the active compound may be incorporated without producing an excessively large particle.

Conine and Hadley [37] were the first to describe the production of pellets via extrusion-spheronization in the pharmaceutical industry, and Reynolds [36] elaborated this work through the further description of the equipment and process mechanisms. Extrusion-spheronization is a multi-step process consisting of the following consecutive stages (Figure 2.3):

- (i) *dry mixing* of drug and excipient(s) to achieve a homogeneous powder blend
- (ii) addition of binder liquid to the dry mass (i.e., *wet granulation*) to produce a (sufficiently) plastic wet mass
- (iii) shaping of the wet mass into cylinders called extrudates of uniform diameter (i.e., *extrusion*)
- (iv) breaking of the extrudates into smaller cylindrical rods and rounding these into spherical granules (i.e., *spheronization*)

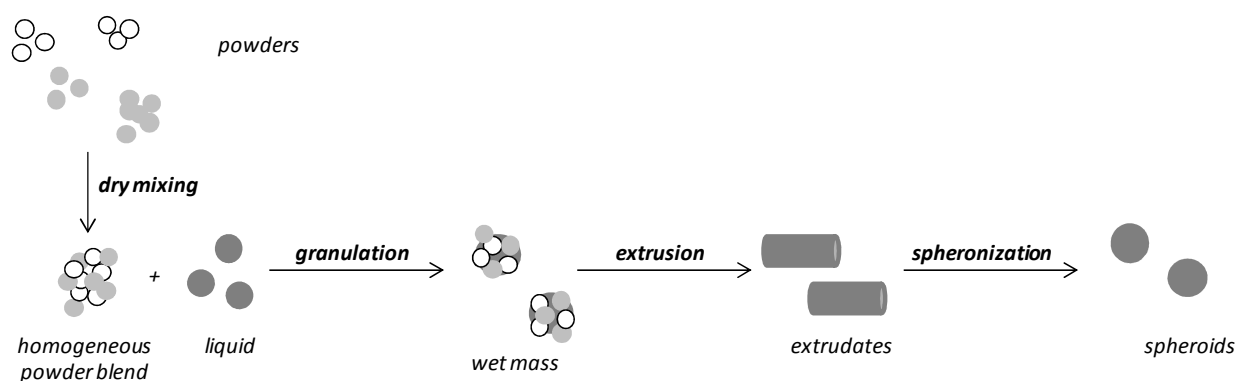


Figure 2.3. Schematic overview of the steps involved in an extrusion-spheronization process.

The spherical particles are then dried at room temperature or at an elevated temperature (in an oven, a fluidized bed or microwave oven) until the desired residual moisture level is achieved. As the different process steps are influenced by a number of interrelated process and formulation variables, the extrusion-spheronization process requires the necessary control to obtain the required pellet quality. The pellet size distribution, shape, friability, density, porosity, flow properties and dissolution behavior are generally evaluated to assess the pellet quality [38, 39].

2.4.2. Process equipment

- Dry mixing and wet granulation

A uniform blend has to be obtained before wet granulation can take place, as it affects the pellets' content uniformity. An uneven distribution may also result into local overwetting during granulation, for materials with large differences in size and solubility properties [40]. Dry mixing and wet granulation are usually carried out in the same equipment (e.g., planetary mixer, high shear mixer, sigma blade mixer), unless a continuous granulator is used. The required amount of granulation liquid is greater than that for conventional wet granulation techniques and in combination with the dispersion of the fluid, it greatly influences the downstream process steps of extrusion and spheronization.

- Extrusion

During extrusion, the plastic wet mass is forced through a die and shaped into cylindrical particles with a uniform diameter. The resultant extrudates' diameter is determined by the diameter of the die, and its length depends upon the properties of the wet mass and the extruder type. A variety of extruder types has been developed, and can be divided into three classes based on their feed mechanism (i.e., the way by which the wet mass is transported through the extrusion zone): screw feed extruders, gravity feed extruders, and piston feed extruders, shown in Figure 2.4 [41].

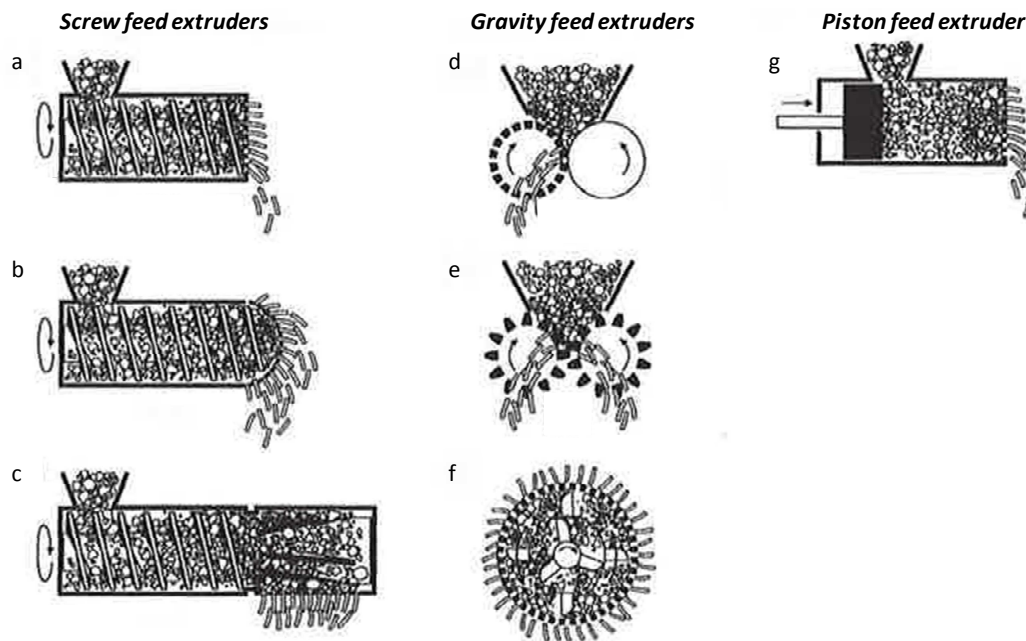


Figure 2.4. Schematic overview of the extruder types applied in extrusion-spheronization. Screw feed extruders with axial (a), dome (b) and radial (c) type, gravity feed extruders with cylinder (d), gear (e) and radial type (f) and piston feed ram extruders (g) [42].

- Spheronization

A spheronizer consists of a bowl with fixed sidewalls and a bottom plate or disk that rotates at a high speed (Figure 2.5). The spheronizer is filled with extrudates, and due to frictional forces generated by particle-particle and particle-equipment interaction, the extrudates are initially broken into smaller cylinders and then rounded into spheres. To enhance the forces generated as particles move across its surface, the bottom plate generally exhibits a grooved surface (cross-hatched pattern or radial pattern).

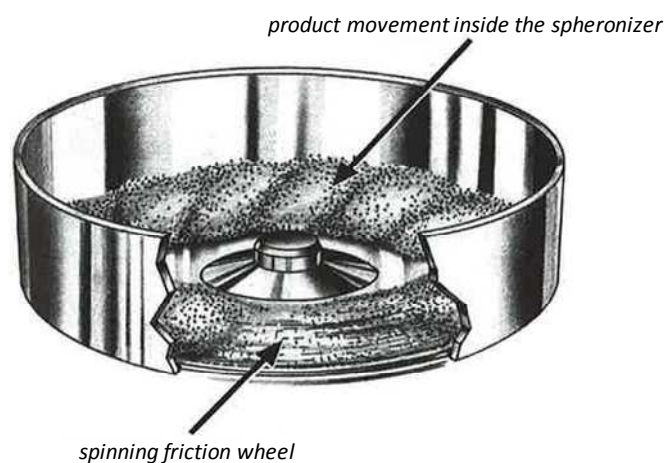


Figure 2.5. Schematic of the particle movement in a spheronizer [42].

The transformation from a cylindrical extrudate in a spherical particle occurs in various stages, and two models have been proposed to describe this process (Figure 2.6a and b). According to Rowe [41] (Figure 2.6a), the cylinders are rounded off at the edges, followed by the formation of dumbbell-shaped particles, ellipsoids and finally spheres. The model proposed by Baert and Remon [43] (Figure 2.6b) suggests that the cylinders are rounded off at the edges, but are additionally bent resulting in the formation of a rope-shaped particle. Next, a dumbbell with a twisted middle is formed, initiating particle breakage into two spherical particles with a cavity on their flat side. Further rounding in the spheronizer creates completely spherical particles. Recently, Koester and Thommes [44] reported that these generally adopted pelletization mechanisms need to be extended, to account for the material transfer between pellet particles (Figure 2.6c). In addition to plastic deformation, the authors also observed a material transfer between pellet particles for different formulations. Herewith, regional distinctions in the amount of mass transfer and an influence of the water content were observed.

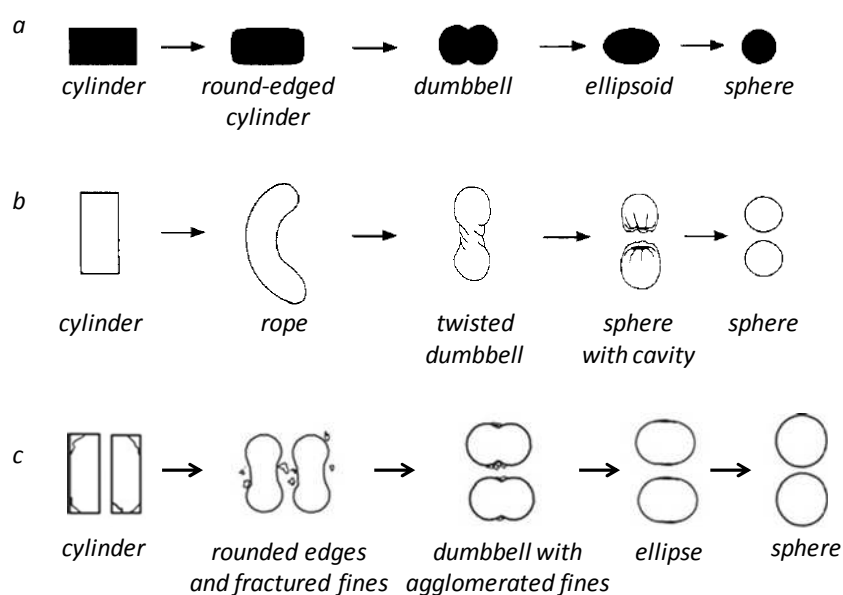


Figure 2.6. Schematic presentation of the different pellet formation stages during spheronization according to Rowe [41] (a), Baert and Remon [43] (b) and Koester and Thommes [44] (c).

2.4.3. Traditional methods of process control and endpoint detection

Extrusion-spheronization can be an efficient method to manufacture pellet dosage forms, but the process exhibits a lack of reliable and readily measured parameters to establish adequate control of the process [45]. Various process parameters affect pellet quality, and therefore a strictly controlled manufacturing procedure needs to be followed.

Control of the temperature during extrusion is of significant importance as the energy dissipated during the extrusion cycle can increase the extruder temperature and cause some of the liquid to

evaporate from the extrudate (particularly from its surface). This may lead to a difference in the quality of the extrudates produced at the beginning versus the end of the batch. The reduced (surface) water content may affect the spheronization stage. In addition, extrusion temperature control is especially important when processing a thermolabile drug formulation.

The total output of the extruder is mainly determined by the extrusion speed. Hence, for economical reasons one would prefer high extrusion speeds. However, surface defects become more pronounced with increased extrusion speed, leading to lower quality pellets during spheronization [46].

The spheronization speed and time must also be controlled, as both influence the final pellet quality by a number of pellet properties [39].

REFERENCES

- [1] B.J. Ennis, J.D. Litster, in: R.H. Perry, D.W. Green (Eds.), *Perry's Chemical Engineers' Handbook*, McGraw-Hill, New York, 1997.
- [2] J.B. Schwartz, *Drug Development and Industrial Pharmacy*, 14 (1988) 2071-2090.
- [3] L.L. Augsburger, M.K. Vuppala, in: D.M. Parikh (Ed.), *Handbook of Pharmaceutical Granulation Technology*, Marcel Dekker Inc., New York, 1997, p. 7-23.
- [4] S.M. Iveson, J.D. Litster, K. Hapgood, B.J. Ennis, *Powder Technology*, 117 (2001) 3-39.
- [5] C. Bacher, P.M. Olsen, P. Bertelsen, J.M. Sonnergaard, *International Journal of Pharmaceutics*, 358 (2008) 69-74.
- [6] Z.H. Loh, D.Z.L. Er, L.W. Chan, C.V. Liew, P.W.S. Heng, *Expert Opinion on Drug Delivery*, 8 (2011) 1645-1661.
- [7] C. Appelgren, *Drug Development and Industrial Pharmacy*, 11 (1985) 725-741.
- [8] D.M. Parikh, J.A. Bonck, M. Mogavero, in: D.M. Parikh (Ed.), *Handbook of Pharmaceutical Granulation Technology*, Marcel Dekker Inc., New York, 1997, p. 227-302.
- [9] D.M. Newitt, J.M. Conway-Jones, *International Journal of Pharmaceutical Technology and Product Manufacture*, 36 (1958) 422.
- [10] C.G. Barlow, *The Chemical Engineer*, 220 (1968) CE196-CE201.
- [11] R. Dixit, S. Puthli, *Journal of Pharmaceutical Sciences*, 98 (2009) 3933-3960.
- [12] D.E. Wurster, *Journal of the American Pharmaceutical Association*, 48 (1959) 451-454.
- [13] D.E. Wurster, *Journal of the American Pharmaceutical Association*, 49 (1960) 82-84.
- [14] T. Liske, W. Mobus, *Drugs made in Germany*, 11 (1968) 182-189.
- [15] Niro Pharma Systems (GEA), *Pharmaceutical Technology Europe* (May 1998).
- [16] D.M. Parikh, in: M. Levin (Ed.), *Pharmaceutical Process Scale-Up*, Marcel Dekker Inc., New York, 2002, p. 171-220.
- [17] M. Jacob, in: A.D. Salman, M.J. Hounslow, J.P.K. Seville (Eds.), *Handbook of Powder Technology*, Elsevier, Amsterdam, 2007, p. 417-476.
- [18] D.M. Jones, *Pharmaceutical Technology*, 9 (1985) 50-62.
- [19] M. Banks, M.E. Aulton, *Drug Development and Industrial Pharmacy*, 17 (1991) 1437-1463.
- [20] L. Gu, C.V. Liew, P.W.S. Heng, *Drug Development and Industrial Pharmacy*, 30 (2004) 111-123.
- [21] X.H. Hu, J. Cunningham, D. Winstead, *Journal of Pharmaceutical Sciences*, 97 (2007) 1564-1577.
- [22] S.H. Schaafsma, N.W.F. Kossen, M.T. Mos, L. Blauw, A.C. Hoffman, *ALChE Journal*, 45 (1999) 1202-1210.

- [23] J.A. Hersey, *International Journal of Pharmaceutical Technology and Product Manufacture*, 2 (1981).
- [24] G.H. Kristensen, T. Schaefer, *Drug Development and Industrial Pharmacy*, 13 (1987) 803-872.
- [25] P.J. Sherrington, R. Oliver, in: A.S. Goldberg (Ed.), *Powder Science and Technology*, Heyden, London, 1981.
- [26] W.J. Thiel, *International Journal of Pharmaceutical Technology and Product Manufacture*, 2 (1981).
- [27] S. Srivastava, G. Mishra, *International Journal of Pharmaceutical Sciences and Drug Research*, 2 (2010) 236-246.
- [28] A. Hemati, R. Cherif, K. Saleh, V. Pont, *Powder Technology*, 130 (2003) 18-34.
- [29] A. Faure, P. York, R.C. Rowe, *European Journal of Pharmaceutics and Biopharmaceutics*, 52 (2001) 269-277.
- [30] K.A. Macias, M.T. Carvajal, in: D.M. Parikh (Ed.), *Handbook of Pharmaceutical Granulation Technology - Third edition*, Informa Healthcare, New York, 2010, p. 567-577.
- [31] K.R. Morris, S.L. Nail, G.E. Peck, S.R. Byrn, U.J. Griesser, J.G. Stowell, S.J. Hwang, K. Park, *Pharmaceutical Science & Technology Today*, 1 (1998) 235-245.
- [32] M. Alden, P. Torkington, A.C.R. Strutt, *Powder Technology*, 54 (1988) 15-25.
- [33] T. Lipsanen, O. Antikainen, H. Raikkonen, S. Airaksinen, J. Yliruusi, *International Journal of Pharmaceutics*, 357 (2008) 37-43.
- [34] S. Matero, S. Poutiainen, J. Leskinen, S.P. Reinikainen, J. Ketolainen, K. Jarvinen, A. Poso, *Chemometrics and Intelligent Laboratory Systems*, 96 (2009) 88-93.
- [35] H. Bechgaard, G. Hegermann Nielsen, *Drug Development and Industrial Pharmacy*, 4 (1978) 53-67.
- [36] A. Reynolds, *Manufacturing Chemist and Aerosol News*, 41 (1970) 40-43.
- [37] J. Conine, H. Hadley, *Drug & Cosmetic Industry*, 106 (1970) 38-41.
- [38] V.R. Sinha, M.K. Agrawal, A. Agarwal, G. Singh, D. Ghai, *Critical Reviews in Therapeutic Drug Carrier Systems*, 26 (2009) 275-331.
- [39] C. Vervaet, L. Baert, J.P. Remon, *International Journal of Pharmaceutics*, 116 (1995) 131-146.
- [40] D.F. Erkoboni, in: D.M. Parikh (Ed.), *Handbook of Pharmaceutical Granulation Technology*, Marcel Dekker Inc., New York, 1997, p. 333-368.
- [41] R.C. Rowe, *Pharmacy International*, 6 (1985) 119-123.
- [42] D.F. Erkoboni, in: I. Ghebre-Sellassie, C. Martin (Eds.), *Pharmaceutical Extrusion Technology*, Marcel Dekker Inc., New York, 2003, p. 277-322.
- [43] L. Baert, J.P. Remon, *International Journal of Pharmaceutics*, 95 (1993) 135-141.
- [44] M. Koester, M. Thommes, *Aaps Pharmscitech*, 11 (2010) 1549-1551.

- [45] D.I. Wilson, S.L. Rough, in: A.D. Salman, M.J. Hounslow, J.P.K. Seville (Eds.), *Handbook of Powder Technology*, Elsevier, Amsterdam, 2007, p. 189-217.
- [46] P.J. Harrison, J.M. Newton, R.C. Rowe, *Journal of Pharmacy and Pharmacology*, 37 (1985) 81-83.

CHAPTER 3

PROCESS ANALYTICAL TECHNOLOGY IN FLUIDIZED BED GRANULATION & EXTRUSION-SPHERONIZATION

Parts of this chapter are published/accepted for publication in:

T. De Beer, **A. Burggraeve**, M. Fonteyne, L. Saerens, J.P. Remon, C. Vervaet, Near infrared and Raman spectroscopy for the in-process monitoring of pharmaceutical production processes, *International Journal of Pharmaceutics*, 417 (2011) 32-47.

A. Burggraeve, T. Monteyne, J.P. Remon, C. Vervaet, T. De Beer, Process analytical tools for monitoring, understanding and control of pharmaceutical fluidized bed granulation: a review, *European Journal of Pharmaceutics and Biopharmaceutics*, accepted with minor revisions.

CHAPTER 3

PROCESS ANALYTICAL TECHNOLOGY IN FLUIDIZED BED GRANULATION & EXTRUSION-SPHERONIZATION

3.1. PROCESS ANALYTICAL TECHNOLOGY

3.1.1. Introduction

For decades, pharmaceutical manufacturing consisted of batch processing with laboratory testing conducted on randomly collected samples to assess the intermediate or end product quality. In addition to the off-line testing, product quality is ensured by determining raw material properties and having a fixed drug product manufacturing process [1]. Simple univariate sensors such as pressure, temperature and pH are used to control the production processes. The processes themselves are often not fully understood and are therefore considered as inefficient black-boxes (Figure 3.1, top). Limited relevant product information is mainly obtained after manufacturing, making process control difficult which can lead to batch losses.

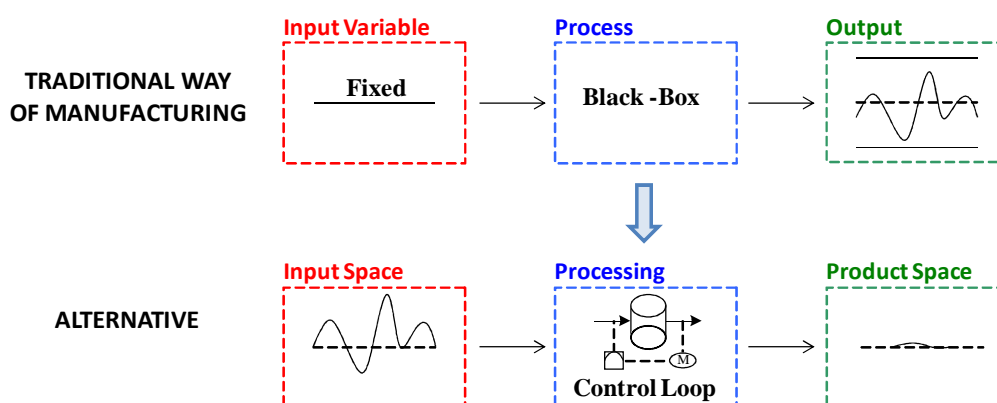


Figure 3.1. Comparison between the traditional fixed way of pharmaceutical manufacturing (top) and the PAT-based approach leading to a robust and adjustable process, guaranteeing the end product quality (bottom).

Through the development of real-time analyzers, several traditional off-line laboratory techniques have been replaced by real-time quality measurements in many industries (e.g., chemical, food,

agricultural, etc.) [2]. These real-time process analytical methods differentiate from the off-line laboratory techniques by the measurement time, with the former on the timescale of seconds (or minutes) as opposed to hours or days for the latter. By eliminating manual sample handling, the sample integrity is retained and the risk of errors by the operator is reduced. The growing interest in the implementation of more complex process analytics within manufacturing industries is driven by the increased capabilities of these systems with regard to both scientific and engineering controls [3]. The complex chemical and physical analyses performed in, on or immediately at the process stream enable (automatic) process control with feedback and/or feed-forward, the reduction of cycle time and safety mitigation. In that way, the product quality and yield may be increased and labor costs reduced. In the long run, the increased process information allows the continuous improvement of the process. Next to these financial drivers, the use of process monitoring data may support the changes in a manufacturing process, by showing the equivalency of an enhanced process to the prior registered version. A key aspect to real-time process analysis and control is the high level of complexity associated with its design, implementation, data interpretation and maintenance, which requires the necessary expertise [4].

Due to the strictly regulated environment of the pharmaceutical industry, the sector has been hesitant to introduce these innovative systems into their manufacturing processes [5, 6]. Therefore, several guidelines have been written by the United States *Food and Drug Administration* [7-9] and the *International Conference of Harmonization* (ICH) [10-12] to improve process performance and product quality in the pharmaceutical industry. The FDA's initiative on Process Analytical Technology encourages to develop and implement effective and efficient innovative approaches in pharmaceutical development, manufacturing and quality assurance. Controlling the quality of the product during instead of after processing, and quantifying (and reducing) herewith the process variability in pharmaceutical manufacturing is promoted. The continuous gathering of critical process information during production should enable the transition from a fixed to a robust manufacturing process with real-time process adjustments, hence ensuring the quality of each end product and avoiding batch losses (Figure 3.1, bottom) [13]. Through this real-time quality control approach, the concept of *real-time release* is introduced in the PAT guidance, i.e., release as soon as the batch manufacture is complete. The paradigm shift from batch to continuous processing also drives the pharmaceutical industry to adopt PAT [14]. The benefits of continuous processing (e.g., reduction in scale-up issues, more flexible response to changes in demand, lower cycle time) would be annulled without the use of process analytics and feedback and feed-forward control loops to keep the processes under control [15].

3.1.2. The PAT Framework

The FDA has defined PAT as *a system for designing, analyzing and controlling manufacturing through timely measurements (i.e., during processing) of critical quality and performance attributes of raw and in-process materials and processes, with the goal of ensuring end product quality* [9]. Herewith, the term analytical in PAT is viewed broadly, including chemical, physical, microbiological, mathematical, and risk analysis to be conducted in an integrated manner.

The aim of PAT is to *enhance understanding and control of the manufacturing process*, which is consistent with the FDA's current drug quality system stating that *quality cannot be tested into products, it should be built-in*.

To completely understand the process, all critical sources of variability should be identified and explained, and the variability should be managed by the process. In that way, the accurate and reliable prediction of the product quality (over the design space) is established given that the materials used, process parameters, and manufacturing, environmental and other conditions are identified.

There are several PAT tools and principles available enabling and advancing the implementation of a PAT system in a pharmaceutical production process. The PAT tools provide relevant information about the chemical, physical and biological properties to enhance process understanding and will therefore enable process control and optimization. Process endpoint will no longer be defined in terms of a fixed process time, but rather by the real-time measured product quality, improving process efficiency. A combination of suitable PAT tools is always necessary to achieve the desired level of understanding and control, and these tools can be categorized as followed [9]:

- Multivariate tools for design, data acquisition and analysis

Through the use of multivariate mathematical approaches such as statistical design of experiments, response surface methodologies, process simulation and pattern recognition tools in conjunction with knowledge management systems, a scientific understanding of the relevant multi-factorial relationships between product and process can be achieved. Data processing and chemometrics enable extracting useful information from the complex instrumental and other data streams to enhance process understanding and enable the development of deterministic models for process control [16, 17].

- Process analyzers

Process analysis by performing univariate process measurements (e.g., pressure, temperature and pH) has evolved towards the non-destructive measurements of chemical, physical and biological

material attributes by novel process analyzers. The measurement position of these analyzers relative to the manufacturing process can be categorized as followed (Figure 3.2):

- *in-line*: the sample interface is located in the process stream (invasive or non-invasive), and product information is derived without removing sample from the process
- *on-line*: the sample is diverted from the process via a sampling loop, to the measurement equipment and may be returned to the process stream
- *at-line*: the sample is removed from the process and analyzed in close proximity to the process equipment, within the timescale of manufacturing

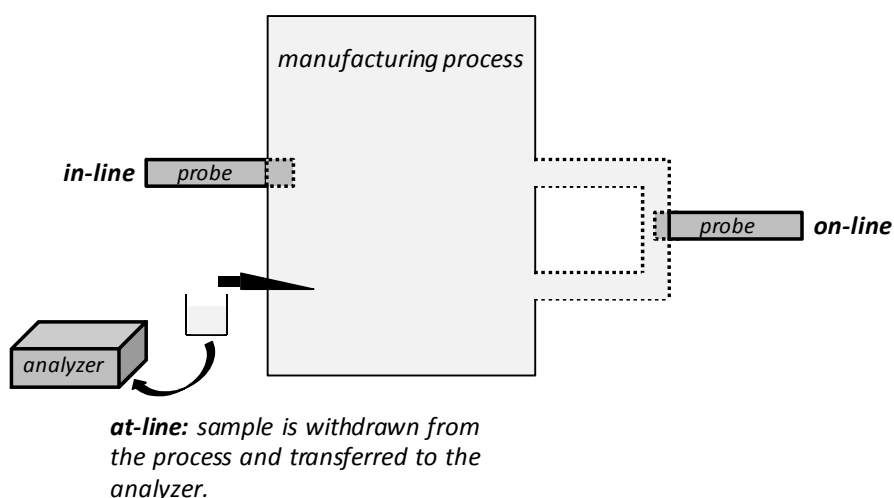


Figure 3.2. Illustrating the difference between in-line, on-line and at-line product measurements during manufacturing.

An at-line application may involve errors related to the sampling and is more time-consuming than the in-line and on-line techniques. Although in-line measurements are quickest in providing product information, the process interfacing is a common pitfall when developing an in-line PAT approach [18]. The location of the in-line probe, its angle of insertion and penetration depth requires extensive investigation to assure a superior measurement performance with minimal impact on the process. Various mechanical interface designs have to be evaluated and modifications to the process equipment have to be considered.

- Process control tools

By use of process monitoring and control strategies, the state of a process can be monitored and actively manipulated to maintain the desired state. In that way, the consistent quality of the output materials and the final product can be ensured (Figure 3.1). Hence, the success (or failure) of PAT not only depends upon the process fingerprints obtained by the real-time process analyzers, but also

on the development of a theoretical or empirical process model that adequately describes the processes occurring within the unit operation [19].

- Continuous improvement and knowledge management tools

The continuous data collection and analysis over the life cycle of a product contribute to the continuous learning about the product and justify proposals for post-approval changes.

The type and function of PAT tools may vary during the lifespan of a product or process [20]. The methods applied during the initial development phases allow defining and understanding the process design space and its relationship to the product quality attributes. In addition, the most efficient and robust operating conditions to produce high quality products are identified (process optimization). During scale-up, further process knowledge is provided by the process analytics, and the process data obtained during initial development are compared to the pilot plant or full-scale data. The process analytics applied during full commercial manufacturing allow process monitoring and control to maintain process robustness and/or reduce process variability. The practical implementation aspects with regard to safety, reliability, validation and maintenance also have to be considered at this stage.

3.2. MEASUREMENT PRINCIPLES OF THE APPLIED PROCESS ANALYZERS

In this thesis, several process analyzers were applied during two wet granulation techniques (i.e., fluidized bed granulation and extrusion-spheronization, Chapter 2), capturing the granule product information in real-time. In the following sections, the measurement principles and characteristics of these PAT sensors are discussed.

3.2.1. Spatial filter velocimetry

The Parsum IPP 70 probe (Gesellschaft für Partikel-, Strömungs- und Umweltmesstechnik, Chemnitz, Germany) uses the established principle of spatial filter velocimetry (SFV) to simultaneously measure the velocity and size of individual moving particles [21-23]. Figure 3.3 schematically displays the Parsum probe design.

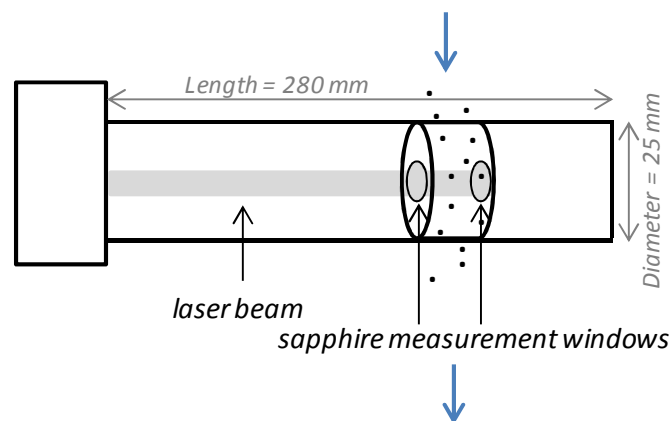


Figure 3.3. Schematic of the Parsum probe design and its components. The blue arrows indicate the direction of particle movement through the measurement zone.

The Parsum probe is equipped with a measurement zone inside the probe comprised of two sapphire measurement windows (Figure 3.3). During SFV measurements, a laser light travels through the probe, and particles passing through the measurement zone block the light received by the detector array (Figure 3.4). In that way, a burst signal is generated, and the frequency of this signal (f_0) is measured by photo detectors. Its value is proportional to the particle velocity v_p :

$$v_p = f_0 * g \quad (3.1)$$

with g the spatial filter constant, corresponding to the distance between each detector (Figure 3.4). Knowing the spatial filter constant, the particle velocity can be calculated.

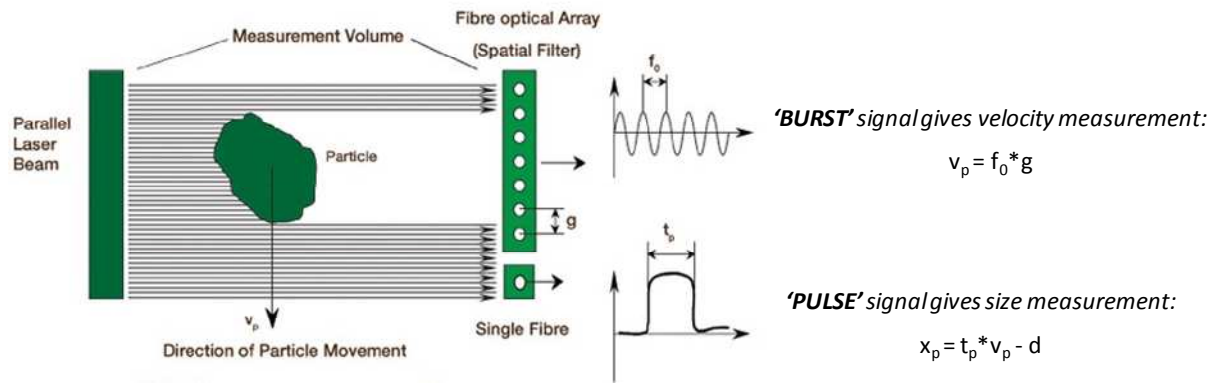


Figure 3.4. The measurement principle of spatial filter velocimetry [24].

Determination of the particle size is based on a secondary pulse (i.e., pulse signal), which is generated by a single optical fiber when the particle passes through the laser beam (Figure 3.4). The size of the moving particle (x_p) is calculated using the time of the pulse signal (t_p) and the velocity of the particle (v_p):

$$x_p = t_p * v_p - d \quad (3.2)$$

with d the diameter of the optical fiber.

The x_p value in Eq. 3.2 depends upon the shape and the trajectory of the particle when crossing the laser beam (Figure 3.5). Therefore, the size value measured by the SFV principle represents a particle chord length, which is defined as the straight line between any two points on the edge of a particle. The chord length can be measured anywhere on the particle, from every aspect.

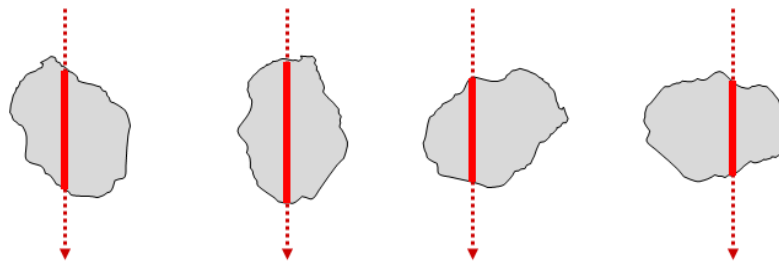


Figure 3.5. Depending on the trajectory, size and shape of the particle, different chord lengths are calculated.

The SFV data captured from individual particles are accumulated in a circular buffer, resulting in the calculation of chord length (and velocity) distributions. The total number of measured particles is kept constant in this circular buffer, providing a continuously updated particle size distribution through replacement of the oldest measured sizes by the newest values. A low (number of particles in the) particle buffer results in more volatile size results, while a larger ring buffer creates a smoothing of the measured size. Size parameters derived from the chord length distribution (e.g., D_{10} , D_{50} , D_{90}) can be correlated against the size data from other particle size analyzers, keeping in

mind that the SFV technique does not assume the particles to be spherical. The SFV technique provides both volumetric and linear number size distributions.

The Parsum IPP70 probe (Figure 3.6, left) is compact, yet robust, constructed from stainless steel, requires no calibration and can be installed directly in a process line to provide continuous particle size and velocity measurements. A range of accessories (Figure 3.6, right) is available to extend the probe's application to difficult process measurement conditions (e.g., greasy and sticky materials). The accessories can be installed in the measurement zone (clip-in cells), protecting the optical windows and adapting the probe for different particle flows. In addition, in the IPP 70-S system, a compressed air connection ensures a constant air blowing in front of the measurement windows, and dilution of sample flow when particle loading is too high. The system is suitable for size measurements in the particle size range of 50 μm – 6000 μm and the particle velocity range of 0.01 m/s – 50 m/s with a data rate up to 20000 particles/s.



Figure 3.6. Picture of the Parsum probe (left) and the clip-in cells (right, top-view).

3.2.2. Photometric stereo imaging

The FlashSizer 3D imaging unit (FS3D, Intelligent Pharmaceuticals Ltd., Finland) consists of a monochrome CCD camera connected to a metal cuvette with a glass window and a computer [25, 26]. A variant of photometric stereo [27] with two white light sources, placed 180° from each other in a horizontal plane and an illumination angle of 30°, is used to create a 3D surface of the measured sample (Figure 3.7).

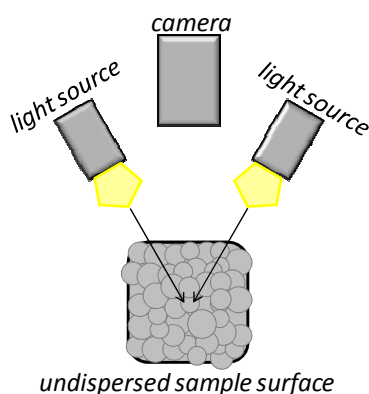


Figure 3.7. Schematic presentation of the photometric stereo imaging setup.

During measurement, the particle sample is presented to the imaging instrument's glass window, and the undispersed sample is illuminated by the two light sources. The viewing direction of the camera is kept constant, but the direction of the incident illumination is varied. In that way, two digital images are captured during each measurement (Figure 3.8, left). The resulting gradient fields obtained with this setup contain direct information about surface normal in xz plane and indirect information about surface normal in yz plane. By line integration in the horizontal direction, a 3D surface is obtained (Figure 3.8, right). Peaks on the 3D surface are assumed to be particles, and by use of the peaks' area in the xy direction, the volume based particle size (V) is calculated:

$$d = \sqrt{a} * c \quad (3.3)$$

$$V = d^3 \quad (3.4)$$

with d the particle diameter, a the area of the peaks and c the calibration constant.

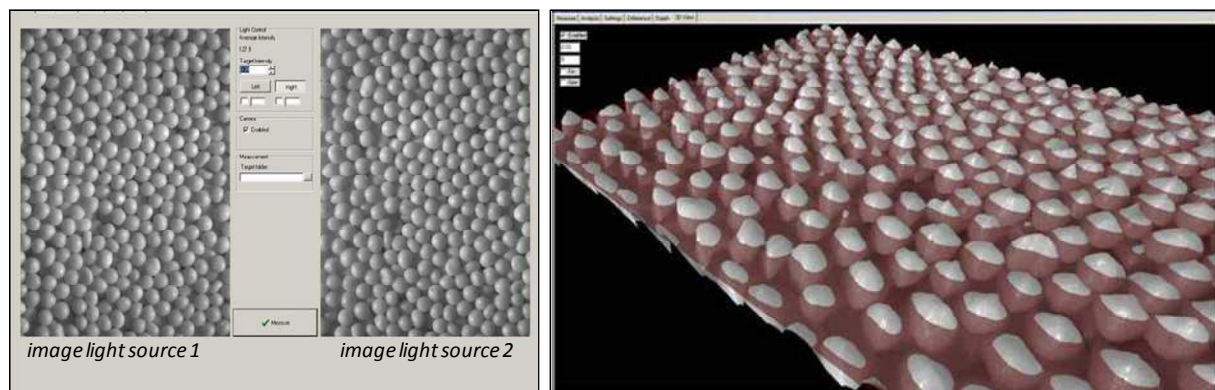


Figure 3.8. Example of the photometric stereo image acquisition (left) and 3D visualization (right).

In addition to the particle size distribution (expressed as sieve distributions and size percentiles), 2D images and brightness values are derived from a single FS3D measurement. The grey scale values in the digital images of sample surfaces correspond to the brightness of the surfaces and are characterized by a number in the range from 0 – 255, where 0 is totally black and 255 is completely white. Calculation of the particle surface brightness index is based on differences in these grey scale values.

In-process FS3D measurements can only be accomplished through a suitable window, and the particles have to be static for the duration of the measurement in order to capture the FS3D images. The non-invasiveness of the technique eliminates the problems associated with going inside the process, but a suitable process interfacing of the measurement equipment has to be designed. The FS3D imaging system used in this thesis exhibited a pixel resolution of 10 μm and image area dimensions of 1.2 x 1.6 cm. The system was calibrated to measure sizes up to 5000 μm .

3.2.3. Focused beam reflectance measurement

Similar to the SFV technique, the focused beam reflectance measurement technology (FBRM, Mettler Toledo, USA) is a laser based technique that provides in-process characterization of particles [28]. A beam of monochromatic laser light is sent through the FBRM probe, and by use of a set of lenses the laser light is focused to a small spot (Figure 3.9). This focal spot needs to be carefully calibrated to have a position at the interface between the probe window and the moving particles. Through rotation of the probe optics at a high speed, the focused laser beam scans in a circular path across the moving particles in front of the measurement window (located at the probe tip). When the focused beam hits a particle, the laser light is backscattered and propagated through the probe. The duration of each pulse of backscattered light is multiplied by the (known) scan speed to calculate the particle chord length. The scan speed of the FBRM technique can be varied between 2 m/s and 8 m/s, enabling the measurement of thousands of chord lengths each second. The resulting FBRM chord length distributions are based on the chord length measurements of individual particles, collected within a pre-selected measurement time.

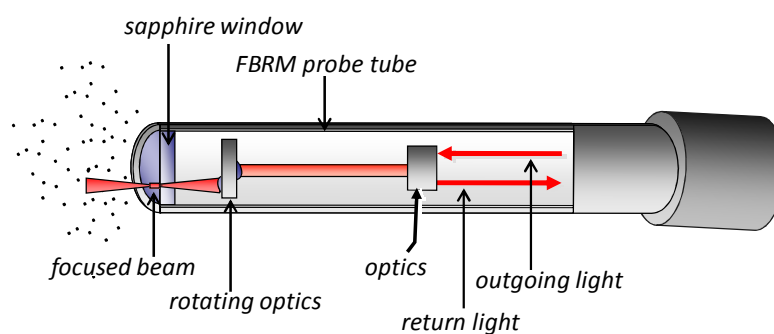


Figure 3.9. Schematic of the FBRM probe design and its key internal components (length = 400 mm, diameter = 34.2 mm).

Unlike the output from SFV measurements, the FBRM software does not transform the measured chord lengths into well-known volume or number distributions, but provides the measured raw chord length distributions. Correlations between FBRM chord length distributions and size data from other, off-line size analyzers such as laser diffraction and sieving have been reported for granulation processes [29]. The goodness of the correlation typically depends upon [30]:

- the particle shape: laser diffraction assumes the particles to be spherical, whereas FBRM does not
- fines in the presence of more coarse particles: FBRM is sensitive to fines, whereas laser diffraction and sieving are not

The FBRM technique requires no calibration and the probe can be installed directly in a process line to continuously provide particle size measurements. The originally designed probe was sensitive to window fouling by the moist product mass during granulation [31, 32]. Recently, the FBRM C35 probe has been commercialized, which is equipped with a mechanical scraper (wiper) on the measurement window to clear the optical window at a pre-defined time interval. The system is suitable for size measurements in the particle size range of 3 μm – 3000 μm .

3.2.4. Near infrared spectroscopy

Near infrared (NIR) spectroscopy studies the absorption of electromagnetic radiation in the NIR region, which is according to the American Society of Testing and Materials defined as the wavelength range 780 – 2526 nm (corresponding to the wavenumber range 12820 – 3959 cm^{-1}) [33]. All the NIR absorption bands result from overtones or combination bands of the fundamental mid-infrared vibrations.

During NIR measurements, samples are irradiated by NIR light. Some of this NIR light is absorbed by the molecules, bringing them to a higher vibrational state (Figure 3.10).

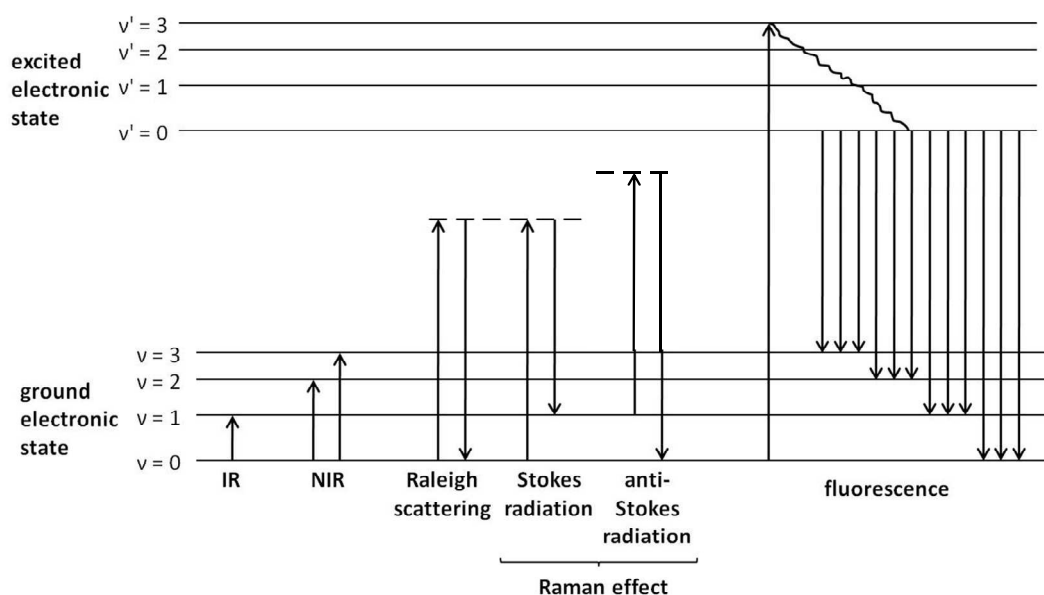


Figure 3.10. Schematic overview of the energy level transitions associated with IR and NIR absorption, the Raman effect and fluorescence.

Only vibrations associated with changes in molecule dipole moment can absorb NIR radiation. A dipole is the product of charge (positive and negative) and distance. Figure 3.11a shows that there is no change in dipole moment during the stretch vibration of an X_2 molecule, while for the stretch vibration of an XY molecule (Figure 3.11b) this is not the case. Hence, diatomic molecules require a permanent dipole to be NIR active, while polyatomic molecules only require a dipole induced by the

vibration. Therefore, H_2 does not absorb NIR radiation while O-H, N-H, C-H and S-H bonds are strong NIR absorbers. Molecules that absorb NIR energy vibrate in two modes: stretching and bending. Stretching is defined as a continuous change in the interatomic distance along the axis of the bond between two atoms. Bending corresponds to a change in bond angle.

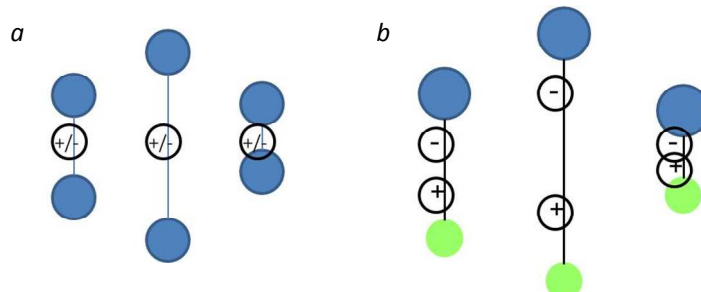


Figure 3.11. Schematic of the possible changes in dipole moment during the stretch vibration of an X_2 (a) and XY (b) molecule, respectively.

Figure 3.12a shows three possible vibration states of a diatomic molecule. The potential energy of these vibrations is dependent on the bond length as can be seen in Figure 3.12b, representing an anharmonic vibration model. At equilibrium, the potential energy is low. Bringing the atoms closer to each other induces repulsion, resulting in an increase in potential energy. Pulling the atoms away from each other leads in first instance to attraction, resulting in an increased potential energy. Further displacement of the atoms will result in dissociation. However, derived from quantum theory, only some vibrational energy levels are allowed, represented by the horizontal lines in Figure 3.12b. These energy levels are not equidistant in an anharmonic model.

An NIR spectrum contains overtones and combinations of the fundamental mid-infrared bands. The overtones occur at about two and three times the frequency of the fundamental vibration, with a decreasing absorption intensity as overtones increase. Combination bands are the sum of several fundamentals from different vibrations. Combination bands are typically situated at lower energies than overtones.

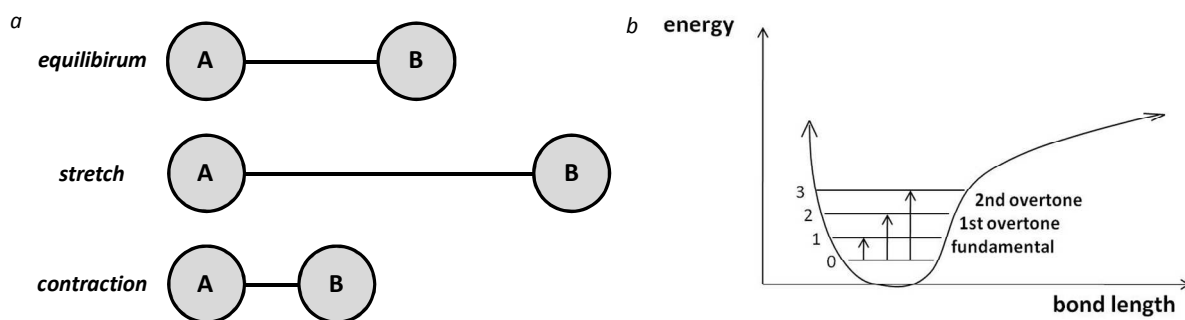


Figure 3.12. Vibration states of a diatomic molecule (a) and the energy levels according to the anharmonic vibration model (b).

The NIR absorption bands in an NIR spectrum are typically broad, overlapping and weaker than the corresponding fundamental mid-infrared absorptions. Therefore, chemometric data processing is always applied to relate the NIR spectral information to sample properties. Due to the dual dependence of the NIR signal on the chemical as well as the physical sample properties (resulting from absorption and scatter effects), a large extent of analyte information can be derived from one single NIR measurement. On the other hand, if one is not interested in the physical sample properties, the scatter effects in the NIR spectra may interfere the detection of the target compound. Therefore, spectral pretreatment before chemometric analysis is often desired to reduce the effect of interfering variance in which one is not interested, thereby increasing the variance due to the parameters of interest [34].

NIR spectroscopy enables a rapid sample measurement (order of seconds), at a relative low cost and is non-destructive. An NIR process analyzer, intended for real-time in-line or on-line process measurements, is equipped with fiber optics to transfer the NIR light and perform NIR measurements away from the operator. In addition, specially designed probes enable a straightforward process interface.

3.2.5. Raman spectroscopy

The Raman effect was theoretically predicted by Smekal [35] in 1923 and observed for the first time by Raman and Krishnan in 1928 [36]. The Raman effect is the inelastic scattering of electromagnetic radiation as a result of the energy exchange between the incident radiation and molecular vibrations [37].

During Raman measurements, samples are irradiated with monochromatic laser light. Typically, lasers producing light in the visible (e.g. 532 nm) or near infrared (e.g. 785 nm and 1064 nm) region are used. The energy of this light is too high to bring molecules to a higher vibrational state (Figure 3.10). Most of the incident radiation is elastic scattered by the sample molecules at the same frequency (= energy), which results into the so-called Rayleigh radiation. Only 10^{-8} is inelastic scattered by the sample molecules, resulting from an energy exchange between the incident light and the sample. This inelastic scattering is called the Raman effect. The inelastic scattered radiation can have a lower energy (lower frequency) than the incident radiation or a higher energy (higher frequency) than the incident radiation. The former type of inelastic scattering is called Stokes radiation, the latter anti-Stokes radiation (Figure 3.10). The shift in energy (or wavelength) between the incident light and the Stokes or anti-Stokes scattering provides information about the vibrational states of the measured molecule. The intensity of both inelastic scattering processes is proportional to the number of molecules that can undergo the processes. Hence, at room temperature mainly

Stokes radiation will occur, while at high temperatures (e.g., 500 °C) many sample molecules are already in a higher vibrational state as can be derived from the Boltzmann distribution, hence favoring anti-Stokes radiation. Therefore, the Stokes radiation is more common used in Raman spectroscopy since its intensity is usually higher than the anti-Stokes intensity at most operating conditions.

Molecules are Raman active if a change in molecule's polarizability occurs upon excitation. The polarizability of a molecule is the ease with which the electron cloud of a molecule can be distorted after bringing the molecule in an electromagnetic field (i.e., by light irradiation) [38]. In the different selection rules for Raman and NIR activity (change in polarizability and change in dipole moment, respectively) lies the complementarity of these two molecular vibrational spectroscopic techniques. Molecules producing good signals in NIR spectra might produce weak signals in Raman spectra and vice versa. Figure 3.11a showed that the stretch vibration of H₂ is NIR inactive due to the absence of a change in dipole moment. However, the larger the bond distance, the further the electrons are apart from the nuclei and thus the easier they can be moved. This change in ease with which the electron cloud of a molecule can be distorted (i.e.; change in polarizability) is needed for Raman activity and therefore the stretch vibration of H₂ is Raman active.

A Raman spectrum displays the intensity of the scattered radiation versus the frequency difference between the incident radiation and the scattered radiation, expressed as wavenumbers. Plačzek developed the following equation to express the intensity of Raman scattering, I_R :

$$I_R = \frac{2^4 \pi^3}{45 * 3^2 * c^4} \frac{h I_L N (v_0 - v)^4}{\mu v [1 - e^{(-hv/kT)}]} [45(\alpha'_a)^2 + 7(\gamma'_a)^2] \quad (3.5)$$

where: c is the speed of light

h is Planck's constant

I_L is the intensity of the incident light

N is the number of light scattering molecules

v_0 is the frequency of the incident light (Hz)

v is the vibration frequency of the molecule (Hz)

μ is the reduced mass of the vibrating atoms

k is the Boltzmann's constant

T is the temperature (K)

α'_a is the mean value invariant of the polarizability tensor

γ'_a is the anisotropy invariant of the polarizability tensor.

Eq. 3.5 shows that the intensity of the scattered light is proportional to the number of molecules N (enables quantitative analysis), the intensity of the incident laser light I_L and $(\nu_0 - \nu)^4$. Therefore, a higher laser intensity and a higher laser frequency enhance the intensity of the Raman scattering. Besides these parameters, the Raman intensity is also determined by instrumental (e.g., detector, length of glass fiber when using probes, etc.) and sample (e.g., sampling volume, sample particle size, refractive index of sample, etc.) parameters. Furthermore, as scattering occurs in all directions, only a fraction is detected. When probes are implemented into process streams, only the light which is scattered into the same direction as where the incident light originated from is measured.

As the Raman effect is inherently weak, other phenomena such as light absorption and fluorescence can interfere strongly. Moreover, heating, photodecomposition and laser ablation can occur. The incident laser light can be absorbed when the wavelength of the laser light corresponds to an absorption band in the spectrum of the molecule, resulting in the transition of the molecule to the excited state. Depending on the laser wavelength, a transition to the excited vibrational or electronic state can occur. The absorbed energy is then transformed via radiation-less transitions into thermal energy. This absorption interferes with the Raman effect as the intensity of Raman scattering is proportional to the intensity of the laser light (Eq. 3.5). Light absorption can be avoided by use of another wavelength laser. Fluorescence can produce substantial interferences in Raman spectra when the molecule is excited to an electronic excited state. The molecule decays to a lower energy level by a radiation-less transition (the vibrational ground state in the electronic excited state), followed by the decay to the electronic ground state (Figure 3.10). During this last decay, fluorescent radiation is emitted, interfering with the Raman signal. Interference by fluorescence can be avoided employing lasers with other (longer) wavelengths to make sure that no excitation to the electronic excited state occurs.

As the intensity of the Raman signal is proportional to the intensity of the laser light, it is favorable to use as high as possible laser intensities. However, destructive effects can occur by a high energy supply. Absorption of the radiation with insufficient energy transfer to the surroundings, results into sample heating (and possibly destruction). Laser ablation is a phenomenon where material is removed from the sample. When the energy added to the sample per time unit is larger than the bond energy and when the energy is dissipated, ablation occurs resulting in a crater [37].

Raman spectroscopy enables to perform rapid and non-destructive measurements without the need for sample preparations. Probes can be coupled to the spectrometer by fiber optic cables and implemented directly into the process stream (with the proper interfacing). A Raman spectrum contains both qualitative and quantitative chemical and physical information. Unlike NIR spectra

that mainly exhibit broad, overlapping peaks of O-H, N-H, C-H and S-H vibrations, Raman spectra consist of distinctive peaks that can be assigned to functional groups and are easier to interpret.

3.3. LITERATURE OVERVIEW OF THE PROCESS ANALYZERS APPLIED IN FLUIDIZED BED GRANULATION

The detection of granule growth during fluidized bed granulation and the process endpoint is traditionally based on the measurement of process parameters (Chapter 2). However, these are considered as indirect measurements as the parameter values are correlated with the granule properties. At times, these methods are inadequate since they do not account for changes in feed material properties or external disturbances. The completion of a granulation process after a fixed time period may then cause over- or under-drying of the granules and reduce the batch quality. Through the development of innovative analysis tools that rapidly provide information related to the physical or chemical material properties, granulation process monitoring and control has incorporated the direct measurement of granule characteristics. These techniques enhance the collected granulation information and enable to determine the granulation endpoint by the achievement of desired granule attributes. The techniques are non-destructive, provide a short measurement time and allow various measurement set-ups (Figure 3.2).

The moisture level of the fluid bed is mostly determined by the rates of binder addition and binder evaporation, which need to be well balanced in order to obtain proper fluidization and high-quality granules [39]. Hence, the first granule product measurements during processing consisted of in-line moisture determinations using an infrared moisture sensor, to strictly control the bed moisture level during granulation and drying [40-42]. Table 3.1 summarizes the most frequently studied analytical process sensors in fluid bed granulation, the real-time captured granule information and the challenges encountered during their application. This will be more extensively discussed in the following sections.

Table 3.1. Overview of the most frequently studied analytical process sensors in fluid bed granulation, the captured granule information and the challenges encountered during their application.

Technique	In-line measured granule property during fluid bed granulation	Challenges
NIR spectroscopy	moisture content	Fouling of the measurement window during invasive measurements.
	solid-state	Fouling of the measurement window during invasive measurements.
	size	Fouling of the measurement window during invasive measurements and extraction of relevant information from the collected spectra.
	bulk density	Fouling of the measurement window during invasive measurements and extraction of relevant information from the collected spectra.
image analysis	size size distribution shape	Adequate presentation of granules to the measurement equipment and data handling.
FBRM	chord length (distribution)	Fouling of the measurement window. The FBRM probe should be installed at a height that is not influenced by size segregation during fluidization. The technique measures chord lengths and therefore a comparison of the FBRM size data with size results from conventional sizing techniques is often desired.
SFV	chord length (distribution)	The SFV probe should be installed at a height that is not influenced by size segregation during fluidization. The technique measures chord lengths and therefore a comparison of the SFV size data with size results from conventional sizing techniques is often desired.
acoustic emission	moisture content size (fluidization)	Extraction of relevant information from the collected signals.
Raman spectroscopy	solid-state	Fouling of the measurement window during invasive measurements.

To a lesser extent, triboelectric probes [43-45], microwave resonance technology [46, 47] and electrical capacitance tomography [48] have also been investigated as potential real-time analyzers in fluidized beds. The effectiveness of each of these methods to accurately determine the moisture content during fluid bed drying was examined and the main results are summarized in Table 3.2.

Table 3.2. Application of triboelectric probes, microwave resonance technology and electrical capacitance tomography during fluid bed drying.

Technique	Main results	Reference
triboelectric probes	Reliable granule moisture measurement with triboelectric probes during fluid bed drying (Karl Fischer as reference).	[43, 44]
	Use of triboelectric probes to qualitatively monitor fluid bed drying and examine the effect of vibration on drying.	[45]
microwave resonance technology (MRT)	Good correlations between granule water content determined by MRT and reference methods (i.e., loss on drying and Karl Fischer) during fluid bed drying.	[46]
	Time saving in the drying process through real-time monitoring of water content by MRT.	
electrical capacitance tomography (ECT)	Increase of process knowledge by combining MRT with multivariate data analysis techniques, applied to an industrial scale granulator.	[47]
	Use of ECT to measure granule moisture during fluid bed drying. Development of a feedback control strategy based on ECT measurements to improve process efficiency and product quality.	[48]

3.3.1. Near infrared spectroscopy

Frake et al. [49] installed an NIR probe into the product bed of a top-spray fluid bed granulator, continuously collecting granule information. The probe was positioned in the downward flow at a point of high product density. The second derivative absorbance changes at 1932 nm were calibrated against moisture content data and an acceptable standard error of calibration for the required level of control was calculated. Changes in zero order absorbance across the entire spectrum as granulation proceeded, resulted from the variation in granule size. Plotting the absorbance of a single wavelength versus process time showed the gradual increase in granule size, but it was not possible to generate suitable granule size calibration models for quantitative determination.

Rantanen et al. [50, 51] applied a novel NIR reflectance spectroscopic method during fluid bed granulation and drying, detecting four wavelengths simultaneously and using three of them for the measurement of moisture content. The 1990 nm characteristic combination band was used for water detection and the 1740 nm and 2145 nm signals for baseline correction. Critical to the in-line

measurements was the sight glass, which was continuously blown with heated supplied air. The results showed that the entire NIR spectrum was not necessary for the measurement of water. By use of only a few NIR wavelengths around the NIR water band, reliable and rapid detection of moisture was possible throughout the entire granulation process. Combining NIR information with trend charts of the temperature difference between process inlet air and granules, and the water content of process air enabled the identification of different process phases, characteristic for different formulations [52]. This provided a novel tool for the monitoring and control of water during fluid bed granulation. The method was further investigated by studying the effect of binder choice and particle size on the accuracy of NIR moisture measurement [53]. Principal component analysis (PCA) proved a promising tool in the reduction of the high-dimensionality of granulation process data (e.g., granule and air temperature, humidity, NIR signal, etc.) [54]. By use of this multivariate data analysis technique, the granulation process was described in a 2-dimensional space where the three process phases (i.e., mixing, spraying and drying) were clearly visible. As the NIR moisture measurement is affected by the varying physical properties of the granules (e.g., temperature, particle size, bulk density), the process-related variables describing the state of granulation were included in NIR moisture calibration models [55]. This approach improved the models' prediction capability. Multivariate calibration of in-line collected NIR spectra and process parameters was performed using two techniques. The artificial neural network (ANN) model with back-propagation algorithm showed the most predictive power of the independent test data, compared to the partial least squares (PLS) model. The NIR setup was also successfully applied for particle size measurement of various grades of microcrystalline cellulose during fluidization, using two of the four simultaneously detected wavelengths [56]. Different inlet airflow rates did not significantly influence the recorded absorbances.

Also Räsänen et al. [57] used only three NIR wavelengths to determine the moisture content by in-line NIR spectroscopy. The authors were able to study the dehydration behavior of theophylline granules using a novel multi-chamber micro-scale fluid bed dryer with a process air control unit and in-line NIR spectroscopy. The stepwise dehydration of materials was monitored by the water content difference of inlet and outlet air, the pressure difference over the bed and in-line NIR spectroscopy.

Morris et al. [58] introduced a fast-drying method to accelerate fluid bed drying by use of NIR and temperature probes. NIR spectra collection was accomplished with an MM55 gauge, continuously monitoring the bed externally, through a lower inspection window. The strategy involved the identification of critical NIR readings corresponding to the end of evaporative cooling (Chapter 2) and using this as a temperature-independent endpoint. The authors showed that no physical changes of compounds occurred during the evaporative cooling stage of drying at an inlet air temperature above

the melting point of a low-melting compound. Hence, using real-time and non-invasive NIR measurements, the drying cycle of a low-melting active ingredient was optimized by reducing the overall drying time. This work was extended by Wildfong et al. [59], who examined the effectiveness of the method using different formulations. A simple computer program was developed to predict the expected drying time reduction and therefore determine any benefit associated with the use of accelerated drying before changing the current process.

Findlay et al. [60] used NIR spectroscopy to simultaneously monitor moisture content and particle size in a fluid bed granulator and determine its endpoint. Spectra were collected with an MM55+ NIR gauge through a glass window into the bed of the granulator. The window was fitted with a special gasket to reduce fouling. In practice, the NIR measurements during the early stages of granulation were not as accurate as measurements performed later in the process since the glass window became partially fouled by powder during the first 10 min of granulation. The NIR determined moisture content and particle size correlated well with off-line reference measurements (i.e., loss on drying and image analysis). However, it was necessary to correct the particle size measurements (due to moisture) when the moisture content of the material was greater than 3% w/w. Using the developed system, fluid bed granulation can be controlled by determining when binder addition should be stopped (desired particle size) and when granule drying is completed (desired moisture content). Nieuwmeyer et al. [61] also applied NIR spectroscopy to simultaneously determine granule water content and size. High shear manufactured granules were dried in an Aeromatic fluid bed dryer (Niro), with the NIR probe placed into the wall of the dryer, at the same height of the sampling probe. The PLS granule moisture model predicted residual water content continuously during drying with errors comparable to the reference method (i.e., Karl Fischer), whereas the PLS granule size model was influenced by the humidity of the granules (as observed by Findlay et al.). After removal of the interfering moisture through initial drying, the NIR granule size model can be used to monitor granule size and attrition effects.

Hartung et al. [62] monitored the fluid bed granulation of an Enalapril formulation by means of in-line NIR spectroscopy with the NIR probe installed in the product container. The moisture content profiles of several granulation batches, derived from an NIR moisture PLS model (Karl Fischer as reference), enabled to examine how granulation influences tableting properties. Results showed that the tablet characteristics not only depended on the residual moisture content of the granules, but also on the moisture profiles during the entire fluid bed granulation process.

NIR spectroscopy was applied non-invasively to monitor fluid bed granulation on an industrial scale (Glatt WSG300) [63]. Spectra of continuously moving samples were acquired by attaching the NIR

optical probe to the glass window (without interfering the process or formulation). PLS calibration models were developed to predict granule moisture content, size distribution and bulk density using the on-line recorded NIR spectra. By principal component analysis of the NIR spectra, each step of the granulation process was identified and monitored. An NIR method for in-line determination of the fluidized bed drying endpoint based on moisture content prediction was developed and analytically validated on commercial scale (300-L) of an approved solid dosage product [64]. An interface/adaptor plate was manufactured to insert the NIR probe into the fluid bed. To demonstrate the applicability of the NIR model, validation was performed following the ICHQ2 (r1) guidelines. However, the in-process method was developed and validated exclusively with in-line samples which necessitated a customized interpretation of these guidelines.

An in-depth investigation on the NIR moisture prediction accuracy with regard to sampling effects was presented by Green et al. [65]. Granulations were performed at three different drying scales (65-L, 300-L and 600-L) and NIR spectra of both dynamic, flowing and stationary solids were collected through insertion of the probe directly into the vessel. The authors demonstrated that process heterogeneity played a major role in determination of apparent prediction accuracy. Mattes and co-workers [66] also recorded NIR spectra of static granules by use of an NIR probe that was equipped with a collection spoon and purge vents on the probe tip. Following each NIR spectrum collection during the fluid bed granulation process, software sent a data-complete-signal that initiated an air purge, cleaning the spoon for a new sample.

Fouling of the measurement window by the moist mass challenges the reliable collection of NIR spectra during fluid bed granulation. Solutions generally involve the use of an air supply system and specialized interfacing. Once a suitable interfacing is found, acceptable prediction of granule moisture content is achieved throughout the granulation process and real-time end point detection of the drying phase (based on residual granule moisture content) is possible. Several studies showed that combining the NIR moisture information with the traditionally collected process parameters increased granulation information, improved the predictability of models and contributed to the process optimization. The use of NIR spectroscopy has not been restricted to R&D scale. A few studies already reported the application of NIR spectroscopy as moisture determination technique on a larger commercial scale showing that the technique allows real-time control of the process, leading to a reduced operation time and an improved consistency of the granule product. Deriving accurate particle size information from in-line collected NIR spectra of fluidizing granules is more challenging and requires further research.

3.3.2. Image analysis

In addition to NIR spectroscopy, image-processing was one of the earliest techniques applied during fluid bed granulation to directly measure granule characteristics. Information regarding the physical granule properties (e.g., granule size, size distribution, shape) is retrieved from the images, which requires a large extent of computational processing. Therefore, imaging devices are usually equipped with powerful computers to handle the data.

The early work of Tanino et al. [67] capturing granules on adhesive tape located on the side wall of the container and taking images with a CCD camera, was followed by a series of papers by Watano and co-workers [68-71]. Watano and Miyanami [68] developed an on-line image-processing system consisting of a CCD camera, optical fibers, a telephoto lens and an air purge unit. The imaging probe was attached to the upper sidewall of the container enabling on-line monitoring of granule growth in an agitation fluidized bed granulator. By use of heated purge air, powder adhesion onto the measurement window was prevented. Extensive preprocessing and image processing was necessary before determining granule size distribution, median diameter (Feret diameter) and shape factors (circularity and aspect ratio). As the image-derived granule size distribution is number-based, transformation into a mass-based distribution was performed to compare image results with conventional sieve analysis. A close agreement between both sizing methods was obtained. Plotting the shape factors in function of granulation time showed that granules became more spherical in the progress of granulation. The median granule diameter value was influenced by the position of the imaging probe due to particle segregation in the fluid bed granulator when low fluidizing air velocities were used [70]. It was concluded that when measuring a broad particle size distribution, the imaging sensor should be placed in the lowest position (closest to the air distributor) or the air velocity should be large. Sensor location should not be considered when measuring granule shape factors. The authors also developed an automated fluid bed control system by use of the image-processing unit and a control algorithm based on fuzzy logic [69]. The developed system was able to control granule growth with high accuracy, under various operating conditions (i.e., agitator rotational speed) and powder sample properties (mass ratio of lactose in starting material).

Whereas traditional imaging studies process 2D black-and-white pictures, a novel 3D imaging method (SAY-3D) was introduced by Närvänen et al. [72] to determine the particle size of granules both off-line and on-line in a fluid bed granulator. The imaging apparatus (i.e., camera, cuvette and Red-Green-Blue leds) was attached 13 cm above the granulator distributor plate for on-line measurements. Samples were collected into the cuvette, images were taken and a pulsed air

pressure returned the sample to the process between images. The described method seemed promising, and limitations and further method development are discussed.

Laitinen et al. [73, 74] developed a photometric concept to calculate the particle size from undispersed powder surfaces under controlled illumination conditions. The photometric approach allowed at-line monitoring of granule growth kinetics in a fluidized bed granulator [75]. Image information of endpoint samples was evaluated regarding the prediction of granule tableting behavior. The technique was also employed for on-line monitoring of fluid bed granulation [25]. The cuvette system described in the study of Närvänen et al. [72] was applied to simultaneously measure the granule size distribution by image analysis and the granule moisture content with NIR spectroscopy during the entire batch granulations.

Granule images are usually captured via a suitable window that allows non-invasive data collection and avoids the problems associated with instrument fouling and process disturbances during invasive measurements. However, the process interfacing can be difficult for fluid bed granulation processes where granules are constantly moving at high velocities. Overlaying particles, large size distributions and non-spherical particles challenge the extraction of physical information related to the granule size (distribution) and shape from the captured images. Therefore, extensive image processing and expertise are necessary. The limited work found in literature suggests that the use of image analysis during fluid bed granulation is not easy and still far from the actual application on a commercial scale production.

3.3.3. Focused beam reflectance measurement

The focused beam reflectance measurement instrument is designed to track in real-time any changes to the particle size and its distribution. The technique has already been used to monitor crystallization [76, 77] and flocculation [78, 79], and its application to granulation has received interest over the recent years.

Hu et al. [29] used the FBRM technique to at-line investigate the granule growth kinetics during fluidized bed granulation. As the particles need to move in front of the measurement window to calculate the particle chord length distribution, the FBRM (S400) probe was immersed in a suspension of silicon oil and sampled granules. By rotating a magnetic stir bar, the suspension was gently agitated and granules passing in front of the sapphire probe window were measured. The trends of the chord lengths (e.g., D_{10} , D_{50} , D_{90}) at-line measured by FBRM were identical to those measured by off-line laser diffraction and sieve analysis. The distinctive differences between FBRM and laser diffraction/sieve analysis particle size values were attributed to the different measurement mechanisms.

In-line FBRM (D600) measurements were performed during fluid bed granulation with the probe installed inside the granulator at two different positions [31]. The probe window was located in the center of the distributor plate and both horizontal and sloped (45°) positions of the probe were employed. The latter was preferred as the former was sensitive to window fouling during the spraying phase. Nevertheless, using the sloped position, the FBRM probe window remained fouled with sticky particles during granulation under certain experimental conditions. In addition, noise was present during the first 20 min of each granulation batch, caused by powder particles covering the measurement window due to their high static electrical charge during mixing.

The at-line FBRM application showed that the technique adequately describes the granule growth kinetics, but the fouling observed during in-process measurements impedes the reliability of the FBRM technique as an in-line process analyzer. Adaptations to the probe have been made to solve these fouling issues. The FBRM C35 probe is equipped with a pressurized air activated mechanical scraper on the sapphire measurement window to prevent powder sticking. The effectiveness of the scraper has already been proven in the harsh conditions of a high shear granulator [30]. Once applied in fluid bed granulation, the technique may play a prominent role in the real-time monitoring and control of fluid bed granulation processes.

3.3.4. Spatial filter velocimetry

In addition to FBRM, spatial filter velocimetry is also able to real-time measure the chord length of a moving particle. Both techniques are designed for in-process particle characterization and enable the real-time size measurement of agitated particles and granules during fluid bed granulation. Nevertheless, the techniques differ substantially in probe design and measurement mechanism (see Section 3.2).

Schmidt-Lehr et al. [80] examined optimum installation and software parameters for the SFV probe during fluid bed granulation in a Glatt WSG 5 granulator. The granulation behavior under various experimental conditions was examined using the SFV probe, and SFV measured *D*50 values were compared with laser diffraction sizes. In addition, the reproducibility of measurement results, the transferability of the technique to a larger sized granulator (WSG 15) and the influence of process anomalies on the SFV technique were assessed.

Närvänen et al. [81] obtained granule size information during fluid bed granulation (in a Glatt WSG 5) using an in-line, at-line and off-line experimental setup of the SFV technique. Although in-line and at-line obtained data were susceptible to size segregation, real-time monitoring of the granule growth

was achieved. Sieve analysis of the final granules was performed as a reference and its results correlated well with off-line SFV data.

Multivariate statistical control methods based on SFV measurements were developed by Huang et al. [82] for an Aeromatic fluid bed granulator capable of manufacturing 35 kg batches.

The applications of SFV during fluid bed granulation demonstrate the technique's ability to continuously measure the granule size distribution during processing, without experiencing fouling problems. However, with the in-line application of a sizing technique, one also has to consider the height with which the sensor is installed in the fluid bed, as size results may be influenced by size segregation during fluidization.

3.3.5. Acoustic emission

Particle-particle or particle-chamber collisions and frictions during fluid bed granulation generate vibrations that contain embedded physical and chemical information. These vibrations can be measured by applying acoustic emission (AE) sensors to the fluid bed container. Acoustic emissions are usually measured in the high frequency range (70 - 500 kHz) as they can easily propagate through solid materials but attenuate rapidly in air. Therefore, the interference from background noise generated by mechanical vibrations (e.g., from the fan) is minimized. The resultant acoustic spectra contain information about several process-relevant properties and chemometric techniques such as PCA and PLS are always necessary to extract the desired information and calibrate the acoustic signals [83]. Hence, often the term acoustic chemometrics is applied. The sensors have small dimensions and can be easily mounted onto the (outside of the) granulator, enabling non-invasive measurements of the granulation progress. In addition, acoustic measurements offer real-time response, are relatively inexpensive and can be performed in hazardous process environments without further protection.

Tsujimoto et al. [84] developed and applied an AE sensor to monitor the fluidization conditions in a small-scale agitation fluidized bed granulator. The effects of several operating variables on the mean AE amplitude were examined and results showed that the mean AE amplitudes correlated with the fluidization activity. Halstensen and Esbensen [85] designed a new acoustic chemometric approach, which was later applied in a semi-industrial fluid bed granulator to monitor the granulation process state and product quality [86]. By use of score plots based on acoustic data, the process state and the quality of the product inside the granulator were identified. In that way, the acoustic chemometric approach was more sensitive to the early detection of critical granulation situations (e.g., lump formation leading to process shutdown) than the traditional process data. The feasibility

study showed that acoustic chemometrics can be used to predict fluidization airflow, reflux of fines to the reactor and granule moisture content.

Matero et al. [87] described the results of applying AE during fluid bed granulation in two different case studies, developing separate models for granule size and moisture. By use of multivariate methods, the granule size information hidden in the AE spectra was extracted, despite the contribution of other granule properties to the AE signals. However, accurate granule size prediction was not achieved. The prediction errors were attributed to sieve analysis as a reference technique, which assumes that granules are spherical and form a narrow, normal size distribution in the sieve cut. The granule water content was tracked throughout the granulation process, but the relative humidity of ambient air was crucial in determining granule moisture. The relative humidity induced batch-to-batch variations and influenced the reliability of the model. The authors also used the AE signals acquired in the early phase of granulation to estimate end product size distribution via N-way PLS modeling [88]. The applied multi-way methods provided a deeper understanding of fluidized bed granulation showing for the first time that the AE signals captured during the nucleation phase can be used to predict end product granule size distribution.

The non-invasiveness and inexpensiveness of AE measurements has encouraged its application in fluid bed granulation. The AE signals contain both chemical and physical granule information, but the extraction of the relevant information is not straightforward. Nevertheless, acoustic chemometrics has allowed to monitor granulation process state and product quality, which provided early warnings of critical process situations.

3.3.6. Raman spectroscopy

The application of Raman spectroscopy in fluid bed granulation has contributed to the real-time monitoring and understanding of solid-state transformations. Hausman et al. [89] applied Raman spectroscopy to monitor the drug (i.e., risedronate sodium) hydration state during fluid bed drying. The Raman probe head was inserted into a lab-scale fluid bed granulator through its solution addition port. By use of the collected Raman information, the relationship between drug hydration state and tablets' physical stability was understood. Kogermann et al. [90] were able to quantify the solid-state transformations of carbamazepine granules during drying in a micro-scale multi-chamber fluidized bed dryer by means of in-line Raman spectroscopy and PLS regression. The granule Raman spectra were non-invasively collected through a quartz sight window of the fluid bed granulator.

Walker et al. [91] proposed the novel use of Raman spectroscopy to measure the product composition within the fluid bed in three spatial dimensions and as a function of time. A Raman

probe was positioned above the fluidized bed on a long-travel x-y-z stage. In that way, a 3D mapping of discrete volumes in the fluidized bed within a relatively short time window (120 s) was obtained. This work was extended by shortening the time window of the Raman spectral acquisition to 10 s, allowing the in-situ real-time characterization of a fluidized bed granulation process [92]. Particle density profiles were calculated over granulation time and these indicated how the volume of the fluidized bed decreased with increasing mean granule size. The authors propose the novel use of Raman spectra to represent particle movement in the fluidized bed.

3.3.7. Combining complementary process analyzers

Previous sections demonstrate that numerous reports have been published on the application of individual process analyzers during fluidized bed granulation. A few studies were found to describe the simultaneous implementation of two or more process sensors. Multiple process analyzers, installed at different locations in the granulator may provide complementary granulation information or contribute to the detection of sample heterogeneity during granulation. The selected sensor location must provide accurate granule product information, but may not disturb the granulation mechanisms. Combining several analyzers can increase the understanding of a granulation process and product during initial development stages and scale-up. A selection of these process sensors can be sufficient to monitor and control the process at full production scale, maintaining process robustness and minimizing process variability.

Aaltonen et al. [93] applied in-line NIR and Raman spectroscopy to quantitatively monitor the solid-state conversion of theophylline monohydrate to theophylline anhydrate during fluid bed drying. In that way, drying insight at the molecular level was achieved, which was not possible using the traditional approach (i.e., monitoring the outlet air humidity or the pressure difference over the bed). The micro-scale fluid bed drying chamber was made of glass and modified with a quartz sight window for spectroscopic analysis. The study showed the complementarity of the two spectroscopic techniques as NIR spectroscopy was particularly sensitive to water and Raman spectroscopy to crystal structure changes.

Tok et al. [32] compared the results of three process analyzers simultaneously applied during fluid bed granulation. Acoustic emission sensors were attached onto the external walls of the fluidized bed chamber. An FBRM and NIR probe were inserted into the container and an anti-static spray was applied onto the measurement windows before each run to reduce the coating of fines. The three process analyzers were able to detect the three granulation rate processes (see Chapter 2) with varying degrees of sensitivity. Fouling of the in-line probes' windows and disruption of the AE signals

by the airflow rate and external disturbances (e.g., heavy footsteps), interfered with the continuous measurement of granule properties.

Leskinen et al. [94] applied an AE sensor, a flash topography particle size analyzer and multi-point NIR probes (eight probes) during fluid bed granulation. All instruments were non-invasively installed, with the NIR probes and topographic camera looking through the glass windows of the granulation chamber. Both the topographic camera and AE technique provided size values that were in good agreement with the off-line reference values. In addition, the multi-point NIR and AE method were able to differentiate between mixing, agglomeration and drying.

3.4. LITERATURE OVERVIEW OF THE PROCESS ANALYZERS APPLIED IN EXTRUSION-SPHERONIZATION

The wet granulation step in an extrusion-spheronization process involves the addition of granulation liquid in much greater amounts, compared to those required for conventional granulation [95]. Interactions between the active pharmaceutical ingredient (API) and water may induce phase transformations altering the pharmaceutical and biopharmaceutical performance of the drug. Hence, research on *real-time* monitoring of extrusion-spheronization has mainly focused on the detection of process-induced transformations of the API throughout the different steps of the extrusion-spheronization process.

Sandler et al. [96] investigated the phase transitions in nitrofurantoin and theophylline formulations during pelletization. An at-line PAT approach consisting of Raman spectroscopy, NIR spectroscopy and X-ray powder diffraction (XRPD) was used to increase the understanding of the solid-state behavior of the APIs during pelletization. Samples were collected at the end of dry mixing, wet granulation, extrusion, spheronization and drying. The at-line collected NIR spectra provided real-time data on the state of water in the system. Due to the saturation of the water signal, detection of hydrate formation in the theophylline and nitrofurantoin formulations during granulation, extrusion and spheronization was not possible. Raman and XRPD results on the other hand enabled the identification of pseudopolymorphic changes, indicating the benefits of using complementary process analyzers to gain an enhanced understanding of the process. More recently, Römer et al. [97] applied at-line NIR spectroscopy and XRPD to better understand the process-induced transformations of erythromycin dihydrate during extrusion-spheronization and drying (at 30 °C and 60 °C). During pelletization and drying at 30 °C, no dehydration or phase transformation occurred. Drying at 60 °C induced the partial transformation to the dehydrated form, which was real-time observed by NIR spectroscopy. This work was extended with the application of in-line NIR spectroscopy during miniaturized fluid bed drying of erythromycin dihydrate pellets [98]. The in-line collected NIR spectra together with PCA increased the understanding of the pellets' dehydration phenomena.

Mantanus and co-workers published several papers related to the rapid determination of pellet properties by NIR spectroscopy immediately after processing. An NIR method was developed and validated for the accurate determination of pellet moisture content (between 1% and 8%) [99]. Accuracy profiles were used to demonstrate the suitability of the proposed method, by assessing the NIR method's ability to predict the moisture content of new samples. A similar approach was taken in the development of an NIR method to quantify the active content of non-coated pharmaceutical

pellets [100]. This was further investigated by interfacing a pellet particle stream with an NIR spectrometer and developing an NIR method that is able to determine the API content of moving pellets [101]. Real-time API quantification of pellets directly from the production line by the NIR method was established, which may reduce the post-manufacturing laboratory tests and enable real-time release.

REFERENCES

- [1] L.X. Yu, *Pharmaceutical Research*, 25 (2008) 781-791.
- [2] T. Kourti, *Analytical and Bioanalytical Chemistry*, 384 (2006) 1043-1048.
- [3] R. Guenard, G. Thureau, in: K.A. Bakeev (Ed.), *Process Analytical Technology*, John Wiley & Sons Ltd, United Kingdom, 2010, p. 17-36.
- [4] D. Lively, J. Thompson, (<http://iom.invensys.com>), White Paper, 2010.
- [5] P. Kanneganti, in: D.M. Parikh (Ed.), *Handbook of Pharmaceutical Granulation Technology - Third edition*, Informa Healthcare, New York, 2010, p. 597-616.
- [6] D.C. Hinz, *Analytical and Bioanalytical Chemistry*, 384 (2006) 1036-1042.
- [7] Food and Drug Administration, *Pharmaceutical cGMPs for the 21st century - a risk-based approach*, (2004)
- [8] Food and Drug Administration, *PAT - A framework for innovative pharmaceutical manufacturing and quality assurance*, (2004)
- [9] Food and Drug Administration, *Guidance for Industry; PAT - A framework for innovative pharmaceutical development, manufacturing and quality assurance*, (2004)
- [10] International Conference on Harmonisation, *Pharmaceutical Development Q8*, (2009)
- [11] International Conference on Harmonisation, *Quality Risk Management Q9*, (2005)
- [12] International Conference on Harmonisation, *Pharmaceutical Quality System Q10*, (2008)
- [13] K.V. Gernaey, J.M. Woodley, G. Sin, *Biotechnology Journal*, 4 (2009) 593-599.
- [14] Z.H. Loh, D.Z.L. Er, L.W. Chan, C.V. Liew, P.W.S. Heng, *Expert Opinion on Drug Delivery*, 8 (2011) 1645-1661.
- [15] M. Fonteyne, J. Vercruyse, D.C. Diaz, D. Gildemyn, C. Vervaet, J.P. Remon, T. De Beer, *Pharmaceutical Development and Technology*, doi:10.3109/10837450.2011.627869.
- [16] M.L. Balboni, *Pharmaceutical Technology* (2003) 54-67.
- [17] T. Kourti, *Critical Reviews in Analytical Chemistry*, 36 (2006) 257-278.
- [18] J. Rantanen, *Journal of Pharmacy and Pharmacology*, 59 (2007) 171-177.
- [19] W. Chew, P. Sharratt, *Analytical Methods*, 2 (2010) 1412-1438.
- [20] G. Vudathala, S. Rodgers, J.E. Simmons, in: D.M. Parikh (Ed.), *Handbook of Pharmaceutical Granulation Technology - Third edition*, Informa Healthcare, New York, 2010, p. 617-636.
- [21] D. Petrak, *Particle & Particle Systems Characterization*, 19 (2002) 391-400.
- [22] D. Petrak, H. Rauh, *Particulate Science and Technology*, 24 (2006) 381-394.
- [23] D. Petrak, S. Dietrich, G. Eckardt, M. Koehler, *Advanced Powder Technology*, 22 (2011) 203-208.

- [24] J.J. Ng, S. Dietrich, In-line particle sizing: a PAT solution for high shear granulation, (2010) http://www.pharmaqbd.com/inline_particle_sizing_pat_solution/.
- [25] N. Sandler, *International Journal of Pharmaceutics*, 417 (2011) 227-234.
- [26] I. Soppela, S. Airaksinen, J. Hatara, H. Raikkonen, O. Antikainen, J. Yliruusi, N. Sandler, *Aaps Pharmscitech*, 12 (2011) 476-484.
- [27] R.J. Woodham, *Optical Engineering*, 19 (1980) 139-144.
- [28] A. Ruf, J. Worlitschek, M. Mazzotti, *Particle & Particle Systems Characterization*, 17 (2000) 167-179.
- [29] X.H. Hu, J.C. Cunningham, D. Winstead, *International Journal of Pharmaceutics*, 347 (2008) 54-61.
- [30] J. Huang, G. Kaul, J. Utz, P.W. Hernandez, V., D. Bradley, A. Nagi, D. O'Grady, *Journal of Pharmaceutical Sciences*, 99 (2010) 3205-3212.
- [31] F. Alshihabi, T. Vandamme, G. Betz, *Pharmaceutical Development and Technology* (2011) 1-12.
- [32] A. Tok, X.P. Goh, W. Ng, R. Tan, *Aaps Pharmscitech*, 9 (2008) 1083-1091.
- [33] G. Reich, *Advanced Drug Delivery Reviews*, 57 (2005) 1109-1143.
- [34] J. Luybaert, S. Heurding, Y. Vander Heyden, D.L. Massart, *Journal of Pharmaceutical and Biomedical Analysis*, 36 (2004) 495-503.
- [35] A. Smekal, *Die Naturwissenschaften*, 11 (1923) 873-875.
- [36] C.V. Raman, K.S. Krishnan, *Nature*, 121 (1928) 501-502.
- [37] R.L. McCreery, *Raman spectroscopy for chemical analysis*, John Wiley and Sons, New York, 2000.
- [38] M.J. Pelletier, in: P. M.J. (Ed.), *Analytical applications of Raman spectroscopy*, Blackwell Science Ltd, Oxford, 1999, p. 1-52.
- [39] W.L. Davies, W.T. Gloor, *Journal of Pharmaceutical Sciences*, 60 (1971) 1869-1874.
- [40] S. Watano, K. Terashita, K. Miyanami, *Advanced Powder Technology*, 3 (1992) 255-265.
- [41] S. Watano, H. Takashima, Y. Sato, K. Miyanami, T. Yasutomo, *Advanced Powder Technology*, 7 (1996) 279-289.
- [42] S. Watano, H. Takashima, Y. Sato, T. Yasutomo, K. Miyanami, *Chemical & Pharmaceutical Bulletin*, 44 (1996) 1267-1269.
- [43] F. Portoghese, F. Berruti, C. Briens, *Chemical Engineering Science*, 60 (2005) 6043-6048.
- [44] F. Portoghese, F. Berruti, C. Briens, *Powder Technology*, 181 (2008) 169-177.
- [45] W. Brennan, M. Jacobson, G. Book, C. Briens, L. Briens, *Powder Technology*, 181 (2008) 178-185.

- [46] C. Buschmüller, W. Wolfgang, C. Döscher, J. Dressler, J. Breitzkreutz, *European Journal of Pharmaceutics and Biopharmaceutics*, 69 (2008) 380-387.
- [47] V. Lourenço, T. Herdling, G. Reich, J.C. Menezes, D. Lochmann, *European Journal of Pharmaceutics and Biopharmaceutics*, 78 (2011) 513-521.
- [48] H.G. Wang, P.R. Senior, R. Mann, W.Q. Yang, *Chemical Engineering Science*, 64 (2009) 2893-2902.
- [49] P. Frake, D. Greenhalgh, S.M. Grierson, J.M. Hempenstall, D.R. Rudd, *International Journal of Pharmaceutics*, 151 (1997) 75-80.
- [50] J. Rantanen, S. Lehtola, P. Ramet, J.P. Mannermaa, J. Yliruusi, *Powder Technology*, 99 (1998) 163-170.
- [51] J. Rantanen, O. Antikainen, J.P. Mannermaa, J. Yliruusi, *Pharmaceutical Development and Technology*, 5 (2000) 209-217.
- [52] J. Rantanen, A. Jorgensen, E. Räsänen, P. Luukkonen, S. Airaksinen, J. Raiman, K. Hänninen, O. Antikainen, J. Yliruusi, *Aaps Pharmscitech*, 2 (2001) article 21.
- [53] J. Rantanen, E. Rasanen, J. Tenhunen, M. Kansakoski, J.P. Mannermaa, J. Yliruusi, *European Journal of Pharmaceutics and Biopharmaceutics*, 50 (2000) 271-276.
- [54] J. Rantanen, M. Käsäköske, J. Suhonen, J. Tenhunen, S. Lehtonen, T. Rajalahti, J.P. Mannermaa, J. Yliruusi, *Aaps Pharmscitech*, 1 (2000) article 10.
- [55] J. Rantanen, E. Rasanen, O. Antikainen, J.P. Mannermaa, J. Yliruusi, *Chemometrics and Intelligent Laboratory Systems*, 56 (2001) 51-58.
- [56] J. Rantanen, J. Yliruusi, *Pharmacy and Pharmacology Communications*, 4 (1998) 73-75.
- [57] E. Räsänen, J. Rantanen, J.P. Mannermaa, J. Yliruusi, H. Vuorela, *Journal of Pharmaceutical Sciences*, 92 (2003) 2074-2081.
- [58] K.R. Morris, J.G. Stowell, S.R. Byrn, A.W. Placette, T.D. Davis, G.E. Peck, *Drug Development and Industrial Pharmacy*, 26 (2000) 985-988.
- [59] P.L.D. Wildfong, A.-S. Samy, J. Corfa, G.E. Peck, K.R. Morris, *Journal of Pharmaceutical Sciences*, 91 (2002) 631-639.
- [60] W.P. Findlay, G.R. Peck, K.R. Morris, *Journal of Pharmaceutical Sciences*, 94 (2005) 604-612.
- [61] F.J.S. Nieuwmeyer, M. Damen, A. Gerich, F. Rusmini, K.M. van der Voort, H. Vromans, *Pharmaceutical Research*, 24 (2007) 1854-1861.
- [62] A. Hartung, M. Knoell, U. Schmidt, P. Langguth, *Drug Development and Industrial Pharmacy*, 37 (2011) 274-280.
- [63] M. Alcalá, M. Blanco, M. Bautista, J.M. Gonzalez, *Journal of Pharmaceutical Sciences*, 99 (2010) 336-345.

- [64] A. Peinado, J. Hammond, A. Scott, *Journal of Pharmaceutical and Biomedical Analysis*, 54 (2011) 13-20.
- [65] R.L. Green, G. Thureau, N.C. Pixley, A. Mateos, R.A. Reed, J.P. Higgins, *Analytical Chemistry*, 77 (2005) 4515-4522.
- [66] R.A. Mattes, D.E. Root, A.P. Birkmire, *Spectroscopy* (2005).
- [67] T. Tanino, Y. Yawata, S. Otani, H. Inoue, K. Sato, T. Takeda, T. Mizuta, *Proceedings of the Sixth International Symposium on Agglomeration*, Nagoya, Japan, 1993, p. 548-553.
- [68] S. Watano, K. Miyanami, *Powder Technology*, 83 (1995) 55-60.
- [69] S. Watano, Y. Sato, K. Miyanami, *Chemical & Pharmaceutical Bulletin*, 44 (1996) 1556-1560.
- [70] S. Watano, Y. Sato, K. Miyanami, *Advanced Powder Technology*, 8 (1997) 269-277.
- [71] S. Watano, *Powder Technology*, 117 (2001) 163-172.
- [72] T. Närvänen, K. Seppälä, O. Antikainen, J. Yliruusi, *Aaps Pharmscitech*, 9 (2008) 282-287.
- [73] N. Laitinen, O. Antikainen, J. Yliruusi, *European Journal of Pharmaceutical Sciences*, 17 (2002) 217-227.
- [74] N. Laitinen, O. Antikainen, J. Yliruusi, *Aaps Pharmscitech*, 4 (2003) 383-391.
- [75] N. Laitinen, O. Antikainen, J. Rantanen, J. Yliruusi, *Journal of Pharmaceutical Sciences*, 93 (2004) 165-176.
- [76] P. Barrett, B. Glennon, *Particle & Particle Systems Characterization*, 16 (1999) 207-211.
- [77] E. Kougoulos, A.G. Jones, K.H. Jennings, M.W. Wood-Kaczmar, *Journal of Crystal Growth*, 273 (2005) 529-534.
- [78] R.A. Williams, S.J. Peng, A. Naylor, *Powder Technology*, 73 (1992) 75-83.
- [79] A.R. Heath, P.D. Fawell, P.A. Bahri, J.D. Swift, *Particle & Particle Systems Characterization*, 19 (2002) 84-95.
- [80] S. Schmidt-Lehr, H.U. Moritz, K.C. Jurgens, *Pharmazeutische Industrie*, 69 (2007) 478-484.
- [81] T. Närvänen, T. Lipsanen, O. Antikainen, H. Räikkönen, J. Heinämäki, J. Yliruusi, *Journal of Pharmaceutical Sciences*, 98 (2009) 1110-1117.
- [82] J. Huang, C. Goolcharran, J. Utz, P. Hernandez-Abad, K. Ghosh, A. Nagi, *Journal of Pharmaceutical Innovation*, 5 (2010) 58-68.
- [83] M. Halstensen, K.H. Esbensen, in: K.A. Bakeev (Ed.), *Process Analytical Technology - Second Edition*, John Wiley & Sons Ltd., United Kingdom, 2010, p. 281-302.
- [84] H. Tsujimoto, T. Yokoyama, C.C. Huang, I. Sekiguchi, *Powder Technology*, 113 (2000) 88-96.
- [85] M. Halstensen, K.H. Esbensen, *Journal of Chemometrics*, 14 (2000) 463-481.
- [86] M. Halstensen, P. de Bakker, K.H. Esbensen, *Chemometrics and Intelligent Laboratory Systems*, 84 (2006) 88-97.

- [87] S. Matero, S. Poutiainen, J. Leskinen, K. Jarvinen, J. Ketolainen, S.P. Reinikainen, M. Hakulinen, R. Lappalainen, A. Poso, *Chemometrics and Intelligent Laboratory Systems*, 97 (2009) 75-81.
- [88] S. Matero, S. Poutiainen, J. Leskinen, K. Järvinen, J. Ketolainen, A. Poso, S.P. Reinikainen, *Journal of Chemometrics*, 24 (2010) 464-471.
- [89] D.S. Hausman, R.T. Cambron, A. Sakr, *International Journal of Pharmaceutics*, 299 (2005) 19-33.
- [90] K. Kogermann, J. Aaltonen, C.J. Strachan, K. Pöllänen, J. Heinämäki, J. Yliruusi, J. Rantanen, *Journal of Pharmaceutical Sciences*, 97 (2008) 4983-4999.
- [91] G. Walker, S.E.J. Bell, M. Vann, D.S. Jones, G. Andrews, *Chemical Engineering Science*, 62 (2007) 3832-3838.
- [92] G.M. Walker, S.E.J. Bell, K. Greene, D.S. Jones, G.P. Andrews, *Chemical Engineering Science*, 64 (2009) 91-98.
- [93] J. Aaltonen, K. Kogermann, C.J. Strachan, J. Rantanen, *Chemical Engineering Science*, 62 (2007) 408-415.
- [94] J.T.T. Leskinen, M.A.H. Okkonen, M.M. Toiviainen, S. Poutiainen, M. Tenhunen, P. Teppola, R. Lappalainen, J. Ketolainen, K. Jarvinen, *Chemical Engineering Journal*, 164 (2010) 268-274.
- [95] D.F. Erkoboni, in: D.M. Parikh (Ed.), *Handbook of Pharmaceutical Granulation Technology*, Marcel Dekker Inc., New York, 1997, p. 333-368.
- [96] N. Sandler, J. Rantanen, J. Heinämäki, M. Römer, M. Marvola, J. Yliruusi, *Aaps Pharmscitech*, 6 (2005) E174-E183.
- [97] M. Römer, J. Heinämäki, I. Miroshnyk, N. Sandler, J. Rantanen, J. Yliruusi, *European Journal of Pharmaceutics and Biopharmaceutics*, 67 (2007) 246-252.
- [98] M. Römer, J. Heinämäki, I. Miroshnyk, N. Kivikero, N. Sandler, J. Rantanen, J. Yliruusi, *Journal of Pharmaceutical Sciences*, 97 (2008) 4020-4029.
- [99] J. Mantanus, E. Ziemons, P. Lebrun, E. Rozet, R. Klinkenberg, B. Streel, B. Evrard, P. Hubert, *Analytica Chimica Acta*, 642 (2009) 186-192.
- [100] J. Mantanus, E. Ziemons, P. Lebrun, E. Rozet, R. Klinkenberg, B. Streel, B. Evrard, P. Hubert, *Talanta*, 80 (2010) 1750-1757.
- [101] J. Mantanus, E. Ziemons, E. Rozet, B. Streel, R. Klinkenberg, B. Evrard, J. Rantanen, P. Hubert, *Talanta*, 83 (2010) 305-311.

CHAPTER 4

EVALUATION OF IN-LINE SPATIAL FILTER VELOCIMETRY AS PAT MONITORING TOOL FOR PARTICLE GROWTH DURING FLUID BED GRANULATION

Parts of this chapter are published in:

A. Burggraeve, T. Van Den Kerkhof, M. Hellings, J.P. Remon, C. Vervaet, T. De Beer, Evaluation of in-line spatial filter velocimetry as PAT monitoring tool for particle growth during fluid bed granulation, *European Journal of Pharmaceutics and Biopharmaceutics*, 76 (2010) 138-146.

ABSTRACT

In this study, the feasibility of spatial filter velocimetry as process analytical technology tool for the in-line monitoring of the particle size distribution during top-spray fluidized bed granulation was evaluated. Herewith, the influence of several process (inlet air temperature during spraying and drying) and formulation (HPMC and Tween 20 concentration) variables upon the particle size distribution during processing, and the end product particle size distribution, tapped density and Hausner ratio was examined using a design of experiments (DoE).

The trend in end granule size distribution of all DoE batches measured with in-line SFV, was similar to the off-line laser diffraction size values. The in-line SFV particle size data, obtained every 10 s during processing, allowed to explain and better understand the (in)significance of the studied DoE variables, which was not possible based on the laser diffraction data as this technique only supplied end granule size information. Univariate, multivariate and multiway models were built to relate end granule properties (i.e., tapped density and Hausner ratio) to the in-line measured particle size distribution.

CHAPTER 4

EVALUATION OF IN-LINE SPATIAL FILTER VELOCIMETRY AS PAT MONITORING TOOL FOR PARTICLE GROWTH DURING FLUID BED GRANULATION

4.1. INTRODUCTION

Fluid bed granulation is an extensively used process within the pharmaceutical industry to improve powder properties (i.e., flowability, compressibility, etc.) for downstream processing (e.g., tableting). During fluid bed granulation, a liquid binder is sprayed onto particles of a powder mixture, circulating through the fluidized bed. As a result, these primary powder mixture particles collide with each other, hence forming larger permanent aggregates (granules), in which the original particles are still identifiable [1].

The concept of PAT has been introduced by the American Food and Drug Administration. The general idea is that *quality cannot be tested into products; it should be built-in or should be by design* [2, 3]. Through the identification and understanding of critical process and formulation parameters, one should be able to completely control the manufacturing processes, hence constantly ensuring a predefined end product quality. In that way, rejects and/or reprocessing may be prevented, production cycle time may be reduced, and real-time release is possible. To enable the implementation of this scientific and risk-based framework in pharmaceutical production processes, a combination of suitable PAT tools is needed, such as modern process analyzers for process and endpoint monitoring, chemometrics, control tools, continuous improvement and knowledge management tools.

The particle size distribution is one of the key characteristics of a granulated product. An inappropriate particle size distribution influences granule properties as density, powder flowability

and dustiness which in turn might cause problems during further processing. Hence, understanding and control of the granule growth mechanism during granulation are of major importance.

Sieve analysis, image analysis and laser diffraction are the traditional *off-line* techniques used for granule size determination. These methods can be time-consuming and labor intensive (sample preparation) and do not supply in-process information. As a result, research has been performed on *at-line*, *on-line* and *in-line* particle size measuring tools. The use of on-line *image analysis* for granule size determination was initiated by Watano et al. [4-9] and more recently investigated by Närvänen et al. [10]. As a *near infrared* spectrum is dependent on the chemical and physical properties of a measured sample, NIR spectroscopy has been extensively investigated for the fast and non-destructive (at-line, on-line or in-line) particle size monitoring during granulation, usually combined with moisture content determination [11-16]. A couple of reports can be found on the application of *focused beam reflectance measurements* in-line or at-line during fluid bed granulation [15, 17]. Tok et al. [15] describe the combined use of FBRM, NIR spectroscopy and acoustic emission measurements in a pilot-scale fluidized bed granulation process. In-line FBRM and NIR probes were able to detect the three granulation rate processes to varying degrees of sensitivity due to fouling. Although an anti-static spray was applied onto the surface of the probe windows, FBRM and NIR signals remained susceptible to fouling during granulation. More recently, an FBRM probe equipped with a scraper system designed for removing agglomerates of the probe window in cohesive particle conditions was developed (FBRM C35 technology). The use of *acoustic emission spectroscopy* in granulation has also been described [15, 18-21]. As this is a non-intrusive technique, it has the advantage of not interfering with the fluidizing bed. However, the technique's sensitivity can be highly affected by the fluidizing airflow rate and external uncontrollable factors.

Spatial filter velocimetry is a method similar to FBRM as they both use chord length distribution to express particle size. Both techniques project a laser beam onto the moving particles. However, FBRM uses the backscattered light and converts it to size measurement, while SFV uses the generated shadow. During SFV measurements, particles pass through a laser beam and cast shadows onto a linear array of optical fibers. In that way, a burst signal is generated, which is proportional to particle velocity. As the particles pass through the beam, a secondary pulse is generated by a single optical fiber. Knowing the time of the pulse and the velocity of the moving particles, the chord length can be calculated (see Chapter 3). The measurement cell of the SFV probe is equipped with sapphire windows that are kept clean through the use of an internal compressed air supply system, which prevents fouling of the windows. The internal airflow also ensures the dispersion of highly concentrated particles and optimizes the movement of these particles through the measurement zone. The measurement results are reported in various ways, e.g. sieve distribution (as fraction and

passage), volume distribution, number distribution, velocity distribution, etc. [22-24]. Närvänen et al. [25] compared three different particle size measurement techniques: sieve analysis, laser diffraction and off-line SFV to model process parameters of a fluid bed granulation process. The SFV results were the most consistent among the three studied techniques. Another study by the same group showed that the in-line particle size data measured via SFV could be used to monitor different process phenomena and process failure [26]. However, particle size determination was influenced by size segregation in the fluid bed: the in-line technique underestimated and the at-line method overestimated the final granule size. Lipsanen et al. [27] showed that the pressure difference over the upper filters (indication of blockage of filters) and the fluidization parameter correlated well with the in-line SFV particle size measurements.

In the present study, SFV was evaluated as a PAT tool for the in-line particle size monitoring in a pharmaceutical fluid bed granulation process. A design of experiments was performed to study the influence of different process and formulation variables upon the average granule size and the granule size distribution (response variables), measured in-line with SFV, and compared to off-line laser diffraction results. It was also examined whether the continuously obtained in-line SFV data could improve our understanding about the impact of the DoE variables on the fluidized bed granulation process. Furthermore, we evaluated whether the in-line particle size data could be related to off-line-measured end granule properties (tapped density and Hausner ratio) using univariate, multivariate and multiway models, hence allowing early estimation of these end product properties during processing.

Whereas previous reports about in-line SFV emphasized on the sensitivity of the technique towards the in-line detection of granule size and process failures [26, 27], the present study examines the application of the technique to enhance the understanding of fluidized bed processing through the continuous measurement of particle size, in combination with DoE. Furthermore, models were built using the continuously in-line measured particle size information, enabling the early prediction of end granule properties.

4.2. MATERIALS AND METHODS

4.2.1. Materials

Each batch, consisting of dextrose monohydrate (700 g, Roquette Frères, Lestrem, France) and unmodified maize starch (Cargill Benelux, Sas van Gent, The Netherlands), was granulated with an aqueous binder solution of hydroxypropylmethylcellulose (HPMC) (type 2910 15 mPa s, Dow Chemical Company, Plaquemine, LA, USA) and Tween 20 (Croda Chemicals Europe, Wilton, UK). The amount of HPMC and Tween 20 in the granules was varied according to the DoE (Section 4.2.4). HPMC was always sprayed as a 4% solution and the total amount of solids was kept constant at 1000 g (amount of maize starch was varied accordingly).

4.2.2. Fluid bed granulation

Granulation was performed in a laboratory-scale fluid bed granulator (GPCG 1, Glatt, Binzen, Germany). A top-spray nozzle with a diameter of 1.2 mm was installed at a height of 26 cm from the distributor plate, and an atomization pressure of 1 bar was used during all experiments. The pump was set at a feed rate of 16 g/min. Shaking of the filter bags was necessary every 45 s for a period of 7 s to prevent the entrapment of small particles in the bags. Through visual monitoring of the flowing powder bed, the inlet airflow rate was adjusted when necessary to keep the height of the fluidized bed constant. The inlet air temperature during spraying and drying varied according to the DoE (Section 4.2.4). Granules were dried until an outlet air temperature of 37 °C, and a product temperature of 45 °C was obtained (granulation endpoint).

4.2.3. In-line measurements with spatial filter velocimetry probe

An in-line spatial filter velocimetry probe (Parsum IPP 70; Gesellschaft für Partikel-, Strömungs- und Umweltmesstechnik, Chemnitz, Germany) was installed in the fluid bed granulator at a height of 20 cm and at approximately 5 cm from the sidewall of the granulator (i.e., between the sidewall of the granulator and the outer part of the spray cone, Figure 4.1). If the probe was placed in the centre of the fluid bed (i.e., below the spray cone), probe fouling by the moist product occurred. Using an internal (20 L/min) and external (3 L/min) air connection, the granules were directed through an aperture (4 mm diameter), to ensure the dilution of the product mass (avoidance of aperture obstruction) and to prevent back flush of the measured granules. Measured raw data were collected via an A/D converter and led to a computer. The In-line Particle Probe V7.12a software was operated in the Windows XP environment. SFV measurements started and stopped simultaneously with the

start and end of fluidization, respectively. During the entire granulation process, SFV data were collected every second, but an average granule size distribution was saved every 10 s.

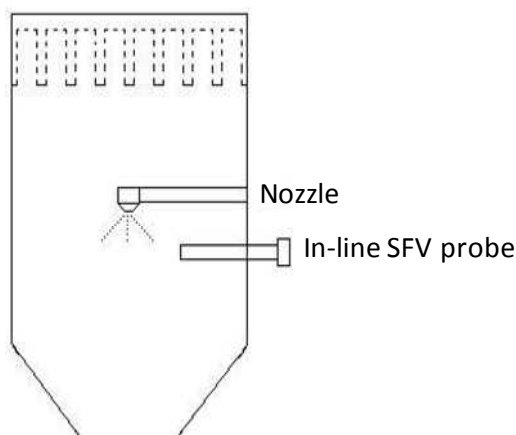


Figure 4.1. Fluid bed granulator with in-line SFV probe (probe at a height of 20 cm and depth of 5 cm).

4.2.4. Design of experiments

A 2-level full factorial design containing four variables (*HPMC concentration, Tween 20 concentration, inlet air temperature during spraying and inlet air temperature during drying*, Table 4.1) and three center point repetition experiments was performed.

Table 4.1. Design matrix 2-level full factorial design.

Batch	HPMC	Tween 20	Inlet air temperature during spraying	Inlet air temperature during drying
1	-1	-1	-1	-1
2	1	-1	-1	-1
3	-1	1	-1	-1
4	1	1	-1	-1
5	-1	-1	1	-1
6	1	-1	1	-1
7	-1	1	1	-1
8	1	1	1	-1
9	-1	-1	-1	1
10	1	-1	-1	1
11	-1	1	-1	1
12	1	1	-1	1
13	-1	-1	1	1
14	1	-1	1	1
15	-1	1	1	1
16	1	1	1	1
17	0	0	0	0
18	0	0	0	0
19	0	0	0	0

In total, 19 experiments were carried out to evaluate the influence of the examined variables and their interactions upon the average particle size and particle size distribution during granulation within the defined knowledge space (Table 4.2). All design granulations were performed in a randomized order.

Table 4.2. Experimental values of the examined variables.

Variable	Unit	Lower level	Upper level
HPMC	%w/w	1	3
Tween 20	%w/w	0.2	0.3
Inlet air temperature during spraying	°C	40	50
Inlet air temperature during drying	°C	50	70

4.2.5. Characterization of granules

After manufacturing, the average particle size, particle size distribution, tapped density and Hausner ratio of the end product of each batch were determined.

A 20-g sample was measured with *laser diffraction (LD)* (Mastersizer S long bench, Malvern Instruments, Malvern, UK). The dry powder dispersing unit was used with a jet pressure of 0.2 bars and a measurement time of 20 s. This low dispersing pressure was selected to prevent the breaking up of the granules. All measurements were performed in triplicate and the particle size distributions were characterized via their $D(v, 0.1)$, $D(v, 0.5)$ and $D(v, 0.9)$ values (10%, 50% or 90% of the distribution has a particle size smaller than this value).

The *tapped density* of the granules was determined as described in the European Pharmacopoeia 6.5. A graduated cylinder of 100 mL was used and samples were tapped 1250 times. All density measurements were performed in triplicate and the average density is reported.

Powder flow characteristics were predicted by calculation of Hausner ratio values, according to the European Pharmacopoeia 6.0 and determined in triplicate.

4.2.6. Data analysis

Analysis of the DoE results was performed with MODDE software (Version 8.0.2, Umetrics, Umeå, Sweden) and Microsoft Excel 2007. Partial least squares models were developed using SIMCA-P+ software (Version 12.0.1, Umetrics, Umeå, Sweden). Matlab 7.1 (The MathWorks, Inc., Natick, MA) with the PLS Toolbox for MATLAB version 4.2 was used for N-way partial least squares (N-PLS) modeling.

4.3. RESULTS AND DISCUSSION

4.3.1. Comparison between in-line SFV and off-line LD results

In a first instance, it was investigated whether the end granule particle size determined by in-line SFV corresponded to the off-line LD results for all DoE batches. Although the measurement principles of both techniques are different (LD assumes spherical particles, SFV does not), similar trends in particle size distributions should be observed. Batches with a small/large particle size should be classified by both techniques as small/large. The SFV volume particle size distribution was used for comparison, and the average of the in-line measured particle size during the last granulation process minute (i.e., 6 data points) was computed. Each batch was measured in triplicate with LD, and the average particle size was calculated. D_{10} , D_{50} and D_{90} values of LD and SFV data demonstrated a similar pattern (only the D_{50} values of both techniques are displayed).

Figure 4.2 shows that an identical trend in D_{50} values for all 19 DoE batches was obtained by the two particle sizing techniques. However, the D_{50} values measured with SFV were always higher than those obtained using LD. An explanation for this observation might lay in the LD measurement technique. Using the dry powder dispersing unit, the particles experience rapid accelerations as the airstream passes through a venturi. Due to the high shear applied during this process and the subsequent collisions with the wall of the apparatus, some granules may break or crumble. During the SFV measurements, pressurized air was also used for dispersing the granules; however, the particles passed directly through the measurement zone. No collisions occurred as no high shear was applied.

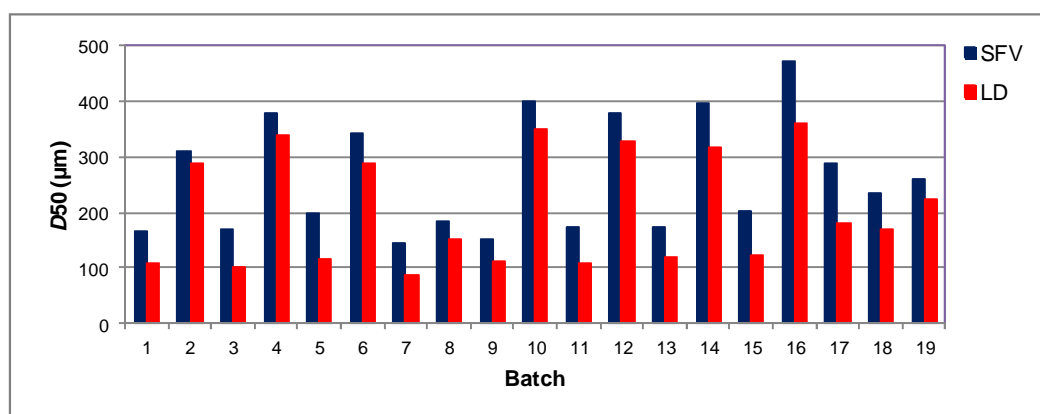


Figure 4.2. Comparison between the D_{50} results obtained with in-line SFV and off-line LD for all DoE batches.

Confirmation of this hypothesis can be found in Figure 4.3, which shows the differences between the D_{10} , D_{50} and D_{90} results of the SFV and LD measurements for the 19 DoE batches. This figure demonstrates that the D_{90} differences are larger for most batches compared to the D_{10} and D_{50}

differences. During the LD measurements, the fragile granules collided with the wall and broke up into smaller particles, which corresponded to a particle size in the range of the D_{10} and D_{50} values. As a consequence, the D_{10} and D_{50} SFV-LD differences were smaller compared to the D_{90} differences.

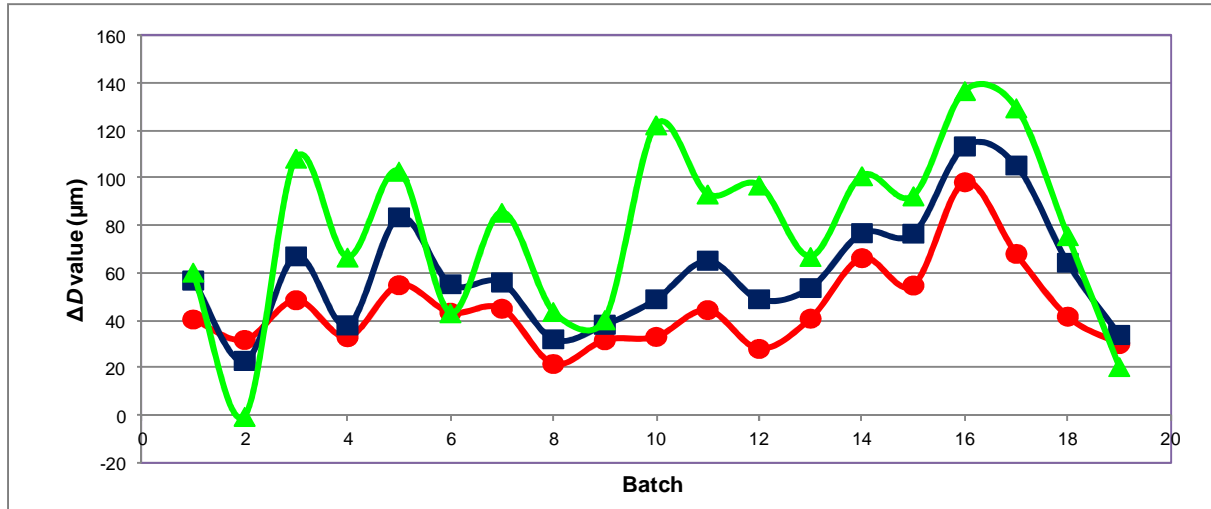


Figure 4.3. Differences between the D_{10} (red circles), the D_{50} (blue squares) and the D_{90} results (green triangles) of the SFV and LD measurements for the 19 DoE batches.

This hypothesis was also confirmed by the particle size measurement of low friable spherical granules (i.e., pellets, Cellets® 100, 200 and 350, Pharmatrans Sanaq Pharmaceuticals, Basel, Switzerland). The particle size of the Cellets® was measured using SFV and LD under identical software settings and experimental setup as during the DoE granule measurements. As these Cellets® have a low friability, the differences between the D_{10} , D_{50} and D_{90} values of SFV and LD, respectively, did not increase due to attrition during LD measurement, in contrast to observations obtained for the ‘breakable’ granules. Moreover, the differences between the D -values were negative or positive, indicating this difference is random.

Besides the LD measurement technique, the assumption of spherical particles during LD measurements might be an additional factor contributing to the discrepancy between SFV and LD values. Especially for larger particles, the effect of these different measurement principles could be expected to be more pronounced as their particle shape will deviate more distinct from a sphere.

Närvänen et al. [26] reported significant differences between the in-line SFV and off-line LD measured particle size, when larger granules ($>200 \mu\text{m}$) were formed during granulation (in-line data underestimated the actual particle size). They explained that size segregation was occurring during fluidization. Hence, a high amount of larger granules was present in the lower part of the fluid bed chamber, and a high amount of smaller granules was present in the upper part of the chamber. As a result, the largest particles could not reach the SFV probe, which was placed in the upper part of the

fluid bed chamber, and were not measured. According to Figure 4.4 (a-b), the in-line SFV data did not underestimate the actual particle size due to size segregation for the present study. This figure presents the difference in SFV and LD D_{50} values for the 19 DoE batches, arranged according to increasing SFV end granule size (Figure 4.4a) and increasing LD end granule size (Figure 4.4b) in the x-axes, respectively. If size segregation would have occurred, these differences should increase according to increasing end granule size (i.e., in function of x-axis), which is clearly not the case in both figures.

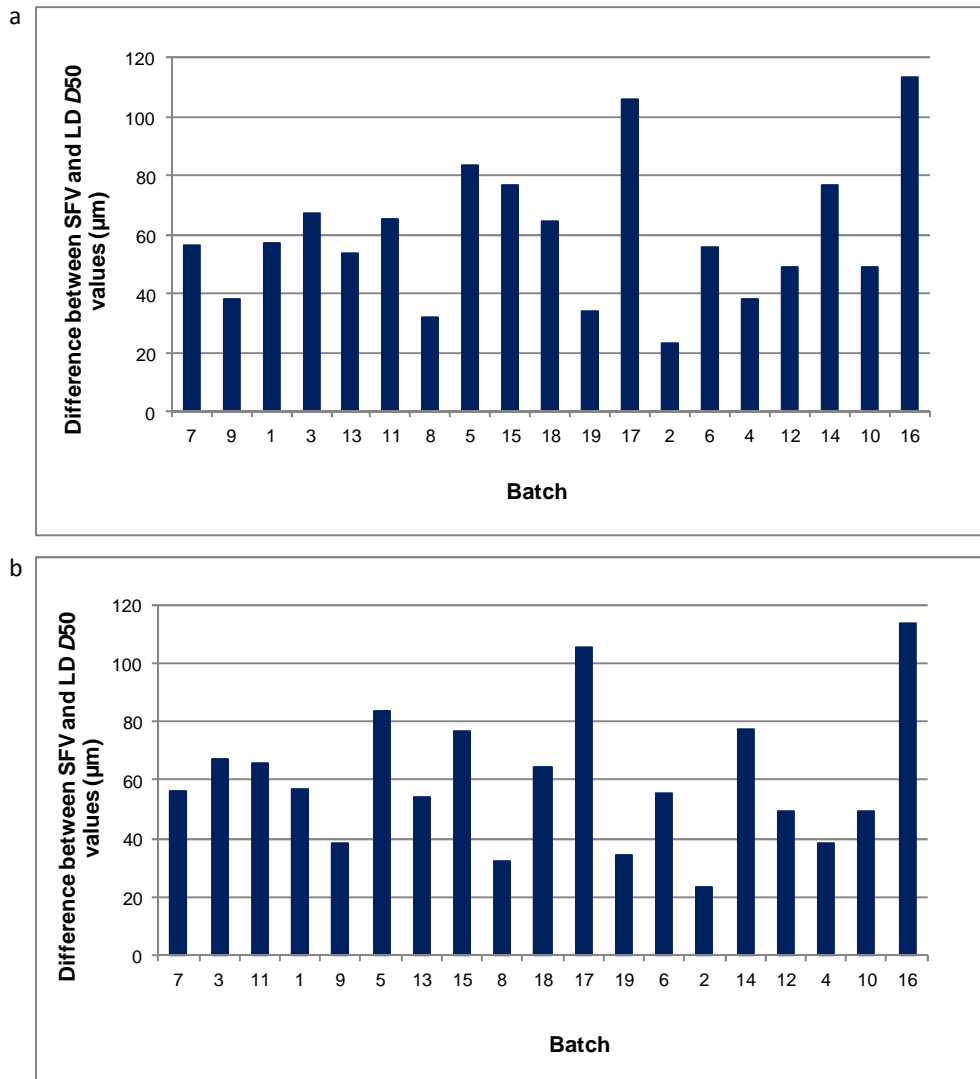


Figure 4.4. Differences between D_{50} values measured by SFV and LD, arranged (x-axis) according to increasing SFV particle size (a), and increasing LD particle size (b).

These primary results suggest that although there is a systematic difference between SFV and LD data due to the granule break-up during the LD measurement, the SFV technique adequately describes the actual particle size distribution during processing.

4.3.2. DoE analysis

4.3.2.1. Comparison between in-line SFV and off-line LD DoE results

The average D_{50} value obtained during the last minute of drying (i.e., 6 data points) was used as SFV response value. LD measurements of the end granules were performed in triplicate, and the average D_{50} value was used as LD response. For each of these responses, a DoE regression model was calculated. Using the MODDE software, the raw data were in first instance evaluated by means of a replicate plot and a descriptive statistics plot in which outliers could be identified. Subsequently, a multiple linear regression model was fitted, and the corresponding parameters, goodness of fit (R^2) and goodness of prediction (Q^2), were evaluated. The least significant model terms were excluded provided that Q^2 increased. R^2 and Q^2 values, and the significant variables can be found in Tables 4.3 and 4.4, respectively.

Table 4.3. R^2 and Q^2 values of SFV- and LD-based models.

	SFV	LD
R^2	0.84	0.87
Q^2	0.73	0.79

Table 4.4. Statistical significance (p) of coefficients in SFV- and LD-based models.

	SFV		LD	
	Coefficient	p	Coefficient	p
HPMC	92.5	***	96.3	***
T_{drying}	28.3	*	21.4	*
HPMC* T_{drying}	25.6	*	15.0	NS

* $p < 0.05$, ** $p < 0.01$, *** $p < 0.001$, NS = not statistically significant

According to Table 4.3, R^2 and Q^2 values of the SFV and LD model are very similar and indicate good models. Both models show the same significant factors (Table 4.4): *HPMC concentration (positive effect on particle size), inlet air temperature during drying (positive effect on particle size) and the interaction between these factors (positive effect on particle size)*. Although the HPMC concentration was the most significant variable, exclusion of T_{drying} and HPMC* T_{drying} (in the LD model, this latter coefficient has a p -value larger than 0.05, Table 4.4) was not done as this resulted in lower R^2 and Q^2 values. Use of the D_{10} and D_{90} values of SFV and LD measurements as responses resulted in the same conclusions. The width ($(D_{90} - D_{10})/D_{50}$) of the particle size distribution was similar for all DoE batches.

Normal probability plots or half-normal plots are another tool to identify significant effects. Normally distributed non-significant effects form a straight line through zero in these plots, while significant effects deviate from this pattern. Development of these plots was done as described in Vander Heyden et al. [28]. Applying the algorithm of Dong, a numerical limit value was obtained which could be plotted onto the half-normal plots and allowed a more objective quantitative identification of the significant effects: effects larger than the calculated margin of error are considered as significant.

Both half-normal plots (Figure 4.5a and b) point out the same conclusion: all effects lie on a straight line except for effect A (HPMC concentration) and only effect A is larger than the margin of error (ME), indicating this was a significant effect. However, both plots also show that effect D (inlet air temperature during drying) is the second most important effect but classified as a borderline case as its value is below the margin of error.

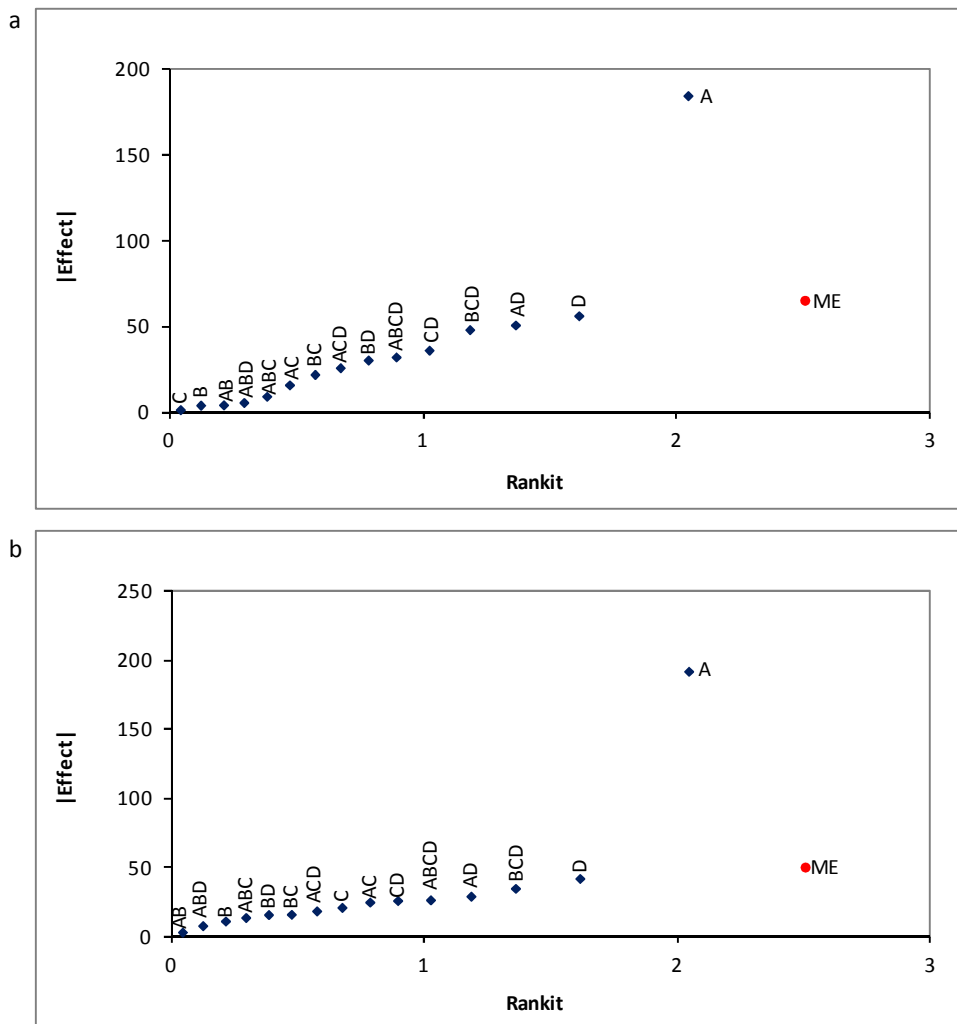


Figure 4.5. Half-normal plots of SFV results (a) and LD results (b), with critical margin of error (ME).

A = HPMC concentration, B = Tween 20 concentration, C = inlet air temperature during spraying and D = inlet air temperature during drying

4.3.2.2. Explanation of the (in)significance of the DoE factors based on in-line SFV data

As granule growth information was obtained every 10 s during granulation using SFV, this in-process information allows thorough explanation and better understanding of the (in)significance of the examined process and formulation variables.

Influence of HPMC concentration

According to the DoE analysis, larger granules were produced by increasing the HPMC amount. These results are in accordance with the well-known adhesive and cohesive properties of HPMC in granule formation. Figure 4.6 shows the influence of the HPMC concentration on the granulation process for batches 13 and 14, containing 1% and 3% HPMC, respectively. The other settings are identical for both batches. The in-line data revealed that the increase in particle size was actually due to two effects:

1. Spraying more binder liquid resulted in larger particles immediately after *spraying* the binding liquid (i.e. before the start of drying). After spraying, batch 13 had a particle size of 200 μm and batch 14 a particle size of 415 μm .
2. Increasing the HPMC concentration created less friable granules, producing less fines during the *drying* period. Batch 13 exhibited a decrease in particle size of approximately 60 μm during drying, while batch 14 decreased only 25 μm in particle size during drying.

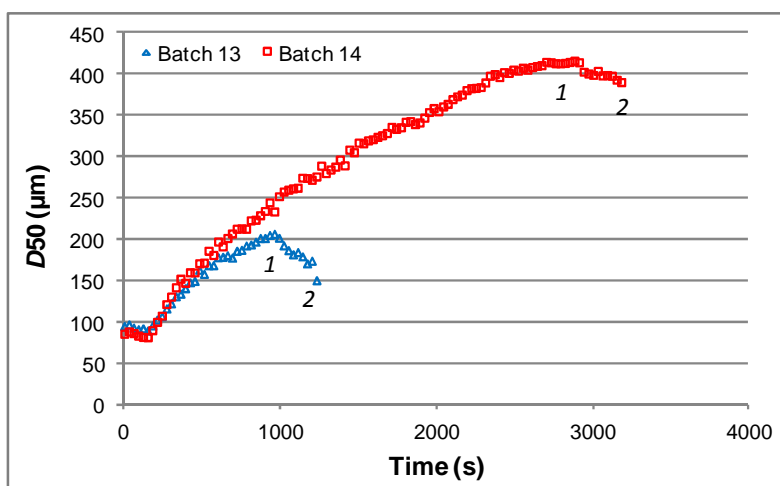


Figure 4.6. In-line SFV data of batches 13/14 (1%/3% HPMC, 0.2% Tween 20, 50 °C spraying T, 70 °C drying T) with 1: end of spraying phase and 2: end of drying phase.

Influence of inlet air temperature during drying

The DoE results indicated that an increase in drying temperature resulted in larger granules, but the significance of this factor was rather small (p -value > 0.01). Figure 4.7a displays the in-line SFV data of batches 6 (50 °C drying temperature) and 14 (70 °C drying temperature) to highlight the effect of the drying temperature on the granulation process. The other settings are the same for both batches.

The plot shows that both batches had approximately the same particle size at the beginning of the drying period (identical spraying phase conditions), but that batch 6, which was dried at a lower temperature for a longer period, resulted in crumbled granules having a smaller end granule particle size.

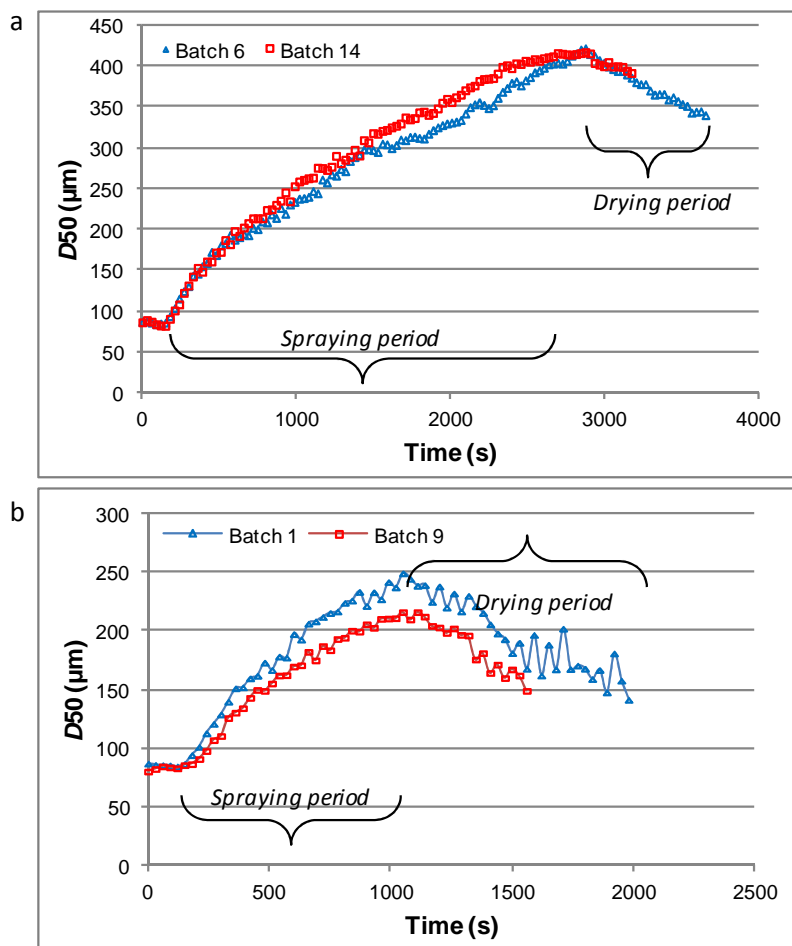


Figure 4.7. In-line SFV data of batches with a different drying temperature. (a) batches 6/14 (3% HPMC, 0.2% Tween 20, 50 °C spraying T, 50 °C/70 °C drying T), (b) batches 1/ 9 (1% HPMC, 0.2% Tween 20, 40 °C spraying T, 50 °C/70 °C drying T).

Figure 4.7b also displays two batches with different drying conditions (batch 1 was dried at 50 °C and batch 9 at 70 °C). Although both batches had initially identical process conditions, after the spraying period, a different particle size was measurement for the batches, which was possibly due to inappropriate fluidization influencing the agglomeration process. Furthermore, there was a clear difference in particle size evolution during drying of batch 1 and 9 (the longer drying period at the lower temperature level of batch 1 caused more attrition of the granules and thus a larger decrease in particle size during the drying period); nevertheless, the batches resulted in similar end granule sizes, used to calculate DoE models. Hence, for both batches, similar response variables were used in the DoE despite the fact that the batches exhibited a very different process progress. Indeed, the

different applied inlet air temperature during drying clearly affected the drying process of batch 1 and 9. However, this was not transposed in the end product particle size (response variable used for the DoE analysis) as the batches did not have the same particle size at the start of the drying period. This might explain why the drying temperature was of limited significance according to the DoE. Only the continuous in-line-obtained information from the SFV probe was able to give this in-depth understanding.

The data in Figure 4.7a and b also display another process phenomenon: shaking of the filter bags. At the beginning of all processes, powders had a small particle size as almost no binder liquid was added yet. As result, the powder particles got trapped into the filter bags. These bags were shaken every 45 s, releasing the small particles which were hence passing the probe, causing a drop in measured particle size after each shaking period. As the granulation process progressed, more binder liquid was sprayed and these small particles were agglomerated into larger granules. Hence, fewer particles were trapped into the bags resulting in less fluctuation in the particle size versus process time plots. During the drying phase of each granulation process, granules could be attrited depending on the process conditions and the smaller particles could get entrapped again into the filter bags, causing a drop in particle size after shaking of the bags (see drying period of batch 1 in Figure 4.7b). This proves that the in-line SFV probe was sensitive to all sudden changes in particle size during granulation.

Influence of inlet air temperature during spraying

The results of the performed DoE showed that the inlet air temperature during spraying had no significant effect upon the end granule size. Figure 4.8 gives an example of the in-line SFV data collected during the spraying phase of two batches where a different spraying temperature was applied.

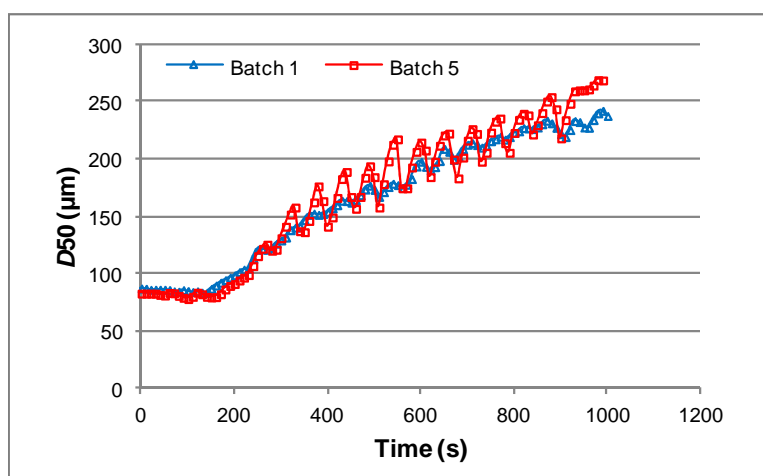


Figure 4.8. In-line SFV data during the spraying phase of batches 1/5 (1% HPMC, 0.2% Tween 20, 40 °C/50 °C spraying T, 50 °C drying T)

During the agglomeration period of batch 5 (with a spraying temperature of 50 °C), there was a higher variability of the particle size compared to batch 1 (with a spraying temperature of 40 °C), due to the continuous entrapment of small particles in and subsequent discharge from the filter bags. Small particles were longer present in batch 5 than in batch 1, as the agglomeration occurred slower in batch 5 due to the faster evaporation of binder liquid at the upper temperature level. However, at the end of the spraying period, a similar particle size was observed at both levels, indicating that the influence of the inlet air temperature during spraying was not pronounced enough to create a difference in particle size at the end of the spraying period.

Influence of Tween 20

According to the performed DoE, the amount of Tween 20 had no significant effect on the particle size. The in-line SFV data profiles of the batches having different Tween 20 settings, but having identical settings for the other examined variables were always similar.

4.3.2.3. Influence of DoE factors upon density and powder flow

The particle size distribution is one of the most important granule characteristics, but other properties, such as density and flowability are also of importance for further processing. These latter properties were determined as described in Section 4.2.5, and it was examined which of the DoE variables had a significant effect on these properties (see Table 4.5). Based on the MODDE software models and the calculated half-normal plots (with algorithm of Dong), similar conclusions were drawn.

Tapped density DoE model

The *HPMC concentration* and *inlet air temperature during drying* had the largest significant negative effect upon tapped density, indicating that by increasing these factors the density of the granules decreased. These effects can be explained by the results in Section 4.3.2.1. The SFV DoE model showed that increasing the amount of HPMC and increasing the drying temperature created larger granules. These larger granules are less cohesive and occupy more volume, thus decreasing the density of the granules.

According to Table 4.5, the *inlet air temperature during spraying* had also a significant negative effect on tapped density, although with a smaller significance compared to the HPMC concentration and the inlet air temperature during drying. The SFV DoE model showed that the spraying temperature did not significantly influence the granule particle size. Hence, the negative effect on density is not caused by a larger volume (larger particle size).

Table 4.5. Statistical significance (p) of coefficients in tapped density and Hausner ratio DoE models.

	Tapped Density		Hausner Ratio	
	Coefficient	p	Coefficient	p
HPMC	-0.0522	***	-0.0238	**
Tween	0.0040	NS	0.0113	NS
T _{spraying}	-0.0156	**	0.0113	NS
T _{drying}	-0.0270	***	-0.0025	NS
HPMC*Tween	-0.0016	NS	0.0025	NS
HPMC*T _{spraying}	-0.0043	NS	0.0175	*
HPMC*T _{drying}	0.0044	NS	0.0012	NS
Tween*T _{spraying}	0.0116	*	0.0125	NS
Tween*T _{drying}	-0.0013	NS	-0.0037	NS
T _{spraying} *T _{drying}	0.0008	NS	-0.0062	NS

*p<0.05, **p<0.01, ***p<0.001, NS = not statistically significant

Hausner ratio DoE model

The granules had passable, fair or good flow characteristics according to the scale of flowability, based on the calculated Hausner ratio. The DoE model (Table 4.5) showed that only the HPMC concentration significantly negatively affected Hausner ratios, indicating that increasing the amount of HPMC, reduced the values of this index, thus increasing the granules' flowability. The explanation was found in the results of the SFV (or LD) DoE model: more HPMC in the binder liquid created larger granules, which reduces the cohesiveness of the granules, thus increasing flow properties.

4.3.2.4. Assessment of granule density and flowability from in-line SFV measurements

In the final part of this study, it was examined whether the density and flowability of the 19 design experiments could be related to the in-line SFV determined particle size distribution, as these granule properties are closely related to the particle size distribution (see Section 4.3.2.3). Univariate, multivariate and multiway approaches were considered (with the tapped density and the Hausner ratio values of the 19 DoE batches as dependent variables: 19 x 1 **y**-vector). Independent models were built for tapped density and Hausner ratio.

- **Univariate:** A *linear* model was built using the *D50* SFV values of the end granules of the 19 design experiments as independent variables (19 x 1 **X**-vector).
- **Multivariate:** A *partial least squares* model was built using the *D01, D10, D25, D50, D63, D75, D90 and D99* SFV values of the end granules of the 19 design experiments as independent variables (19 x 8 **X**-matrix).
- **Multiway:** An *N-way partial least squares* model was built using the *D01, D10, D25, D50, D63, D75, D90 and D99* SFV values of the 19 design experiments *in function of complete batch time* as independent variables (3-way **X**-matrix).

The quality of the models was compared by evaluation of R^2 (explained variance) and RMSEE (root mean square error of estimation, Eq. (4.1)). R^2 reflects the goodness of fit, and the RMSEE specifies the root mean square error of the fit for observations in the work set, hence giving a direct indication of the error in the model (adjusted to the scale of the model):

$$RMSEE = \sqrt{\frac{\sum_{i=1}^N (y_{iobs} - y_{ipred})^2}{N - A - 1}} \quad (4.1)$$

with N = number of experiments, y_{iobs} = observed y -value, y_{ipred} = predicted y -value according to the model, A = number of PLS components in the model.

According to Table 4.6, the multivariate PLS tapped density model and the multiway N-PLS Hausner ratio model had the highest R^2 values in combination with the lowest RMSEE values. For tapped density, the use of a multivariate approach seemed justified as the correlation improved by more than 10%. In case of the Hausner ratio models, the benefits of a more complicated multivariate or multiway approach was not as pronounced, as the amount of variance explained by the model did not increase largely.

As the errors of the models were rather small, the results suggest that the models had a good prediction ability and the in-line SFV data can give an indication towards the magnitude of the off-line measured end granule properties. Nevertheless, better model performance evaluation can be done by using an independent test set as the RMSEE values relate to the errors within the calibration set and may overestimate the actual model performance.

Table 4.6. RMSEE and R^2 values of univariate, multivariate and multiway tapped density and Hausner ratio models with the mean and standard deviation (SD) of actually measured properties.

	Univariate		Multivariate (PLS)		Multiway (N-PLS)		Mean	SD
	RMSEE	R^2 (%)	RMSEE	R^2 (%)	RMSEE	R^2 (%)		
Tapped density	0.0339	69	0.0279	82	0.0360	70	0.53	0.059
Hausner ratio	0.0307	46	0.0281	47	0.0268	52	1.21	0.037

4.4. CONCLUSIONS

In this study, the use of in-line SFV as PAT monitoring tool for particle growth during fluid bed granulation was evaluated. Comparison between in-line SFV and off-line LD data demonstrated that an identical trend in D_{50} values among all different monitored batches was obtained by both methods. Nevertheless, in-line-obtained granule sizes were always larger than the corresponding off-line LD results, due to the measurement method of LD. The in-line SFV data did not underestimate the actual granule size due to size segregation and no probe fouling occurred during any of the granulations. These results suggest that SFV data were reliable and representative to the actual particle size.

Analysis of the SFV and LD DoE models showed that the HPMC concentration had the most significant (positive) effect upon the granule size. The influence of the inlet air temperature during drying was smaller in comparison. The in-line SFV probe provided every 10 s particle size information, which allowed to explain and better understand the (in)significance of the studied variables upon granulation, which was not possible using the off-line LD data. The influence of the DoE variables on granule density and flow properties was explained by the results of the in-line SFV DoE model. The multivariate PLS tapped density model and the multiway N-PLS Hausner ratio model, built to assess these properties during processing, had the highest R^2 values in combination with the lowest RMSEE values.

These results suggest that the in-line SFV technology is a valuable PAT monitoring tool that is sensitive to any particle size changes during granulation and that helps to increase granulation process understanding. This indicates the potential use of the SFV technique during different stages in the development process of new drug molecules. Moreover, the continuous and rapid measurement of the particle size distribution during granulation enables to improve process quality and increase the efficiency and control of the granulation process. The results also indicate the ability to assess end granule properties based on SFV data, which can be beneficial in both development and routine production. Nevertheless, the full use of such an approach requires further testing of model performance on an independent test set as the RMSEE values may overestimate the actual model performance.

REFERENCES

- [1] S.M. Iveson, J.D. Litster, K. Hapgood, B.J. Ennis, *Powder Technology*, 117 (2001) 3-39.
- [2] Food and Drug Administration, *Guidance for Industry; PAT - A framework for innovative pharmaceutical development, manufacturing and quality assurance*, (2004)
- [3] International Conference on Harmonisation, *Guidance for Industry; Q8(R1) Pharmaceutical Development*, (2009)
- [4] S. Watano, K. Miyanami, *Powder Technology*, 83 (1995) 55-60.
- [5] S. Watano, Y. Sato, K. Miyanami, *Chemical & Pharmaceutical Bulletin*, 44 (1996) 1556-1560.
- [6] S. Watano, Y. Sato, K. Miyanami, *Advanced Powder Technology*, 8 (1997) 269-277.
- [7] S. Watano, T. Numa, K. Miyanami, Y. Osako, *Chemical & Pharmaceutical Bulletin*, 48 (2000) 1154-1159.
- [8] S. Watano, *Powder Technology*, 117 (2001) 163-172.
- [9] S. Watano, T. Numa, K. Miyanami, Y. Osako, *Powder Technology*, 115 (2001) 124-130.
- [10] T. Närvänen, K. Seppälä, O. Antikainen, J. Yliruusi, *Aaps Pharmscitech*, 9 (2008) 282-287.
- [11] P. Frake, D. Greenhalgh, S.M. Grierson, J.M. Hempenstall, D.R. Rudd, *International Journal of Pharmaceutics*, 151 (1997) 75-80.
- [12] S.G. Goebel, K.J. Steffens, *Pharmazeutische Industrie*, 60 (1998) 889-895.
- [13] W.P. Findlay, G.R. Peck, K.R. Morris, *Journal of Pharmaceutical Sciences*, 94 (2005) 604-612.
- [14] P. Luukkonen, M. Fransson, I.N. Bjorn, J. Hautala, B. Lagerholm, S. Folestad, *Journal of Pharmaceutical Sciences*, 97 (2008) 950-959.
- [15] A. Tok, X.P. Goh, W. Ng, R. Tan, *Aaps Pharmscitech*, 9 (2008) 1083-1091.
- [16] A.A. Kaddour, B. Cuq, *Powder Technology*, 190 (2009) 10-18.
- [17] X.H. Hu, J.C. Cunningham, D. Winstead, *International Journal of Pharmaceutics*, 347 (2008) 54-61.
- [18] M. Whitaker, G.R. Baker, J. Westrup, P.A. Goulding, D.R. Rudd, R.M. Belchamber, M.P. Collins, *International Journal of Pharmaceutics*, 205 (2000) 79-91.
- [19] M. Halstensen, P. de Bakker, K.H. Esbensen, *Chemometrics and Intelligent Laboratory Systems*, 84 (2006) 88-97.
- [20] J.F. Gamble, A.B. Dennis, M. Tobbyn, *Pharmaceutical Development and Technology*, 14 (2009) 299-304.
- [21] S. Matero, S. Poutiainen, J. Leskinen, K. Jarvinen, J. Ketolainen, S.P. Reinikainen, M. Hakulinen, R. Lappalainen, A. Poso, *Chemometrics and Intelligent Laboratory Systems*, 97 (2009) 75-81.
- [22] D. Petrak, *Particle & Particle Systems Characterization*, 19 (2002) 391-400.

- [23] D. Petrak, H. Rauh, *Particulate Science and Technology*, 24 (2006) 381-394.
- [24] S. Schmidt-Lehr, H.U. Moritz, K.C. Jurgens, *Pharmazeutische Industrie*, 69 (2007) 478-484.
- [25] T. Närvänen, T. Lipsanen, O. Antikainen, H. Räikkönen, J. Yliruusi, *International Journal of Pharmaceutics*, 357 (2008) 132-138.
- [26] T. Närvänen, T. Lipsanen, O. Antikainen, H. Räikkönen, J. Heinämäki, J. Yliruusi, *Journal of Pharmaceutical Sciences*, 98 (2009) 1110-1117.
- [27] T. Lipsanen, T. Narvanen, H. Raikkonen, O. Antikainen, J. Yliruusi, *Aaps Pharmscitech*, 9 (2008) 1070-1077.
- [28] Y. Vander Heyden, A. Nijhuis, J. Smeyers-Verbeke, B.G.M. Vandeginste, D.L. Massart, *Journal of Pharmaceutical and Biomedical Analysis*, 24 (2001) 723-753.

CHAPTER 5

BATCH STATISTICAL PROCESS CONTROL (BSPC) OF A FLUID BED GRANULATION PROCESS USING IN-LINE SPATIAL FILTER VELOCIMETRY AND PRODUCT TEMPERATURE MEASUREMENTS

Parts of this chapter are published in:

A. Burggraeve, T. Van Den Kerkhof, M. Hellings, J.P. Remon, C. Vervaet, T. De Beer, Batch statistical process control of a fluid bed granulation process using in-line spatial filter velocimetry and product temperature measurements, *European Journal of Pharmaceutical Sciences*, 42 (2011) 584-592.

ABSTRACT

Chapter 5 shows the multivariate statistical modeling and control of a fluid bed granulation process based on in-line particle size distribution measurements combined with continuous product temperature registrations, using a partial least squares approach.

Continuously collected particle size distribution and product temperature process data of ten reference batches (**X**-matrix) were used to develop a reference batch PLS model, regressing the **X**-data versus the batch process time (**y**-vector). Score control charts in which the average batch trajectory, and upper and lower control limits are displayed were developed. Next, these control charts were used to monitor four new test batches in real-time and to immediately detect any deviations from the expected batch trajectory. By real-time evaluation of new batches using the developed control charts and by computation of contribution plots for deviating process behavior at a certain time point, batch losses or reprocessing can be prevented. Immediately after batch completion, all collected particle size distribution and product temperature information (i.e., batch progress fingerprint) was used to estimate some granule properties (density and flowability) at an early stage, which can improve batch release time.

CHAPTER 5

BATCH STATISTICAL PROCESS CONTROL (BSPC) OF A FLUID BED GRANULATION PROCESS USING IN-LINE SPATIAL FILTER VELOCIMETRY AND PRODUCT TEMPERATURE MEASUREMENTS

5.1. INTRODUCTION

A fluid bed granulation (batch) process consists of successive spraying and drying phases to create larger permanent aggregates or granules, in which the original particles are still identifiable [1]. A batch process is generally characterized by a predefined processing of raw materials for a *finite* period of time. The granulation process itself is also complex due to many interrelated variables (such as inlet air relative humidity and temperature, fluidizing airflow rate, atomization pressure, spray rate, etc.) and it is susceptible to natural, random variations in process and formulation variables, which can cause significant batch-to-batch variations. However, a high degree of reproducibility is necessary to obtain successful batches that meet the quality requirements.

Traditionally, final product quality is assessed off-line by a number of quality evaluations on end product samples. If these end product quality properties do not meet the predefined criteria, the entire batch is rejected or reprocessed. Moreover, identification of failure cause and prevention of batch failure by real-time adjustments to the process is most difficult or even impossible when using the traditional off-line evaluation. This can be prevented through in-line measurements of critical quality properties and statistical control of the batch process. Using this approach, processing of material via fluid bed granulation is not marked by a predefined duration of time, but the endpoint of the granulation process is defined by the in-line measured end product quality.

The particle size distribution (PSD) is considered as one of the main quality attributes of a granulated product as it influences other granule properties such as density, powder flow and compression. Hence, the change in PSD during granulation gives a direct indication of the batch progress and batch quality. Several techniques have been evaluated to monitor the PSD during granulation in real-time: near infrared spectroscopy [2-8], focused beam reflectance method [5, 9, 10], spatial filter velocimetry [11-13], image analysis [14-21] and acoustic emission monitoring [5, 22-25]. Each technique has its own advantages and shortcomings. Usually, the main challenge is to find the appropriate position of probes and lenses in the process stream to perform representative measurements and to prevent fouling. Fouling is not a problem when using non-intrusive AE measurements. However, as the AE signals are usually weak, external uncontrollable factors and the fluidizing airflow rate may influence the technique's sensitivity.

In this study, spatial filter velocimetry was used in-line during top-spray fluid bed granulation to continuously obtain PSD information. The SFV technique measures simultaneously the velocity and the chord length distribution of particles as they pass through the laser light and cast a shadow onto the detector [26, 27]. Chapter 4 showed that the technique is sensitive to any particle size changes during fluid bed granulation. Hence, the sensitivity of the technique combined with the short measuring time make SFV an appropriate tool to continuously gather PSD information throughout a granulation process. SFV data were combined with a continuous registration of the product temperature to model and statistically control the fluid bed granulation process using a partial least squares approach. The 3-way data matrix [**batch** x **variable** (*in this study: PSD and product temperature*) x batch process **time**] comprising process and product information of ten reference batches (i.e., good batches) was unfolded to new matrices, suitable for PLS analysis (Figure 5.1). The resulting reference PLS model was used to indicate possible deviations from process normality and to detect the process endpoint for new in-line monitored batches (four test batches). Full PSD and product temperature information of completed granulation batches was used to estimate density and flowability at an early stage, immediately after batch production. Individual PLS models relating the computed scores (**X**) of the reference PLS model and these granule properties (**y**-vector) were built.

5.2. MATERIALS AND METHODS

5.2.1. Materials

The powder mixture used during all granulations consisted of 700 g dextrose monohydrate (Roquette Frères, Lestrem, France) and 272.5 g unmodified maize starch (Cargill Benelux, Sas van Gent, The Netherlands). The powder mass was granulated with an aqueous binder solution of 25 g HPMC (type 2910 15 mPa s, Dow Chemical Company, Plaquemine, LA, USA) and 2.5 g Tween 20 (Croda Chemicals Europe, Wilton, UK), resulting into a total solids amount of 1000 g for each batch. HPMC was always sprayed as a 4% solution.

5.2.2. Fluid bed granulation setup

Granulations were performed in a laboratory-scale fluid bed granulator (GPCG 1, Glatt, Binzen, Germany). A nozzle with a diameter of 1.2 mm was installed top-spray at a height of 26 cm from the distributor plate, and an atomization pressure of 1 bar was used during all experiments. For the ten reference batches, granulation liquid was sprayed at a rate of 16 g/min, inlet air velocity was set to 8 m/s and shaking of the filter bags was performed every 45 s for a period of 7 s. The inlet air temperature during spraying and drying was 45 °C and 60 °C, respectively. Granules were dried until an outlet air temperature of 37 °C and a product temperature of 45 °C was obtained.

A spatial filter velocimetry probe (Parsum IPP 70; Gesellschaft für Partikel-, Strömungs- und Umweltmesstechnik, Chemnitz, Germany) was installed in the fluid bed granulator at a height of 20 cm from the distributor plate and at approximately 5 cm from the sidewall of the granulator. Particles passed through an aperture with 4 mm diameter and a pressurized air connection was used to disperse the particles and prevent fouling of the measurement zone. Measured raw data were collected via an A/D converter. The software (In-line Particle Probe V7.12a) operated in the Windows XP environment. The experimental setup and software settings were based on the results described in Chapter 4.

During the entire top-spray granulation processes, an average PSD was saved every 10 s and product temperature values were registered every minute. The batch model was developed using the PSD and product temperature values continuously obtained during processing of the reference batches (i.e. ten batches with identical process and formulation settings; see Section 5.2.4). Four test batches (TB A-D) were granulated to evaluate the batch process model (Table 5.1). The process settings of TB B-D deviated from the reference batches and represented typical errors occurring during fluid bed granulation processes. For example, the blockage of tubing was simulated by interruption of liquid spraying and overwetting of granules was simulated by the use of a higher feed rate.

Table 5.1. Granulation conditions for test batches A, B, C, and D.

Name batch	Granulation conditions
TB A	Identical conditions as reference batches.
TB B	Spraying of granulation liquid was stopped during 1 min.
TB C	Spraying of granulation liquid was stopped during 9 min.
TB D	Rate of spraying granulation liquid was increased to 21 g/min.

5.2.3. Characterization of granules

After manufacturing, the bulk density, tapped density and Hausner ratio of each batch were determined.

Approximately 30-g samples were gently poured into a 100 mL graduated cylinder. The granule weight and volume were used to calculate bulk density. Next, each sample was tapped 1250 times using an automatic tapper (J. Engelsmann AG, Ludwigshafen am Rhein, Germany) and the new volume was used to determine the tapped density. All density measurements were performed in triplicate and the average density was calculated. Bulk and tapped densities were used to determine powder flow characteristics via calculation of Hausner ratio values.

5.2.4. Development of batch model

The batch process model was developed and evaluated using the SIMCA-P+ software (Version 12.0.1, Umetrics, Umeå, Sweden).

During each granulation process, J variables (i.e., product temperature and size percentiles D_{01} , D_{10} , D_{25} , D_{50} , D_{63} , D_{75} , D_{90} , D_{99}) were measured at K time points. Consequently, a set of N batches resulted into a 3-way granulation data matrix \mathbf{X} with dimensions $N \times J \times K$ (Figure 5.1, left).

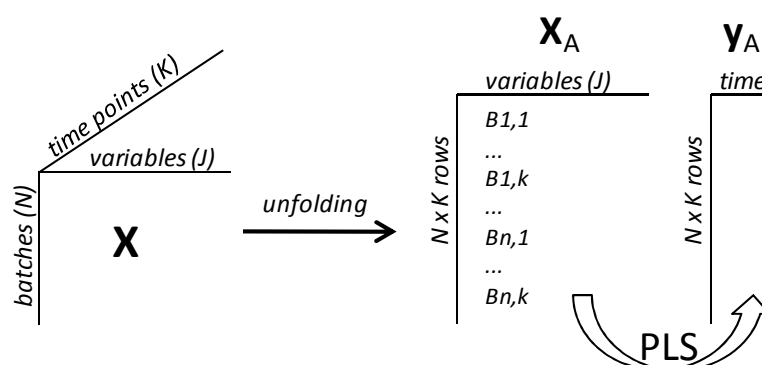


Figure 5.1. Schematic overview of the unfolding of the 3-way batch data matrix preserving variable direction.

Initially, the 3-way batch data matrix was unfolded in such a way that the direction of the J variables was preserved. In the resulting 2-way matrix \mathbf{X}_A (Figure 5.1, middle), the batch and time dimensions are combined, creating a matrix with $N \times K$ observations (rows) and J variables (columns). Hence, each row in \mathbf{X}_A represents the data of batch N at time point K for variable J . A dummy \mathbf{y}_A -vector having a length of $N \times K$ and expressing the local batch time was autogenerated by the software. Partial least squares regression was performed relating \mathbf{X}_A and \mathbf{y}_A . The correct number of PLS components was based on cross validation, using the approach of Krzanowski [28]. The value of local time predicted by the reference PLS model indicates the maturity of a batch (i.e., how far the batch has evolved over time).

In a next step, score control charts were established to identify the characteristic trajectory of a reference batch. These charts were then used to monitor the evolution of the test batches in real-time.

The score control charts were developed by rearranging the scores of each PLS component (PLSC), resulting in a new matrix per PLS component in which each row corresponds to the scores of one batch (Figure 5.2, left: \mathbf{X}_{A1} , \mathbf{X}_{A2} , ...). Consequently, these matrices have N rows and K columns. From these matrices the averages and standard deviations (SD) of each series of scores (each column) were calculated (Figure 5.2, right). Hence, score control charts were obtained for each PLS component with control intervals set to average ± 3 SD [29]. The use of 3 SD ensures that 99.7% of the variation in the accepted reference batches lies within the control limits. The data of the four test batches (Table 5.1) were then projected onto the reference PLS model, allowing the computation of their respective score values. These score values were plotted in the control charts and the quality of the test batch trajectory was compared to the trajectories of the reference batches (i.e., score trajectory is within or outside the control interval).

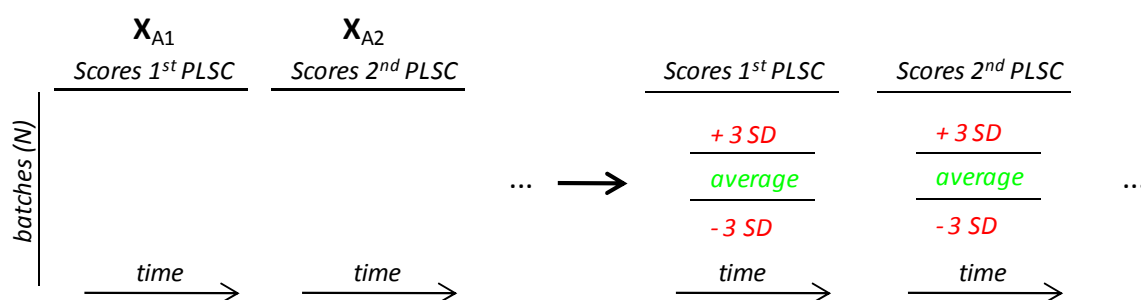


Figure 5.2. Schematic overview of the PLS scores rearrangement, shown for the first 2 PLS components (PLSC), with the calculation of averages and standard deviations (SD) to develop score control charts.

After granulation completion, all PSD and product temperature data collected during the production of the ten reference batches were used to make a principal component analysis model. However, instead of the original measured PSD and product temperature values, the scores of the reference batch PLS model (\mathbf{X}_B -matrix) were used (Figure 5.3). PSD and product temperature information gathered during processing of the four test batches were used as a prediction set. In that way, the quality of the test batches could be determined (i.e. batch acceptance or rejection).

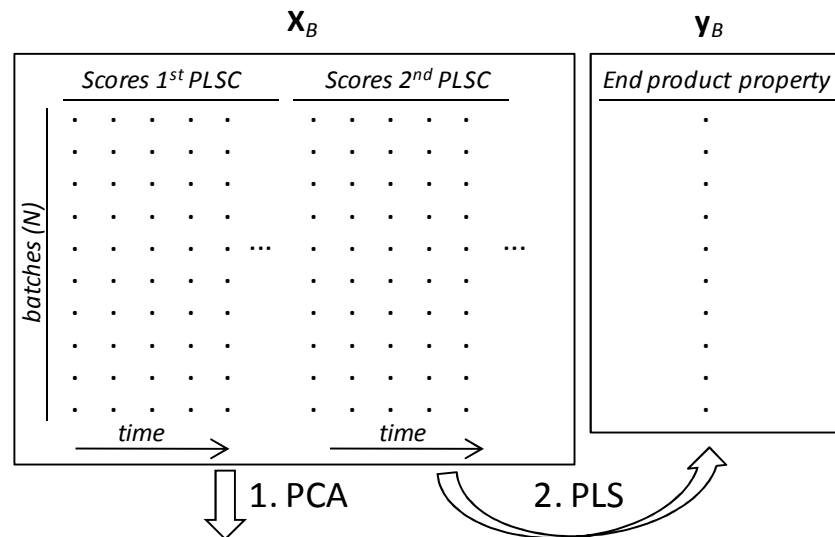


Figure 5.3. Schematic overview of the scores rearrangement to model whole batches. Initially, PCA was performed on \mathbf{X}_B and in a next step PLS analysis was used to regress the \mathbf{X}_B -matrix to end product properties contained in the \mathbf{y}_B -vector.

Finally, PLS regression was performed to relate the measured process information (\mathbf{X}_B) to three end product characteristics (i.e., bulk density, tapped density and Hausner ratio; \mathbf{y}_B), hence allowing to predict the final product quality of new batches from the PSD and product temperature evolution during granulation. In that way, time-consuming off-line analysis might become unnecessary.

5.3. RESULTS AND DISCUSSION

5.3.1. Real-time batch progress evaluation

The training set consisting of the in-line collected PSD and product temperature data for ten reference batches was unfolded and the resulting 2-way \mathbf{X}_A -matrix was regressed versus the batch process time (\mathbf{y}_A -vector) using PLS (Figure 5.1). A reference model with two significant PLS components was developed corresponding to an R^2X (cum) = 0.99 and Q^2 (cum) = 0.97. The R^2X value expresses that 99% of the variation in \mathbf{X}_A was captured by the model. The significance of Q^2 (goodness of prediction) should not be overestimated as the \mathbf{y}_A -vector was artificially generated. The PLS score scatter plot of the 2-component reference PLS model (Figure 5.4) demonstrates that all reference batches had a similar score trajectory. Hence, no deviating reference batches were detected.

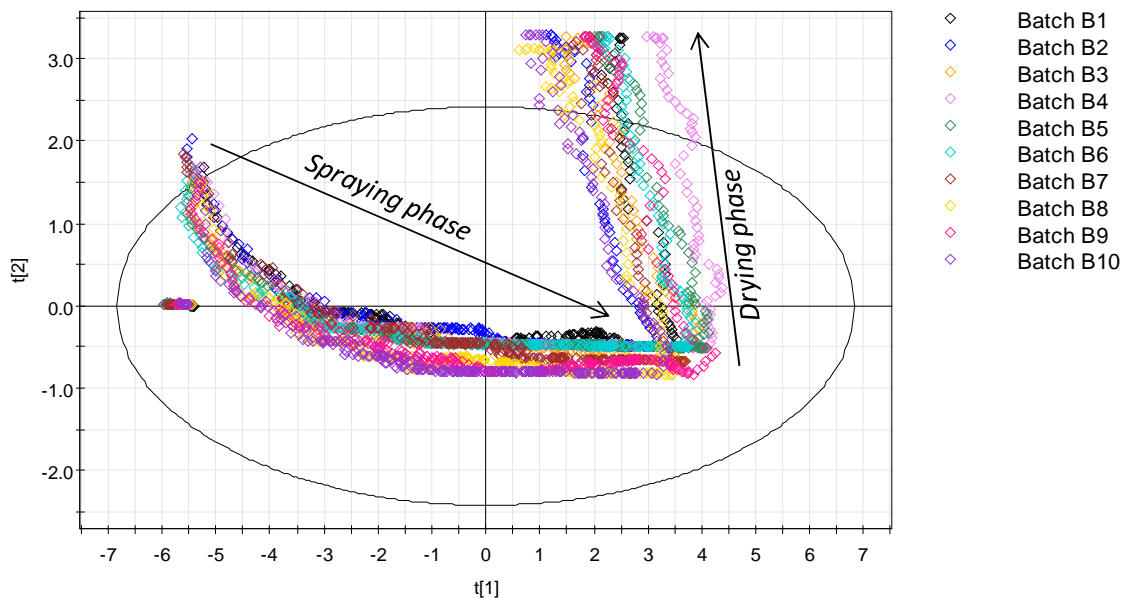


Figure 5.4. PLS t_1/t_2 score scatter plot of the reference PLS model for all ten reference batches.

The scores of all reference batches initialized in the upper left quadrant (negative t_1 , positive t_2) and finished in the upper right quadrant (positive t_1 , positive t_2). In addition, the plot shows that the first PLS component reflected the PSD evolution of a normal batch in function of time: growth (increase in t_1 value) and attrition (decrease in t_1 value) of granules. The second component described the difference between the spraying and the drying phase. During spraying, the product temperature decreased until it reached a minimum value (22°C-23°C). Subsequently, during drying the product temperature increased. This interpretation of the two PLS components was confirmed by the corresponding loading plots (Figure 5.5a and b shows the loading column plot for the first and second

PLS component, respectively). All particle size fractions contributed strongly to the first component, while the product temperature only contributed to the second component.

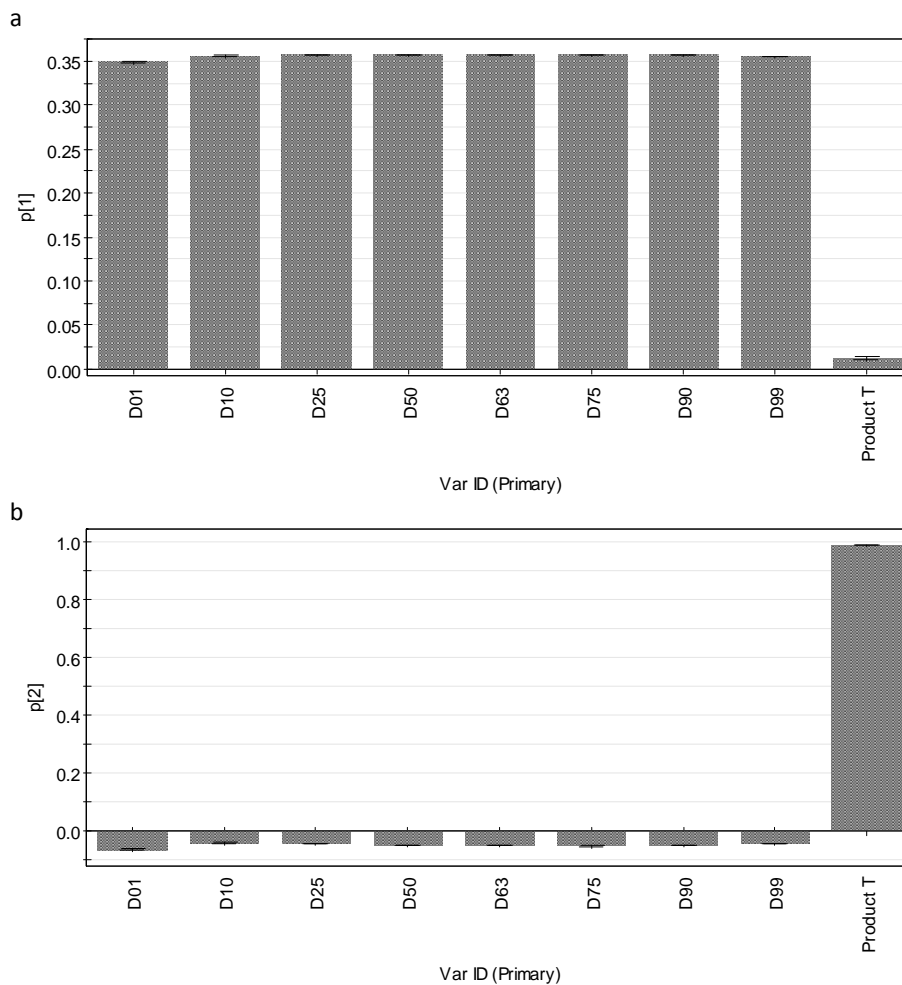


Figure 5.5. Loading column plot of the first (a) and second (b) PLS component.

In a next step, the scores of the reference model were rearranged to develop score control charts for each PLS component, in which the average batch trajectory with an upper and lower control limit in function of process time is displayed (Section 5.2.4 and Figure 5.2). The scores of all training set batches lay between the calculated control limits in the resulting control charts (Figure 5.6a and b), confirming previous results that there were no outliers in the set of reference batches. A clear distinction between the spraying and drying period is visible in both charts.

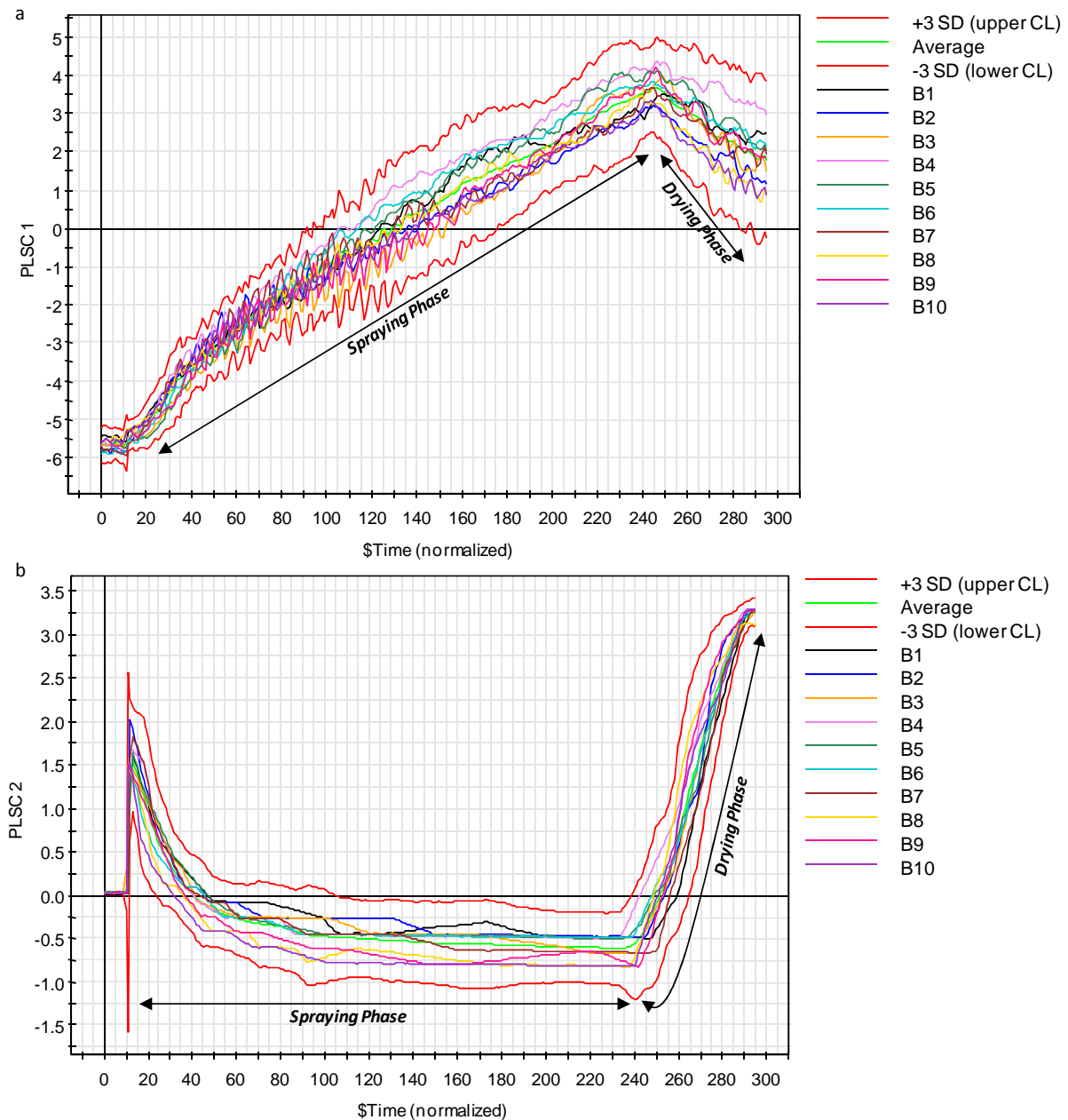


Figure 5.6. Batch control charts for PLSC 1 (a) and PLSC 2 (b). The average batch trajectory, the upper and lower control limits (CL) and the observed trajectories of the ten reference batches (B1-B10) are shown.

The established reference PLS model was then used to monitor the evolution of four test batches (Table 5.1), and the resulting score control charts are displayed in Figure 5.7a-d. In these charts, score values of completed test batches are shown. In practice however, the calculated scores of ongoing batches can be projected in real-time into these plots even though all data has not yet been collected.

Test batch A was performed under identical conditions as the reference batches. The scores of this batch behaved similar to the average score values of the reference batches and were hence within

the set control limits in each score control chart throughout the whole process (black line in Figure 5.7a and c).

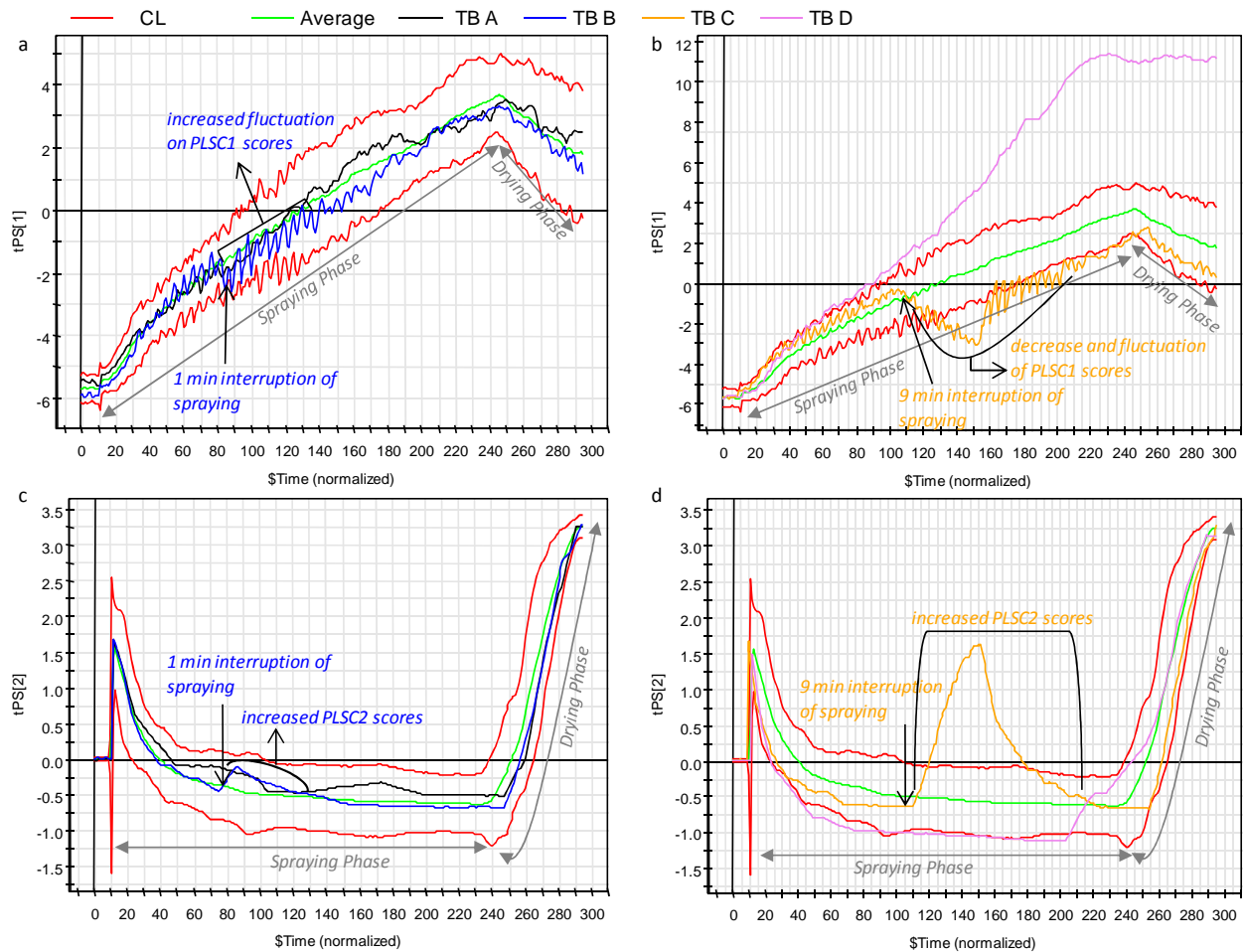


Figure 5.7. Batch prediction control charts for PLSC 1 (a and b) and PLSC 2 (c and d). The average batch trajectory, the upper and lower control limits (CL) and the predicted trajectories of the four test batches (TB A-D) are shown. TB A and TB B are displayed in (a) and (c). TB C and TB D are displayed in (b) and (d).

The pump used for spraying of the granulation liquid was stopped for 1 and 9 min during the spraying phase of **test batch B and C**, respectively, hence simulating a blockage of the tubing. For **test batch B**, this resulted into an immediate fluctuation of the PLSC1 scores (blue line in Figure 5.7a) and an increase in PLSC2 scores (blue line in Figure 5.7c). When interrupting the spraying of the granulation liquid, the already shaped agglomerates dried and created fines due to attrition of the granules. As the fines were trapped in the filter bags, these small particles were released when the bags were shaken every 45 s, which caused a drop in particle size value and hence more fluctuations of PLSC1 scores. Furthermore, due to drying of the granules during the interruption of spraying, the product temperature increased resulting in higher PLSC2 scores. When liquid spraying was restarted after 1 min, the fines adhered to larger granules resulting in less fluctuations in particle size (i.e., PLSC1 scores, Figure 5.7a) and a lower product temperature (i.e., PLSC2 scores, Figure 5.7c). During the

next stage of the spraying phase and the subsequent drying phase, the scores for both components were similar to the average trajectory and the influence of a 1 min liquid feeding interruption was negligible at the end of the granulation process. The scores of **test batch C** (interruption of liquid spraying for 9 min) showed a similar pattern: fluctuation on PLSC1 scores (orange line in Figure 5.7b) and an increase in PLSC2 scores (orange line in Figure 5.7d). However, the scores for both components progressed outside the control limits. When spraying was restarted after 9 min, the agglomeration process continued and the PLSC1 and PLSC2 scores evolved towards the average trajectory. At the end of the granulation process, PLSC1 scores were close to the lower control limit, indicating a batch of low quality. During the 9 min pause of liquid feeding, the PSD of the granules decreased extensively. Although a total identical amount of liquid was sprayed compared to the reference batches, this was not sufficient to ensure a similar particle size at the end of the granulation process. If this phenomenon would occur during routine production, it could possibly be prevented by increasing the amount of binder liquid sprayed onto the powder bed or increasing the granulation feed rate until PLSC1 scores similar to the average values of the reference batches are obtained [13]. Based on the PLSC2 scores, this batch showed a normal drying period.

The liquid feed rate of **test batch D** was increased to 21 g/min. Already during the early stages of the process the PLSC1 and PLSC2 scores were outside the control interval, and throughout the entire granulation process the PLSC1 scores were above the upper control limit (pink line in Figure 5.7b and d). At a higher liquid addition rate, liquid saturation of the powder bed increased (consequently the growth rate of the granules was faster, as reflected in the PLSC1 scores) and the granule temperature was lower (as reflected in the PLSC2 scores) compared to the average batch trajectory. The higher feed rate created granules with more liquid bridges and with stronger cohesive forces which prevented breakage of the granules during drying (constant PLSC1 scores during drying phase, Figure 5.7b). As binder liquid was sprayed at a faster rate, drying of granules initiated earlier and due to the higher moisture content, drying extended over a longer period.

Evaluation of test batches data using the score control charts showed that the developed PLS model allowed the real-time detection of deviations from the normal batch trace. Even when the granulation feeding was interrupted during a single minute, this problem was instantly detected in both control charts, hence permitting early fault diagnosis.

In this study, particle size and product temperature information were gathered during processing, which resulted in a 2-PLS-component model describing 99% of the variation in the process data. However, when monitoring more variables in complex systems (e.g., during fluid bed granulation: pressure difference over the filter; temperature, relative humidity and flow rate of inlet/outlet air), the use of a larger number of PLS components might be needed to model the evolution of the

batches. As the use of many individual score control charts might then become cumbersome, a statistic called Hotelling's T^2 can be calculated enabling to monitor and evaluate the overall performance of a new batch with a single chart. In the Hotelling's T^2 plot the distance from the origin in the score space of the reference PLS model for each selected observation of a test batch is displayed, and the T^2 values are calculated for the 2 PLS components selected. Figure 5.8a and b displays the corresponding Hotelling's T^2 plots for test batches A-B and C-D, respectively. The average reference batch trajectory is displayed in green and deviations can be immediately detected. The 95% confidence limit was not exceeded for test batch A, and only for a limit time period for test batch B, indicating that no deviations for PSD and product temperature (compared to the reference batches) were measured during processing of these test batches. In contrast, in the Hotelling's T^2 plot of test batch C and D, T^2 values differed significantly from the T^2 values of the reference model (similar observations based on the score control charts, Figure 5.7b and d). Hence, PLS score control charts and Hotelling's T^2 plots can both be used to monitor new batches. Based on these different types of charts, same observations can be made. The choice of chart type depends on the examiner's preference.

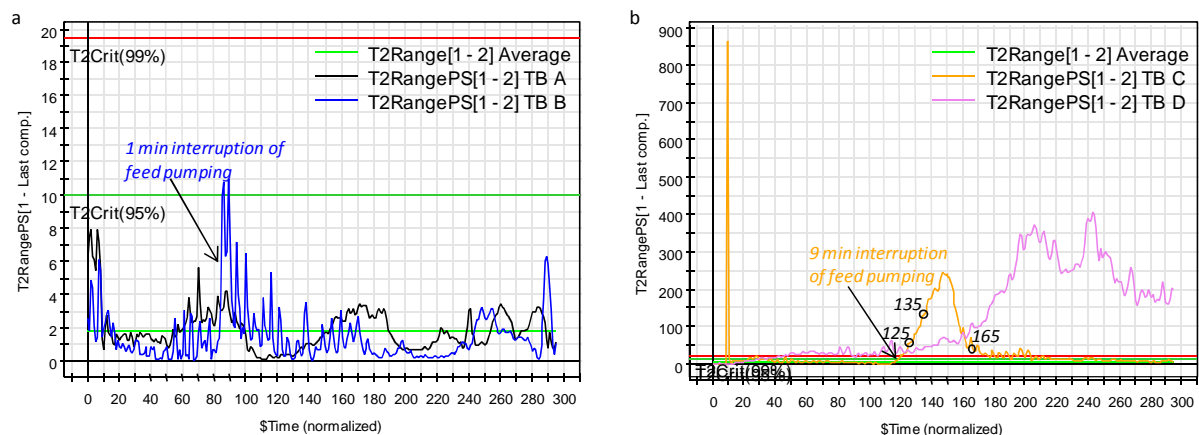


Figure 5.8. Hotelling's T^2 plot for test batches TB A-TB B (a) and TB C-TB D (b), respectively.

When detecting deviations from the normal batch trajectory in the Hotelling's T^2 plot, it is possible to identify the monitored variable(s) responsible for this difference through the computation of contribution plots [30]. A contribution plot displays the differences between the outlying observation and average observation for each **monitored** variable **in the model**. Information from a previously performed design of experiments can then sometimes be used to correctly adjust process variables and lead the scores towards the average direction. The use of contribution plots is exemplified in Figure 5.9a-c for test batch C. At time point 125 (Figure 5.9a) both PSD and product temperature showed a similar deviation from the average observation due to the interruption of spraying prior to this time point. One minute and 40 s later (time point 135, Figure 5.9b), the

deviation was mainly determined by the high product temperature. After restarting the liquid spraying (time point 165, Figure 5.9c), the product temperature recovered rapidly to the average observation while not all fines could adhere to the larger granules.

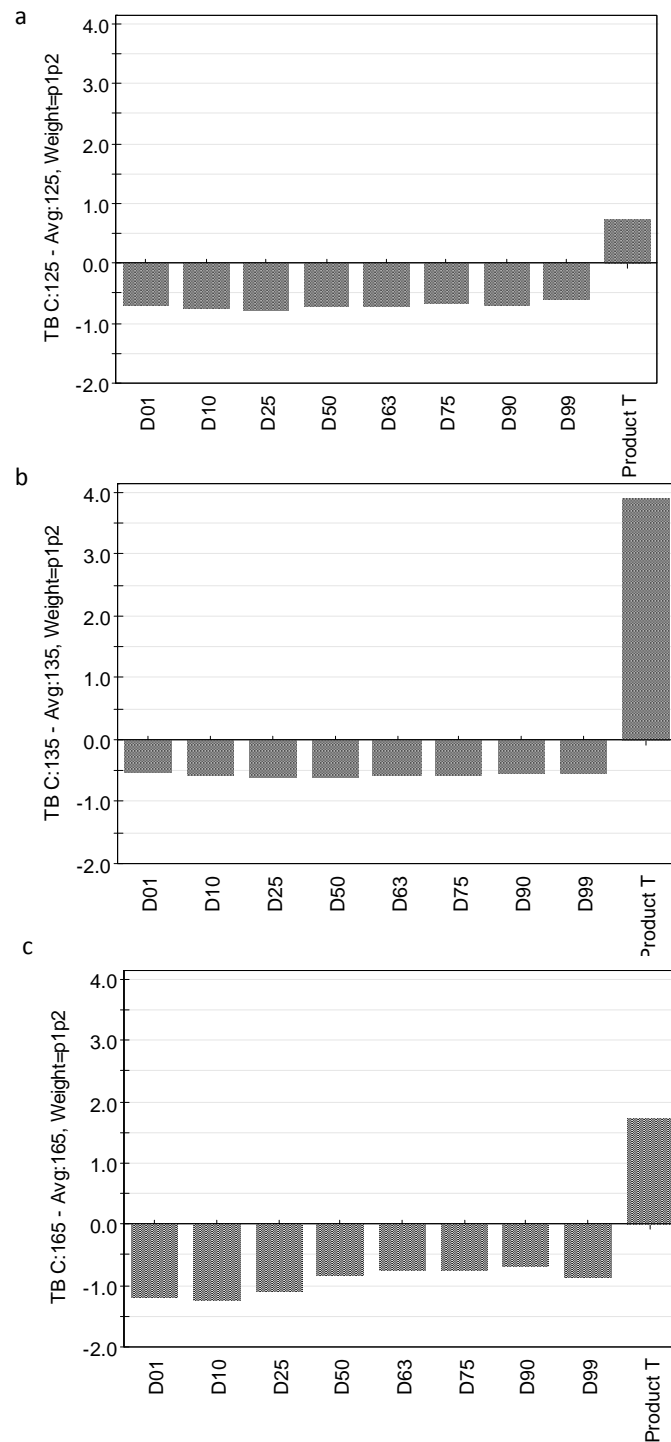


Figure 5.9. Batch contribution plots of how test batch C and the average batch differ at time points 125 (a), 135 (b) and 165 (c), respectively.

In Chapter 4, the influence of process and formulation variables upon the PSD of this formulation was studied in a DoE, which showed that the amount of HPMC had a positive effect upon granule size. A possible action to prevent batch failure due to the large amount of fines, might for example be to spray more HPMC until the scores correspond to the average value. In practice, the granulation kinetics should also be taken into consideration as they might be influenced by the addition of larger HPMC amounts.

5.3.2. Evaluation of completed batches

The scores of the reference PLS model (modeling the ten reference batches, Section 5.3.1) were rearranged to form a new \mathbf{X}_B -data matrix consisting of 10 rows and 2 PLSC x time columns (\mathbf{X}_B matrix, Figure 5.3). Hence, each row corresponded to one batch. Without the use of an external \mathbf{y} -variable, principal component analysis was performed on the \mathbf{X}_B -data block. The resulting PCA model consisted of three principal components, capturing 77% of the total batch process variation. The PCA score plot shows a homogeneous distribution among the ten reference batches (Figure 5.10, B1-B10) indicating the absence of any deviating batches among the reference set. The developed PCA batch model was then used to classify the four test batches. Figure 5.10 indicates that two test batches (TB A and B) were within the confidence ellipse at a significance level of 0.05 and thus of a quality similar to the reference batches. Test batches C and D were outside the confidence ellipse, having a minor product quality. Based on the score control charts in Figure 5.7a-d, similar conclusions were made for test batches A, B and D. In both score control charts, the scores of test batch C were at the end of the process within the control interval. However, based on the whole batch performance, the final batch quality is unacceptable.

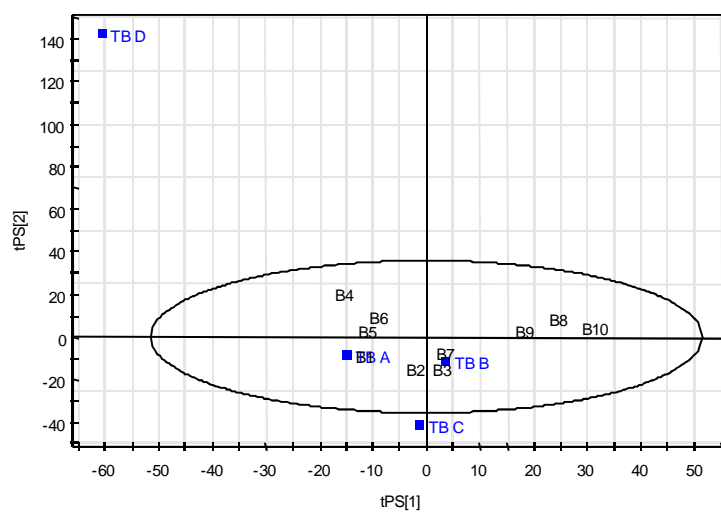


Figure 5.10. PCA score plot showing the distribution of completed reference (B1-B10) and test batches (TB A-TB D) with a confidence ellipse at significance level 0.05.

The granule quality attributes bulk density, tapped density and Hausner ratio were determined after completion of each reference and test batch. Individual PLS models were developed to relate the reference X_B -data matrix to these final product characteristics as response variables (Figure 5.3). These models were then used to predict the final product characteristics of the test batches (Table 5.2) based on their in-line collected PSD and product temperature information. Models with prediction errors of 0.034 g/mL, 0.036 g/mL and 0.022 for bulk density, tapped density and Hausner ratio were established. The final product bulk density, tapped density and Hausner ratio of test batches A and B were similar to the quality of the reference batches and showed a good predictability by the PLS model. The trajectory of test batches C and especially D deviated from the reference batches. Hence, the difference between the measured and predicted granule properties was larger for these batches. This use of PLS to relate monitored process and product values of **good** batches (good/bad classification based on previous score trajectories (Figure 5.7 and 5.8) and PCA (Figure 5.10)) to end product characteristics allows the early estimation of these properties immediately after production.

Table 5.2. End product particle size distribution (PSD), measured and predicted bulk density, tapped density and Hausner ratio according to whole batch PLS model for reference and test batches. Standard deviations were calculated for 3 replicates.

Batch	PSD (μm)			Bulk density (g/ml)		Tapped density (g/ml)		Hausner ratio	
	D10	D50	D90	measured	predicted	measured	predicted	measured	predicted
B1	150	293	510	0.425 \pm 0.009	0.425	0.511 \pm 0.008	0.510	1.203	1.204
B2	139	268	445	0.370 \pm 0.003	0.368	0.447 \pm 0.002	0.445	1.208	1.202
B3	137	283	481	0.390 \pm 0.004	0.391	0.472 \pm 0.001	0.476	1.211	1.216
B4	167	313	538	0.399 \pm 0.003	0.396	0.470 \pm 0.003	0.467	1.179	1.178
B5	147	295	492	0.387 \pm 0.001	0.396	0.473 \pm 0.004	0.480	1.222	1.218
B6	152	294	488	0.391 \pm 0.001	0.388	0.468 \pm 0.005	0.466	1.199	1.203
B7	145	288	486	0.377 \pm 0.001	0.376	0.455 \pm 0.002	0.455	1.208	1.205
B8	129	261	444	0.411 \pm 0.003	0.409	0.492 \pm 0.006	0.490	1.198	1.199
B9	142	288	482	0.415 \pm 0.003	0.410	0.496 \pm 0.001	0.491	1.195	1.198
B10	131	259	435	0.394 \pm 0.006	0.399	0.477 \pm 0.003	0.482	1.209	1.207
TB A	148	290	515	0.425 \pm 0.005	0.420	0.511 \pm 0.006	0.505	1.203	1.198
TB B	99	223	413	0.390 \pm 0.001	0.379	0.478 \pm 0.002	0.462	1.224	1.215
TB C	97	222	408	0.383 \pm 0.005	0.330	0.472 \pm 0.003	0.407	1.231	1.211
TB D	275	513	849	0.456 \pm 0.009	0.507	0.525 \pm 0.002	0.563	1.151	1.111

5.4. CONCLUSIONS

The objective of this study was to model and control a fluid bed granulation process based on in-line particle size distribution measurements combined with continuous product temperature registrations.

A PLS model of ten reference batches allowed to evaluate the process and product quality of four new test batches. In the developed control charts, the scores of complete batches were shown. However, in practice these control charts can be used for ongoing batches, even though all data have not yet been collected. As the reference model was sensitive to small process deviations, the presented approach of real-time monitoring a fluid bed granulation process allows early fault detection. This tool can be used to improve process efficiency and to reduce batch reprocessing and/or batch loss.

The use of full batch information after batch completion allowed to estimate important product characteristics (i.e., density and flowability) at an early stage. This may reduce the lag period between the end of the granulation process and downstream processing, when granules are held for laboratory testing.

REFERENCES

- [1] S.M. Iveson, J.D. Litster, K. Hapgood, B.J. Ennis, *Powder Technology*, 117 (2001) 3-39.
- [2] P. Frake, D. Greenhalgh, S.M. Grierson, J.M. Hempenstall, D.R. Rudd, *International Journal of Pharmaceutics*, 151 (1997) 75-80.
- [3] S.G. Goebel, K.J. Steffens, *Pharmazeutische Industrie*, 60 (1998) 889-895.
- [4] P. Luukkonen, M. Fransson, I.N. Bjorn, J. Hautala, B. Lagerholm, S. Folestad, *Journal of Pharmaceutical Sciences*, 97 (2008) 950-959.
- [5] A. Tok, X.P. Goh, W. Ng, R. Tan, *Aaps Pharmscitech*, 9 (2008) 1083-1091.
- [6] A.A. Kaddour, B. Cuq, *Powder Technology*, 190 (2009) 10-18.
- [7] M. Alcalá, M. Blanco, M. Bautista, J.M. Gonzalez, *Journal of Pharmaceutical Sciences*, 99 (2010) 336-345.
- [8] W.P. Findlay, G.R. Peck, K.R. Morris, *Journal of Pharmaceutical Sciences*, 94 (2005) 604-612.
- [9] X.H. Hu, J.C. Cunningham, D. Winstead, *International Journal of Pharmaceutics*, 347 (2008) 54-61.
- [10] J. Huang, G. Kaul, J. Utz, P.W. Hernandez, V., D. Bradley, A. Nagi, D. O'Grady, *Journal of Pharmaceutical Sciences*, 99 (2010) 3205-3212.
- [11] T. Lipsanen, T. Narvanen, H. Raikkonen, O. Antikainen, J. Yliruusi, *Aaps Pharmscitech*, 9 (2008) 1070-1077.
- [12] T. Närvänen, T. Lipsanen, O. Antikainen, H. Räikkönen, J. Heinämäki, J. Yliruusi, *Journal of Pharmaceutical Sciences*, 98 (2009) 1110-1117.
- [13] T. Närvänen, T. Lipsanen, O. Antikainen, H. Räikkönen, J. Yliruusi, *International Journal of Pharmaceutics*, 357 (2008) 132-138.
- [14] N. Laitinen, O. Antikainen, J. Rantanen, J. Yliruusi, *Journal of Pharmaceutical Sciences*, 93 (2004) 165-176.
- [15] T. Närvänen, K. Seppälä, O. Antikainen, J. Yliruusi, *Aaps Pharmscitech*, 9 (2008) 282-287.
- [16] S. Watano, *Powder Technology*, 117 (2001) 163-172.
- [17] S. Watano, K. Miyanami, *Powder Technology*, 83 (1995) 55-60.
- [18] S. Watano, T. Numa, K. Miyanami, Y. Osako, *Chemical & Pharmaceutical Bulletin*, 48 (2000) 1154-1159.
- [19] S. Watano, T. Numa, K. Miyanami, Y. Osako, *Powder Technology*, 115 (2001) 124-130.
- [20] S. Watano, Y. Sato, K. Miyanami, *Chemical & Pharmaceutical Bulletin*, 44 (1996) 1556-1560.
- [21] S. Watano, Y. Sato, K. Miyanami, *Advanced Powder Technology*, 8 (1997) 269-277.
- [22] J.F. Gamble, A.B. Dennis, M. Tobbyn, *Pharmaceutical Development and Technology*, 14 (2009) 299-304.

- [23] M. Halstensen, P. de Bakker, K.H. Esbensen, *Chemometrics and Intelligent Laboratory Systems*, 84 (2006) 88-97.
- [24] S. Matero, S. Poutiainen, J. Leskinen, K. Jarvinen, J. Ketolainen, S.P. Reinikainen, M. Hakulinen, R. Lappalainen, A. Poso, *Chemometrics and Intelligent Laboratory Systems*, 97 (2009) 75-81.
- [25] M. Whitaker, G.R. Baker, J. Westrup, P.A. Goulding, D.R. Rudd, R.M. Belchamber, M.P. Collins, *International Journal of Pharmaceutics*, 205 (2000) 79-91.
- [26] D. Petrak, *Particle & Particle Systems Characterization*, 19 (2002) 391-400.
- [27] D. Petrak, H. Rauh, *Particulate Science and Technology*, 24 (2006) 381-394.
- [28] H. Eastment, W. Krzanowski, *Technometrics*, 24 (1982) 73-77.
- [29] W. Shewhart, *Economic control of quality of manufactured product*, Van Nostrand, Princeton, N.J., 1931.
- [30] S. Wold, N. Kettaneh, H. Friden, A. Holmberg, *Chemometrics and Intelligent Laboratory Systems*, 44 (1998) 331-340.

CHAPTER 6

DEVELOPMENT OF A FLUID BED GRANULATION PROCESS CONTROL STRATEGY BASED ON REAL-TIME PROCESS AND PRODUCT MEASUREMENTS

Parts of this chapter are published in:

A. Burggraeve, A.F.T. Silva, T. Van Den Kerkhof, M. Hellings, C. Vervaet, J.P. Remon, Y. Vander Heyden, T. De Beer, Development of a fluid bed granulation process control strategy based on real-time process and product measurements, *Talanta*, (2012) <http://dx.doi.org/10.1016/j.talanta.2012.07.054>

ABSTRACT

Chapter 6 describes the results of three case studies conducted consecutively, in order to develop a process control strategy for a top-spray fluid bed granulation process. The use of several real-time particle size (i.e., spatial filter velocimetry and focused beam reflectance measurement) and moisture (i.e., near infrared and Lighthouse near infrared spectroscopy) analyzers was evaluated. A feed-forward process control method was developed, where in-line collected granulation information during the process spraying phase was used to determine the optimum drying temperature of the consecutive drying phase. Via real-time monitoring of process and product parameters during the spraying period, the batch bulk density was predicted at the end of the spraying cycle, using a PLS model. When this predicted bulk density was not meeting the desired value, the developed control method allowed the calculation of an adjusted drying temperature leading to the desired batch bulk density at the end of the granulation process. Besides the development of the feed-forward control strategy, a quantitative PLS model for in-line moisture content prediction of the granulated end product was built using the NIR data. Herewith, the sampling performance of a conventionally designed diffuse reflectance NIR probe was compared to a Lighthouse NIR probe.

CHAPTER 6

DEVELOPMENT OF A FLUID BED GRANULATION PROCESS CONTROL STRATEGY BASED ON REAL-TIME PROCESS AND PRODUCT MEASUREMENTS

6.1. INTRODUCTION

Fluid bed granulation has extensively been used in the pharmaceutical industry since Wurster proposed the agglomeration process for pharmaceutical applications over five decades ago [1, 2]. Top-spray fluid bed granulation entails the suspension of powder particles in an air stream and spraying a binder liquid from the top down (counter-current to the fluidizing air) onto the fluidized bed. In that way, moistened particles collide with each other, agglomerate and form granules. After spraying the required amount of granulation liquid (spraying phase), the product is dried inside the fluid bed granulator until a pre-set exhaust air temperature is achieved corresponding to the desired moisture level (drying phase). Similar to all other wet (or dry) granulation processing techniques, the main objectives of fluid bed granulation are to improve the flow characteristics of a powder mixture, to decrease dustiness and/or to prevent mixture segregation. It is a complex process as many interrelated parameters influence the granule properties and consequently the quality of the resulting tablets.

Traditionally in pharmaceutical batch manufacturing, the critical quality attributes of the end product are assessed via off-line laboratory testing. Depending on the outcome of these tests, the batches are labeled as in- or out-of-specification products and are released or discarded. A more efficient way of operating consists of in-process quality assessments based on timely measurements, offering real-time quality evaluation of intermediate and end products. The PAT framework initiated by the FDA encourages to move from off-line laboratory tests to timely measurements executed directly in or near the process environment [3]. Off-line measurements should be replaced by at-line, on-line or

in-line measurements. The control of fluid bed granulation processes conventionally consists of monitoring process parameters (e.g., process air flow, volume, humidity) [4]. The progress of drying is determined by the outlet air and granule bed temperature combined with the drying time. Fluid bed granulation endpoint is reached when a pre-set exhaust air temperature is obtained. However, also direct product property measurements (e.g., moisture, particle size distribution, material solid-state) should be considered.

Both spatial filter velocimetry [5-14] and focused beam reflectance measurement [15-17] are able to record in real-time any changes to the particle size and its distribution during granulation. These sizing techniques provide a picture of granule growth and breakage as a function of granulation time by measurement of the particle chord lengths. The measuring principle of SFV consists of an extended spatial filter method based on the shadows created onto a detector by the movement of particles through a laser beam [18, 19]. From these shadows, the particle chord length distribution and velocity are simultaneously extracted. FBRM uses the laser beam light backscattered into the probe when the beam crosses the surface of a particle [20, 21]. Multiplication of the duration of each reflection by the known velocity of the scanning beam results into a chord length measurement. Both techniques do not require any calibration. Whereas the FBRM C35 probe is equipped with a mechanical scraper on the sapphire measurement window to prevent probe fouling, the SFV probe utilizes a pressurized air connection to keep the measurement windows clean and disperse the particles.

The binder liquid addition and distribution affect the granule bed moisture level during granulation, contributing to the agglomeration process. The end product residual moisture content influences directly the granule properties, the subsequent post-granulation process steps (e.g., tableting) and the product stability during storage. Near infrared spectroscopy is highly suitable to evaluate moisture in-line during granulation [22, 23]. As primarily vibrations of C-H, O-H, S-H and N-H bonds are observed, water exhibits strong absorption bands in an NIR spectrum. NIR measurements are non-destructive and the instrumentation exhibits a high measurement speed and robustness. Besides chemical product information, NIR spectroscopy is also sensitive to physical (e.g., particle size) sample properties which are both quantitatively and qualitatively interpretable [24, 25]. Hence, NIR spectroscopy has been extensively used for in-line fluid bed granulation monitoring [8, 26-28], determination of (end product) moisture content [8, 24, 26, 27, 29-36] and/or granule size [24, 26, 29, 31].

This chapter describes the results of three case studies conducted consecutively, in order to develop a process control strategy for a top-spray fluid bed granulation process. Figure 6.1 displays the experimental setups for the three case studies.

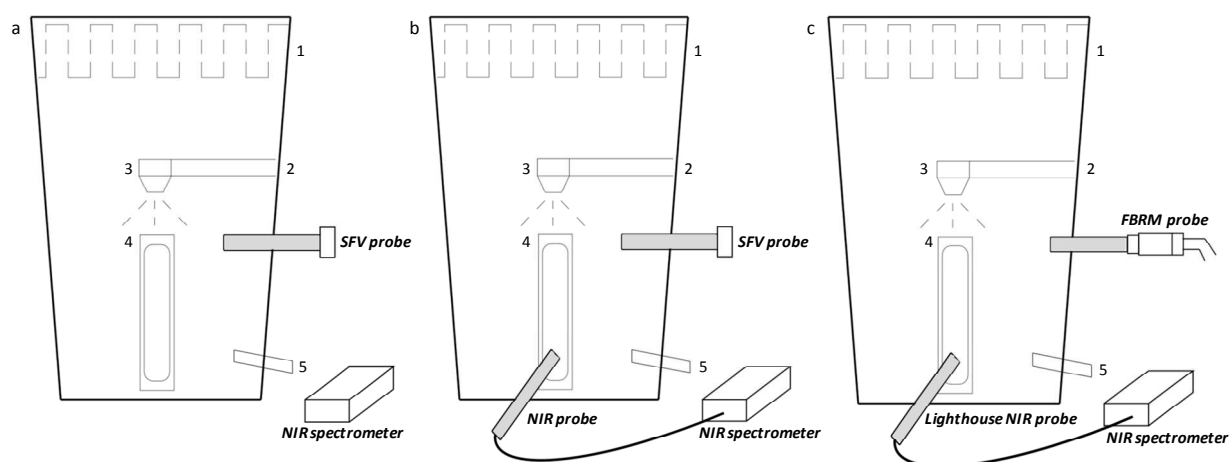


Figure 6.1. Front view schematic of the experimental setup in case studies A (a), B (b) and C (c). Standard components of the fluid bed equipment are indicated by numbers: filter bags (1), spray arm (2), spray nozzle (3), front window (4), sample thief (5).

Real-time granule size distribution information was provided via the implementation of an SFV probe directly into the process environment in case studies A and B, while in case study C an FBRM probe was (identically) installed in the granulator. Simultaneously, NIR spectra were collected at-line (case study A) and in-line (case studies B and C). The rapid data collection offered by these PAT tools enables real-time granulation analysis to control the manufacturing process.

The feed-forward process control strategy developed in this study uses the in-line collected granulation information during the spraying phase, to determine the optimum process setting (drying temperature) of the consecutive drying phase. Via real-time collection of process (i.e., spraying temperature and spray rate) and product (i.e., granule size distribution and moisture) parameters during the spraying period, the batch density is predicted early-on, i.e., at the end of the spraying cycle. When the predicted density does not meet the desired value, the control method proposes the use of an adjusted drying temperature leading to the desired granule density at the end of the granulation process.

In all case studies, two steps were taken to develop this feed-forward control method:

- (i) The performance of a design of experiments resulting in individual regression models for bulk and tapped density by linking three process parameters, i.e., *spraying temperature, spray rate and drying temperature*, to bulk and tapped density.

- (ii) The development of a partial least squares model to predict the end product density (\mathbf{y}) from the granulation process and product information (\mathbf{X}) collected during the spraying period. Separate PLS models were developed for bulk and tapped density.

The resulting control strategy combines the PLS density prediction model with the design regression equation, as is explained later in this chapter.

Besides the development of a fluid bed granulation feed-forward control method, a quantitative NIR model for in-line moisture content prediction of the granulated end product was built. In this context, a conventionally designed diffuse reflectance NIR probe (case study B) was compared to a Lighthouse NIR probe (case study C), hence evaluating the sampling of both probes in the process environment.

6.2. MATERIALS AND METHODS

6.2.1. Materials

Each batch, consisting of dextrose monohydrate (700 g, Roquette Frères, Lestrem, France) and unmodified maize starch (277.5 g, Cargill Benelux, Sas van Gent, The Netherlands), was granulated with an aqueous binder solution of Tween 20 (2.5 g, Croda Chemicals Europe, Wilton) and HPMC (20 g, type 2910, Dow Chemical Company, Plaquemine, LA, USA). Two different HPMC viscosities were used, namely 15 mPa s (case study A and C) and 5 mPa s (case study B). Each batch consisted of a total solids amount of 1000 g. The HPMC binder was always sprayed as a 4% (w/w) solution.

6.2.2. Process description

Granulations were performed in a laboratory-scale fluid bed granulator (GPCG 1, Glatt, Binzen, Germany). A 1.2 mm diameter nozzle was installed top-spray at a height of 26 cm from the distributor plate. The binder liquid was atomized using a pressure of 1 bar during all granulations. Granulator filter bags were shaken every 45 s for a period of 7 s to prevent the entrapment of particles in the bags. The inlet air temperature during the spraying phase, the spray rate and the inlet air temperature during the drying phase were varied according to a 2-level full factorial design with three centre point repetitions (i.e., 11 granulation experiments, Table 6.1). Inlet air, product and exhaust air temperatures were manually recorded every minute during the entire granulation process. The process was stopped when an outlet air temperature of 37 °C and a product temperature of 45 °C were obtained.

Table 6.1. Overview of the performed design experiments.
(2-level full factorial design with three replicates of the center point)

Batch	Inlet air temperature during spraying (°C)	Spray rate (g/min)	Inlet air temperature during drying (°C)
1	30	12	50
2	50	12	50
3	30	20	50
4	50	20	50
5	30	12	70
6	50	12	70
7	30	20	70
8	50	20	70
9	40	16	60
10	40	16	60
11	40	16	60

6.2.3. Collection of granule product information during processing

6.2.3.1. Case study A: in-line SFV and at-line NIR spectroscopy

A spatial filter velocimetry probe (Parsum IPP 70, Gesellschaft für Partikel-, Strömungs- und Umweltmesstechnik, Chemnitz, Germany) was installed in the fluid bed granulator at a height of 20 cm and at approximately 5 cm from the sidewall of the granulator (Figure 6.1a). Particles passed through an aperture with 4 mm diameter and an internal (20 L/min) and external (3 L/min) pressurized air connection were used to prevent fouling of the measurement zone by the moist product and disperse the particles. Optimization of the experimental setup was described in Chapter 4, enabling representative size measurements without disturbing the process. Measured raw data were collected via an A/D converter. The software (In-line Particle Probe V7.12a) operated in the Windows XP environment. The SFV technique expresses the measured particle size distribution as a sieve distribution and via size percentiles (D_{01} , D_{10} , D_{25} , D_{50} , D_{63} , D_{75} , D_{90} , D_{99}). The sieve sizes are selected prior to executing the experiments and cannot be changed afterwards. During the entire granulation process, particle size measurements were continuously performed and an average particle size distribution was saved every 10 s.

At the end of each spraying cycle, a sample was withdrawn from the granulated mass via the built-in sample thief. The sample was at-line measured with diffuse reflectance NIR spectroscopy using a Nicolet Antaris II FT-NIR analyzer (Thermo Fisher Scientific, USA) equipped with an InGaAs detector and a quartz halogen lamp. The instrument was furnished with an integrating sphere module and controlled with the software package RESULT 3.0. The sampled granules were poured in the NIR instrument's sample cup, after which the sample cup was placed on the detection window of the integrating sphere. By rotating the cup in between NIR spectra collection, each sample was measurement at three different positions. All spectra were collected in the $4000 - 10000 \text{ cm}^{-1}$ spectral region with a resolution of 8 cm^{-1} and averaged over 32 scans. Background was measured using the gold-plated inner wall of the integrating sphere.

6.2.3.2. Case study B: in-line SFV and in-line NIR spectroscopy

The granule size distribution was collected in real-time by implementing the SFV probe in the fluid bed granulator identically to the setup described in Section 6.2.3.1 (case study A).

In-line diffuse reflectance NIR spectra were continuously collected during granulation by use of an FT-NIR spectrometer. The NIR instrument described in Section 6.2.3.1 was used and equipped with a fiber-optic non-contact probe for in-line measurements. Spectra were acquired every 20 s in the $4000 - 10000 \text{ cm}^{-1}$ spectral region with a resolution of 8 cm^{-1} and averaged over 32 scans.

Background was measured holding a golden plate (dimensions 7.6 cm x 2.5 cm) to the measurement window of the probe. The NIR probe was mounted into the granulator at a height of 7 cm (identical to the height of the system integrated sampling thief) and depth of 0.5 cm (Figure 6.1b).

6.2.3.3. Case study C: in-line FBRM and in-line Lighthouse NIR spectroscopy

The granule size distribution was continuously monitored by implementing a focused beam reflectance measurement probe (model C35, Mettler Toledo, Columbus (Ohio), USA) in the fluid bed granulator (Figure 6.1c). The pressurized air activated scraper cleaned the probe window every 2 s and the acquisition parameters were set to save the average particle size distribution every 10 s, using a scan speed of 4 m/s. The FBRM probe was positioned at a height of 20 cm (identical to the SFV probe) and depth of 3 cm inside the fluid bed container. Due to the location of the FBRM measurement window at the probe tip (Chapter 3), the instrument was inserted with a smaller depth compared to the SFV probe. Nevertheless, FBRM and SFV measurements were performed at identical locations since SFV windows are approximately 2 cm distant from the probe tip.

In-line diffuse reflectance NIR spectra were continuously collected during granulation using an FT-NIR spectrometer (MATRIXTM-F Duplex, Bruker Optics Ltd., UK) equipped with a fiber-optic Lighthouse ProbeTM (LHP, GEA Pharma Systems nv – Collette, Wommelgem, Belgium). The LHP is an immersion probe with seven radial windows that radiate and collect light. Hence, sampling is performed 360° around the probe. The spectrometer operated in the 4000 – 10000 cm⁻¹ NIR region and spectra with a resolution of 8 cm⁻¹ and averaged over 32 scans were continuously collected. The NIR measurements in case studies B and C were performed at identical locations inside the granulator, but the NIR LHP was inserted with a greater depth as the measurement windows are positioned 3.75 cm from the probe tip. The measurement window of the conventionally designed probe used in case study B was located at the probe tip itself.

6.2.4. Characterization of granules

6.2.4.1. Karl Fischer titration

Reference moisture content of the granule batches was determined off-line using a V30 volumetric Karl Fischer titrator (Mettler Toledo, Gießen, Germany). Hydranal[®]-Composite 5 (1-component, Sigma-Aldrich, Germany) was used as titrant and Hydranal[®]-Methanol dry (Sigma-Aldrich, Germany) as solvent. Three Karl Fischer determinations were performed for each completed batch. The water content in samples was determined via the quantitative reaction of water molecules with iodine and sulfur dioxide in the presence of methanol and imidazole as base. The amount of iodine consumption as a result of the reaction with water was measured.

6.2.4.2. Density measurements

The bulk density and tapped density were determined for each completed batch. Twenty-five g samples were gently poured into a 100 mL graduated cylinder. By use of the granule weight and volume, bulk density was calculated. Next, each sample was tapped 1250 times employing an automatic tapper (J. Engelsmann AG, Ludwigshafen am Rhein, Germany) and the new volume was used to determine the tapped density. All density measurements were performed in triplicate and the average density was calculated.

6.2.5. Development of the granulation feed-forward control strategy

In-process measurements of the agglomerates' properties, performed during the spraying phase of the batch process, were used to predict end product granule characteristics (bulk and tapped density) using a PLS model (see (ii) below). When these predicted densities were not as desired, the drying temperature of the successive drying phase was adjusted. The extent to which the drying temperature had to be adjusted was derived from a DoE model (see (i) below), expressing the granule bulk and tapped density as function of the spraying temperature, spray rate and drying temperature.

(i) A 2-level full factorial design (see Section 6.2.2 and Table 6.1) was carried out, resulting in a polynomial regression model (considering the 3-factor interaction term negligible) for each response:

$$y = \beta_0 + \beta_1x_1 + \beta_2x_2 + \beta_3x_3 + \beta_{12}x_1x_2 + \beta_{13}x_1x_3 + \beta_{23}x_2x_3 \quad (6.1)$$

with y the response (*i.e.*, bulk or tapped density), x_{1-3} the coded process variables (*the inlet air temperature during the spraying phase, the spray rate and the inlet air temperature during the drying phase*), β_0 the intercept and β_i the model coefficients expressing for each factor how much the response is affected by changing the factor from the coded DoE level 0 to +1.

Individual regression models were developed for bulk and tapped density. Analysis of the design experiments and development of the DoE models were done with the MODDE software (Version 9.0, Umetrics, Umeå, Sweden).

(ii) Partial least squares models were built using the SIMCA-P+ software (Version 12.0.1, Umetrics, Umeå, Sweden), correlating two data matrices, \mathbf{X} and \mathbf{y} . The \mathbf{X} -matrix contained granulation information collected during the spraying period of the 11 DoE batches, while the \mathbf{y} -vectors consisted of the design responses, bulk and tapped density. Individual PLS models were developed for bulk and tapped density. Applying these PLS models during new granulations

allows predicting the density of a completed batch (i.e., after spraying and drying phase) at the end of the spraying period.

Hartung et al. [8] reported that not only residual moisture in granules affected subsequent process steps, but also the moisture profile of the entire granulation process. Hence a similar approach, examining whether the complete spraying phase fingerprint contributed to the predictability of the density models, was considered. Therefore, the 3-way data matrix of [*design batches* (I)] \times [*collected granulation process and product variables* (J)] \times [*spraying time* (K)] was unfolded in the direction of the batches, creating a 2-way data matrix [*design batches* (I)] \times [*collected granulation process and product variables \times spraying time* ($J \times K$)] (Figure 6.2) [37].

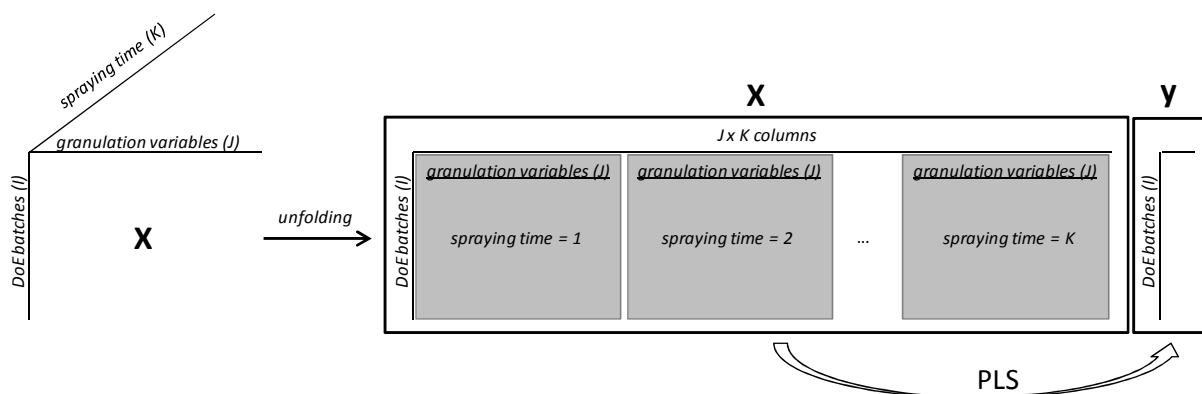


Figure 6.2. Unfolding of the 3-way granulation batch data matrix preserving batch direction.

In that way, the **X**-matrices of the developed PLS models contained 11 rows, corresponding to the 11 design batches, and the number of columns depended on the included spraying phase time-period. This resulted in the development of several PLS models (for bulk and tapped density individually), differing in the number of **X**-matrix columns describing the collected spraying phase data:

- Case study A – In-line SFV and at-line NIR measurements: The first three **X**-matrix columns for the various PLS models developed in case study A, contained the settings of the three process variables (spraying temperature, spray rate and drying temperature) describing the collected granulation *process* data (Figure 6.3a). The following columns of models M0 and M1 consisted of the collected granulation *product* information (based on SFV and NIR measurements) at the end of the spraying phase (i.e., when all granulation liquid has been sprayed) (Figure 6.3a). Hence, the **X**-matrix of **model M0** contained the three process variables and the in-line SFV measured granule size. The 8 percentile descriptors (see Section 6.2.3.1) were used to express the granule size distribution as the size of the smallest SFV sieve was set to 200 μm , which was too large to capture the size distribution variations between the different experiments. The **X**-matrix of **model M1** was identical to the M0 **X**-

matrix, complemented with the at-line collected NIR information. To express the NIR captured spectral variation between the 11 design batches, principal component analysis was performed on all at-line collected NIR spectra (*3 spectra x 11 batches*). The score values on the principal components (PC1 and PC2) were added to the M1 X-matrix.

Models M2-M9 were built by adding each time the granule size distribution collected during the previous spraying phase minutes to the X-matrix (Figure 6.3a).

- Case studies B and C – In-line SFV/FBRM and in-line NIR measurements: The **model M1 X**-matrix included the three process variables, the granule size distribution and the NIR data (expressed by PCA scores) collected at the end of the spraying phase, as described above for case study A. Based on the granule sizes measured in case study A, the SFV sieves were correctly selected and used to describe the collected granule size distribution during granulation (Figure 6.3b).

Since both SFV/FBRM and NIR measurements were continuously performed, **models M2-M5 X**-matrices contained both types of granule product information collected during the previous spraying phase minutes (Figure 6.3b).

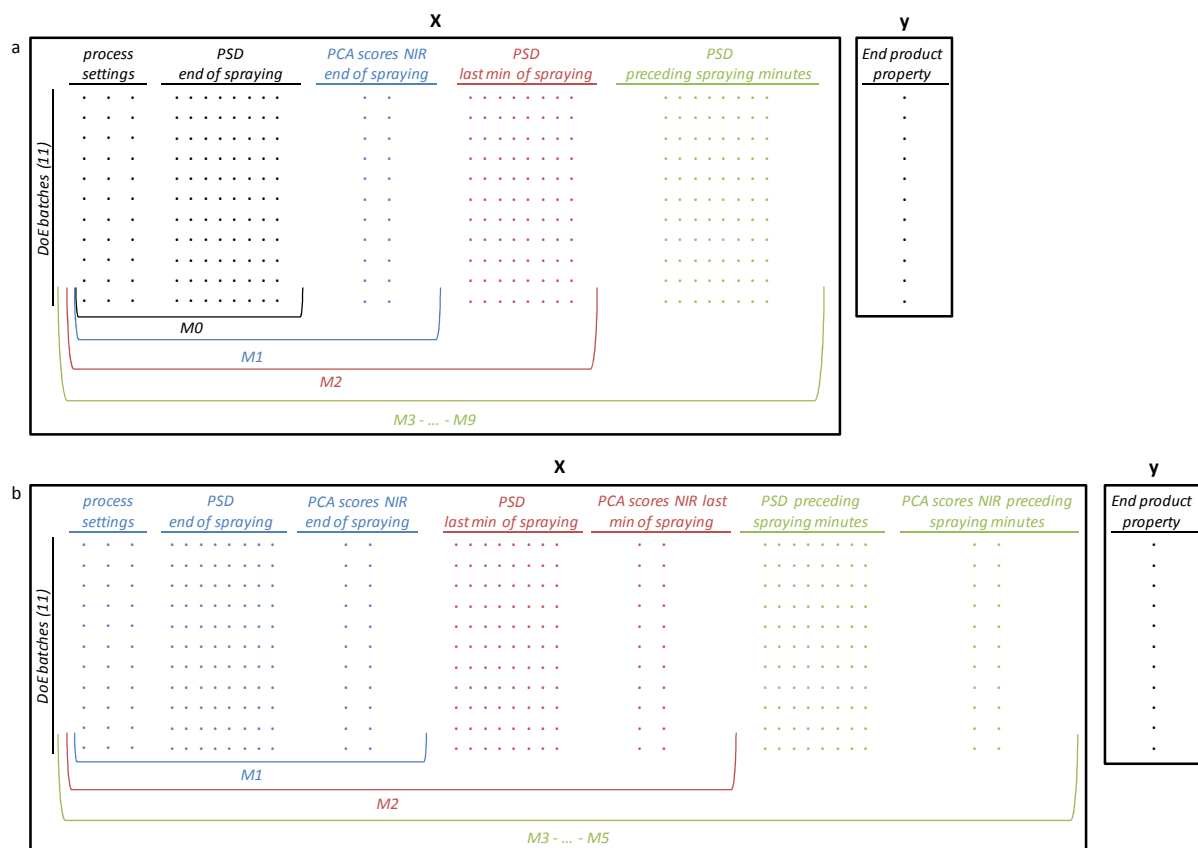


Figure 6.3. The X-matrix and y-vector for the bulk density and tapped density PLS models in case studies A (a) and B/C (b) (PSD = particle size distribution).

The goodness of fit and the predictive power of the PLS models were given by R^2 and Q^2 . R^2 expresses the percent variation of the response explained by the model and Q^2 measures how well the model is able to predict the examined response for new experiments (test batches). In addition to the evaluation of R^2 and Q^2 , the root mean square errors of estimation (RMSEE) and root mean square errors of prediction (RMSEP) were compared to select the best PLS prediction model. Both errors indicate the difference between the experimentally measured value and the value predicted by the model under examination, for the calibration and test batches, respectively.

The feed-forward control strategy, guaranteeing the granule quality of future experiments, combines the optimal predictive PLS model with the DoE regression equation. When a new granulation process is started, the selected PLS model allows the prediction of the end product quality (i.e. density of the end product) at the end of the spraying period based on the real-time collected granule information. If the predicted density does not meet the predefined quality requirements, the DoE model terms (Eq. 6.1) expressing the influence of the drying temperature on the batch density (i.e., β_3x_3 , $\beta_{13}x_1x_3$ and $\beta_{23}x_2x_3$) can be used to calculate by how many (coded) units the drying temperature should be adjusted to lead the granulation process towards the desired density. To exemplify, if the predicted density differs from the desired density by A g/mL, then the level of the pre-set nominal drying temperature (x_3 , coded according to the performed DoE) should be adjusted with Δ units (coded as above) established by the following equations (expressed with coded DoE variables and corresponding coefficients):

$$y + A = \beta_0 + \beta_1x_1 + \beta_2x_2 + \beta_3(x_3 + \Delta) + \beta_{12}x_1x_2 + \beta_{13}x_1(x_3 + \Delta) + \beta_{23}x_2(x_3 + \Delta) \quad (6.2)$$

$$A = \beta_3\Delta + \beta_{13}x_1\Delta + \beta_{23}x_2\Delta \quad (6.3)$$

$$\Delta = \frac{A}{\beta_3 + \beta_{13}x_1 + \beta_{23}x_2} \quad (6.4)$$

6.2.6. Development of an NIR method to predict end product moisture content

An NIR calibration model for in-line moisture content prediction of the granulated end product was developed. The use of a conventionally designed diffuse reflectance NIR probe (case study B) was compared to the Lighthouse NIR probe (case study C). Therefore, separate calibration models were developed for the two probes.

6.2.6.1. Use of conventional NIR probe (case study B)

Calibration and validation batches were manufactured by granulation of the previously described formulation (Section 6.2.1), and terminating the drying period at different exhaust air temperatures to create granules with varying moisture levels. Subsequently, the fluid bed container was removed from underneath the filter housing and by immersion of the NIR probe in the granule bed, static NIR spectra were at-line recorded (at different locations in the bed). The moisture reference value was determined by Karl Fischer titration using the average of three measured samples. In total, 20 NIR spectra of each batch were correlated with the Karl Fischer determined moisture content using PLS regression. The calibration model covered a water content range between 4% and 10% including 9 concentration levels. In the diffuse reflectance measurement, the light travels various distances because the distribution of sample particles and particle sizes are different. Hence, prior to modeling the absorbances in the 4500 – 7500 cm^{-1} spectral region of 180 NIR spectra, standard normal variation (SNV) correction was performed to eliminate these scattering effects and the spectra were mean centered. The calibration of the PLS model was evaluated by calculation of the RMSEE. The model was externally and independently validated by computing the RMSEP using 140 spectra of 7 validation batches.

6.2.6.2. Use of Lighthouse NIR probe (case study C)

Similar to the method described in 6.2.6.1, calibration and prediction granule batches with varying moisture content were manufactured and static NIR spectra were at-line recorded by immersing the NIR LHP in the granule bed. The moisture reference value was determined by Karl Fischer titration using the average of three measured samples. A PLS model was constructed with the Karl Fischer moisture content as dependent variable and the NIR absorbances as predictors. The developed PLS model related 140 NIR spectra to 7 different moisture levels (20 NIR spectra per calibration batch) covering a water content range between 4% and 10%. Hundred spectra of 5 samples in total were used for external model validation. SNV correction and mean centering in the spectral region between 4500 cm^{-1} and 7500 cm^{-1} were selected as spectral pre-processing treatments. RMSEE and RMSEP were used to assess method accuracy and assist in the determination of appropriate data pre-treatment, wavenumber selection and model complexity.

6.3. RESULTS AND DISCUSSION

6.3.1. Case study A: in-line SFV and at-line NIR spectroscopy

For the 11 DoE granulations performed in case study A, batch bulk and tapped densities were determined in triplicate and averages were used as design responses. Individual bulk and tapped density multiple linear regression models were computed and the significance of the coefficients was determined by calculation of the 95% confidence interval. The confidence intervals of the three 2-factor interaction coefficients included zero, indicating the statistical insignificance of the interactions. The insignificant coefficients were removed and the following bulk density (BD) and tapped density (TD) regression equations (based on the coded variables) were obtained after refitting the models:

$$BD = 0.4357 - 0.0268 * T_{spraying} + 0.0204 * spray\ rate - 0.0196 * T_{drying} \quad (6.5)$$

$$TD = 0.5307 - 0.0258 * T_{spraying} + 0.0181 * spray\ rate - 0.0284 * T_{drying} \quad (6.6)$$

As described in 6.2.5, separate PLS models were developed for bulk and tapped densities (\mathbf{y}), predicting the densities of a completed batch (i.e. after spraying and drying phase) based on the collected data during the spraying period (Figure 6.3a). Therefore, all available granulation *process* and *product information* related to batch density were included in the PLS \mathbf{X} -matrices. Herewith, the settings for the three process variables (i.e., spraying temperature, spray rate and drying temperature) were included as they significantly influenced end product density according to the DoE analysis. Furthermore, since the density of a product is defined as the mass of the material divided by the volume the material occupies (i.e., volume of individual particles, inter-particle volume and the internal pore volume), the granule size distribution during the spraying phase is related to batch density. Consequently, the \mathbf{X} -matrix of the initially constructed PLS model (model M0, Figure 6.3a) included the three process variable settings and the particle size distribution determined at the end of the spraying period.

Principal component analysis was performed on all at-line collected NIR spectra for the 11 design batches to examine the spectral differences between the batches. Using the SNV corrected 4500 – 7500 cm^{-1} spectral region, a model consisting of two principal components (PC1 and PC2), describing 99.9% of the spectral variation was computed. The PC1 and PC2 loading plots exhibited large contributions by the 7000 cm^{-1} and 5200 cm^{-1} spectral regions, corresponding to the NIR absorption bands of water. The PC1 versus PC2 scores plot showed clustering of the design experiments along PC1, describing the variability in granule moisture level caused by the process settings of the spraying

cycles (Figure 6.4). Experiments performed at a low spraying temperature and a high spray rate (-1,1; high granule moisture) clustered in the outer positive region of PC1, while experiments executed using a high spraying temperature and low spray rate (1,-1; low granule moisture) grouped in the negative part of PC1. Combinations of spraying temperature and spray rate resulting in a moderate granule moisture state (1,1 ; 0,0 ; -1,-1) lay around the PC1 origin. Hence, instead of including all NIR spectral variables, only the PC1 and PC2 scores were added to the PLS X-matrix (model M1, Figure 6.3a) comprising the NIR captured granule moisture differences between the various batches. The addition of the granule size distributions collected during the preceding spraying phase minutes resulted in the development of models M2, M3, ..., M9 (Figure 6.3a).

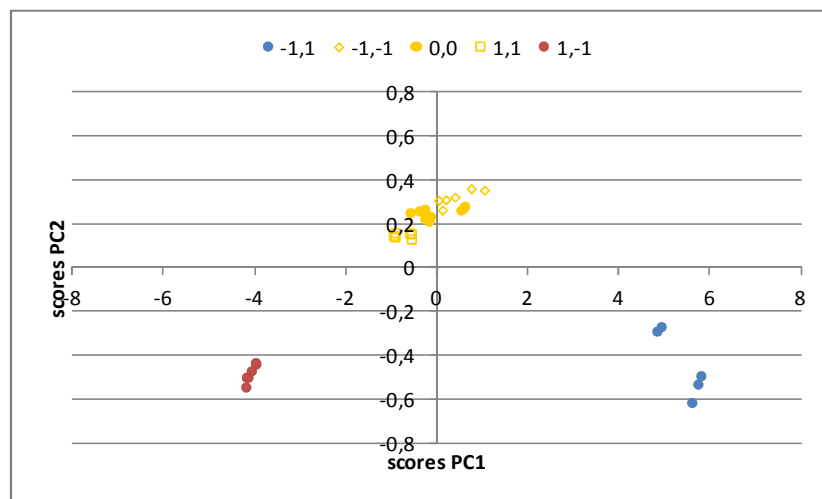


Figure 6.4. PC1 versus PC2 scores plot of the at-line collected NIR spectra for the 11 design experiments performed in case study A. The scores are labeled according to the coded DoE settings for the spraying temperature and spray rate. Three NIR spectra were collected per design experiment.

Figure 6.5 displays the resulting R^2 , Q^2 , RMSEE and RMSEP values for the developed BD and TD PLS models M0 to M9. The calculation of the prediction error (RMSEP) was based on the predicted densities of four new independent batches (not included in the calibration set). Four randomly selected batches from the performed DoE, namely batch 4, 8 and twice the centre point, were granulated a second time covering drying temperatures of 50 °C, 70 °C and 60 °C. The bulk and tapped density R^2 and Q^2 values lay in the same range, with repeatedly higher values for BD models. Adding PCA scores distinctively increased the models' predictability based on the 10% rise in Q^2 values between M0 and M1. Adding the granule size distributions collected during the complete spraying phase to the X-matrices improved only slightly the predictability. Maximum Q^2 was reached by models M3 and M4. According to the estimation and prediction errors, optimal density prediction resulted from the granule information collected at the end of the spraying period. Adding the full particle size fingerprint collected during spraying did not seem to contribute to a better predictability.

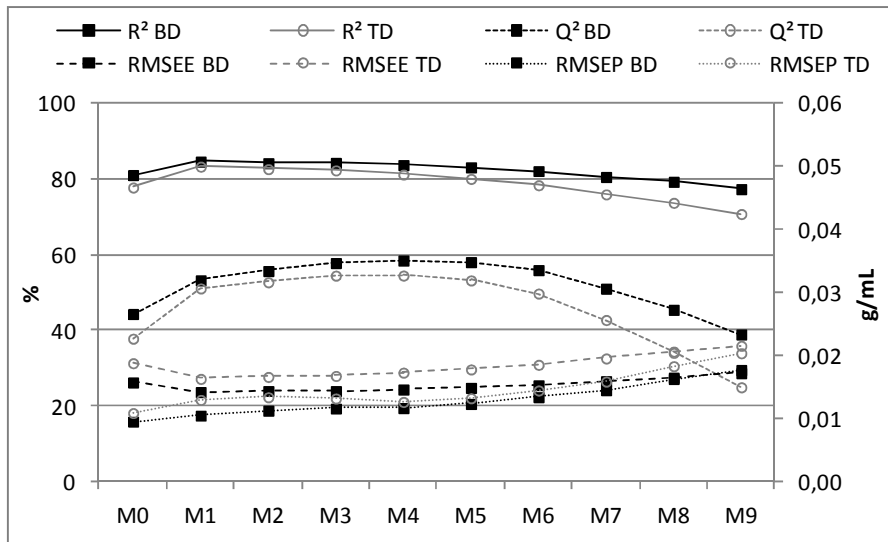


Figure 6.5. R^2 , Q^2 , RMSEE and RMSEP for bulk density (BD) and tapped density (TD) PLS models M0 to M9 in case study A.

The feed-forward control strategy described in Section 2.5 requires (i) a *valid prediction of the batch density* after completion of the spraying period, and (ii) a *reliable estimation of the optimal drying temperature* to obtain the desired density, using the DoE regression equation. The latter was assessed for the previously mentioned four test batches by means of Eq. 6.1. Hence, the drying temperature (x_3) was computed applying the by the PLS model predicted BD (y), the significant regression coefficients (β_i), and the experimentally set spraying temperature (x_1) and spray rate (x_2). The BD values predicted by all 9 PLS models (M0 to M9) were used in these calculations and identical computations were carried out based on the predicted TDs. As the drying phase of the four test batches was experimentally executed, these calculated drying temperatures were compared to the drying temperatures applied during processing (Table 6.2).

Table 6.2. Comparison of the experimentally applied drying temperature with the estimated optimum drying temperature for 4 test batches (case study A) using the process control methodology.

Estimated drying temperature based on predicted bulk density (°C)											
Batch	Used T_{drying} (°C)	M0	M1	M2	M3	M4	M5	M6	M7	M8	M9
T4	50	50	50	50	50	49	49	49	49	49	50
T8	70	76	75	75	74	73	73	72	72	73	73
TCP1	60	60	60	60	60	60	59	58	57	55	54
TCP2	60	61	58	57	56	56	56	55	54	53	53
Estimated drying temperature based on predicted tapped density (°C)											
Batch	Used T_{drying} (°C)	M0	M1	M2	M3	M4	M5	M6	M7	M8	M9
T4	50	49	50	50	50	49	49	49	50	50	50
T8	70	73	73	72	71	70	69	69	69	70	70
TCP1	60	60	60	59	59	59	59	58	57	56	54
TCP2	60	60	57	56	56	56	56	55	54	54	53

The drying temperature predictions were satisfactory, keeping in mind that an increase in drying temperature by 1 °C, reduces the BD and TD by 0.0020 g/mL and 0.0028 g/mL, respectively. In general, the accuracy of drying temperature prediction tends to decrease going from M0 to M9, caused by the growing incorrectness in batch bulk and tapped density predictions when adding spraying phase information collected early in the process (Figure 6.5).

6.3.2. Case study B: in-line SFV and in-line NIR spectroscopy

6.3.2.1. Qualitative monitoring of the granulation process

In-line SFV measurements were appended with in-line NIR spectra collection during the 11 design granulations to describe the continuously evolving granule size and moisture. Figure 6.6a-d exemplifies the change in NIR spectra and SFV measured average particle size (D_{50}) during one of the performed DoE batches (i.e., batch 3).

Examination of the raw NIR data without preprocessing (Figure 6.6a) showed that spraying of the binder liquid onto the fluidizing bed, caused a significant increase in spectrum baseline, most likely due to the increasing particle size [30, 38]. During subsequent drying, water removal and attrition decreased the granule size and therefore influenced the physical state of the measured samples. This was associated with a lowering of the NIR spectrum baseline.

By SNV preprocessing of the NIR spectra, physical light-scattering effects were removed from the chemical light absorbance effects in the spectra [39, 40]. Figure 6.6b and c displays the NIR spectra collected during the spraying and drying operation, respectively, after SNV preprocessing. The color assignment to the spectra is related to the spraying and drying times with dark and light coloring indicating the start, respectively the end of the cycle. The spectral evolution was characterized by a strong increase and subsequent decrease in NIR absorptions in the 5200 cm^{-1} and 7000 cm^{-1} spectral region. These regions are associated with the OH combination band of the fundamental stretching and deformation vibration, and the first overtone of the OH bond in water, respectively. The signal in the first overtone region for CH, CH₂ and CH₃ around 5700 – 6000 cm^{-1} decreased during spraying and increased throughout drying. This might be attributed to the masking effect of water on the NIR signals originating from the formulation components during spraying of the binder. As water was removed during drying, the masking effect faded enabling the formulation's NIR signals to be more prominent.

The PC1 obtained after principal component analysis on the SNV corrected spectra (4500 – 7500 cm^{-1} spectral region) accounted for 90% of the spectral variation. Similarity between the PC1 loading

profile and the NIR spectrum of water confirmed the association of this component with the water addition/removal during granulation.

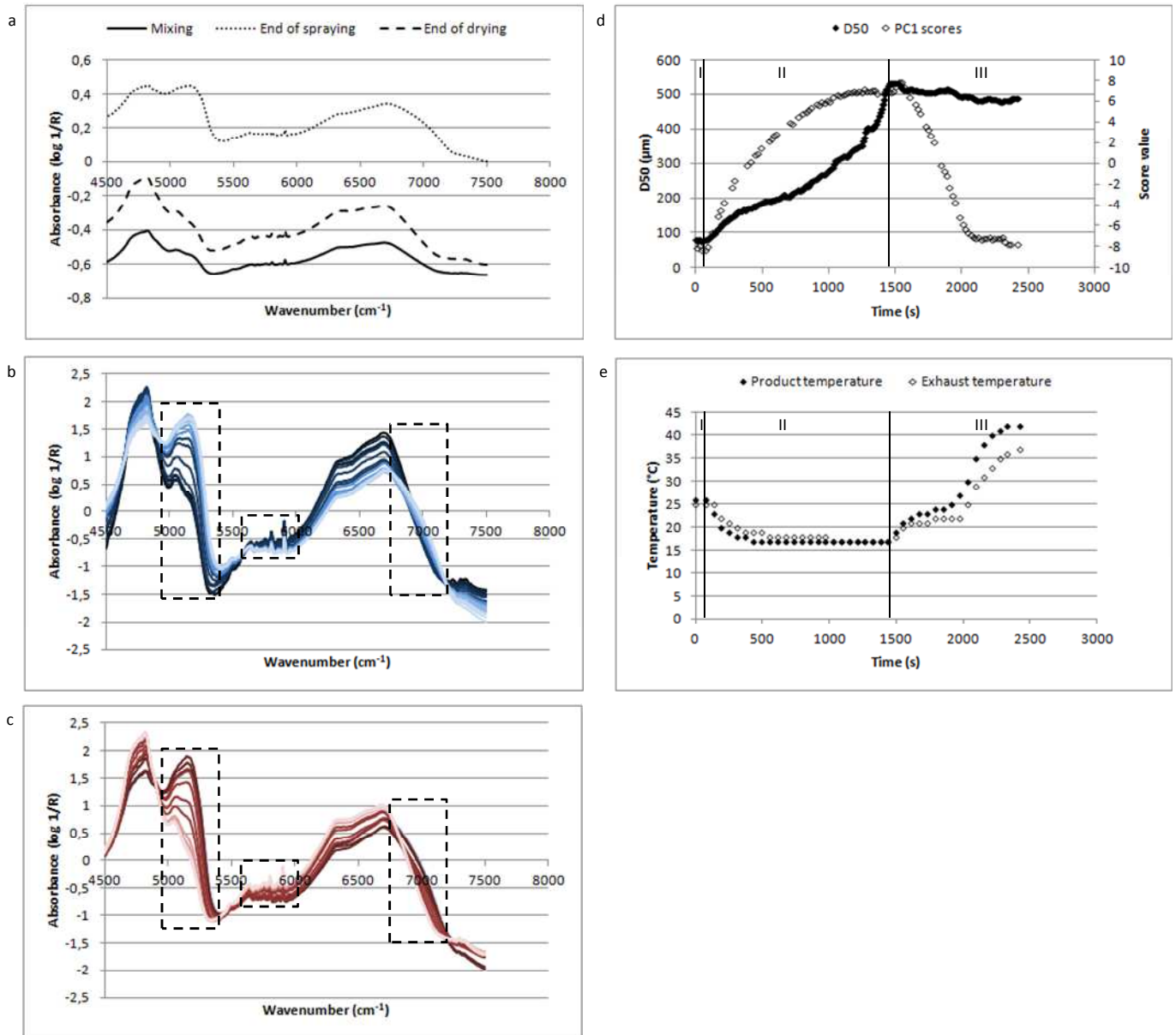


Figure 6.6. Granulation product and process information in-line collected during granulation of batch 3 (case study B). Pure NIR spectra collected during the mixing, spraying and drying steps of the granulation process (a). SNV corrected NIR spectra collected during the spraying phase (b) and drying phase (c). The color assignment to the spectra is related to the spraying and drying times with dark and light colors indicating the start, respectively the end of the cycle. Evolution of D50 and PC1 scores (d), and product and exhaust air temperatures (e) during the granulation process.

The trajectory of PC1 scores as a function of granulation time (Figure 6.6d) displayed a clear distinction between the three granulation process steps. During heating and powder mixing (step I, data shown of the final minute), the score values were similar. The addition of binder liquid in the second step increased the PC1 scores, while drying of the granules caused a score value decrease

until a minimum value was reached similar to the PC1 scores in step I. The trajectory of SFV collected D_{50} values during granulation exhibited a similar sequence of the three granulation process steps. A constant particle size during sample agitation and heating was followed by a particle size increase during the spraying of binder liquid. Drying slightly reduced the average granule size due to inter-particle and particle-fluid bed container collisions. As can be seen from Figure 6.6d, the variation in NIR scores and SFV measured particle size during granulation provided improved knowledge on the batch evolution. A better insight into the granulation under examination is achieved, compared to the traditionally used product and exhaust air temperature control charts. Figure 6.6e shows that after approximately 8 min in the spraying period, the process variables did no longer provide information on the granulation progress as product and exhaust air temperatures remained constant. During routine production, the use of a plot expressing particle size and moisture content trajectories (Figure 6.6d) allows determining whether a batch is developing under the normal operating conditions and granulation is being performed accordingly [6].

6.3.2.2. Development of the granulation feed-forward control strategy

After executing the 11 design granulations, end product bulk and tapped densities were determined and the coefficients of the significant main and interaction effects calculated. The following bulk density and tapped density regression equations (based on the coded variables) were obtained:

$$BD = 0.4733 - 0.0332 * T_{spraying} + 0.0236 * spray\ rate - 0.0164 * T_{drying} + 0.0107 * T_{spraying} * spray\ rate \quad (6.7)$$

$$TD = 0.5744 - 0.0211 * T_{spraying} + 0.0096 * spray\ rate - 0.0246 * T_{drying} + 0.0207 * T_{spraying} * spray\ rate \quad (6.8)$$

To construct bulk and tapped density PLS models, a similar methodology as for case study A (6.3.1) was followed, however with one difference. In addition to the granule size, NIR spectra were continuously in-line collected during the entire DoE granulation processes. Principal component analysis was performed on the SNV corrected 4500 – 10000 cm^{-1} spectral region of all collected NIR spectra (for all batches) to examine the NIR captured granule differences between the 11 design batches. The NIR variables contributing most to the two first principal components were associated with the two water bands. Hence, the scores on PC1 and PC2 were added to the PLS \mathbf{X} -matrices to describe the granule moisture information captured by in-line NIR spectroscopy. Figure 6.7 displays the RMSEE and RMSEP values of the resulting bulk density PLS models M1 to M5, without and with the inclusion of NIR scores in the \mathbf{X} -matrix. Since case study A showed that the information collected during the final minutes of the spraying period produced the best BD predictions, only five PLS models were developed using the granule size and moisture information collected at the end of

spraying, augmented with the granule data collected during the final four minutes of spraying (i.e., models M1 to M5). To calculate the prediction error, four new batches (i.e., batch 1, 5 (twice) and 8), not included in the calibration set were granulated a second time. The resulting RMSEE values decreased by the addition of NIR information, while RMSEP values exhibited a slightly variable trend.

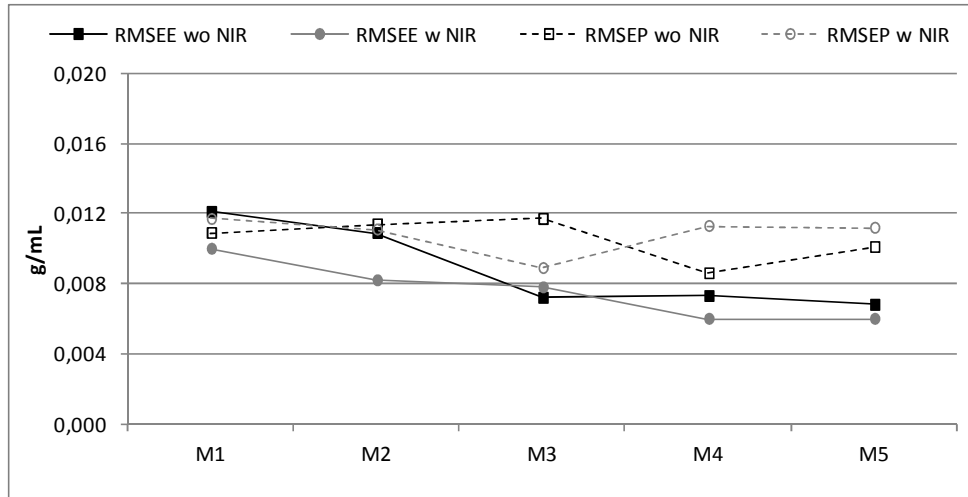


Figure 6.7. RMSEE and RMSEP values of bulk density PLS models M1 to M5 with **X**-matrices containing the granule size distribution either without (wo) or with (w) the inclusion of NIR scores (case study B).

As a result, taking Figure 6.7 into account, the **X**-matrices of the developed BD and TD PLS models in case study B were composed of continuously collected granule size and moisture data (Figure 6.3b). The resulting BD and TD PLS models exhibited an excellent fit and predictability, with the BD models producing slightly higher R^2 and Q^2 values (Figure 6.8).

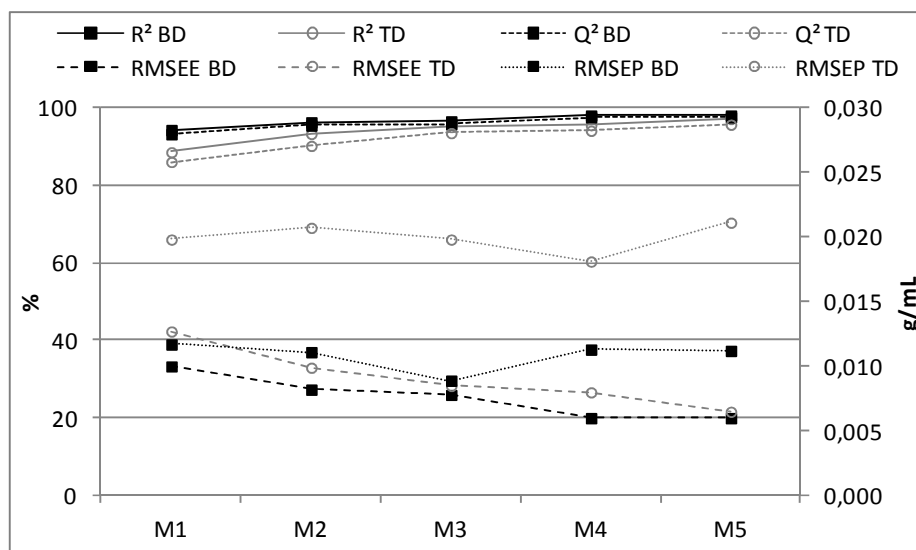


Figure 6.8. R^2 , Q^2 , RMSEE and RMSEP for bulk density (BD) and tapped density (TD) PLS models M1 to M5 in case study B.

Both BD and TD models showed that the addition of size and NIR information collected during the final minutes of the spraying period, improved the fit and predictability of the calibration batches as

R^2 , Q^2 and RMSEE values reached a maximum, respectively minimum for model M5. The density prediction of new, independent batches did not exhibit an identical trend. The initial addition of granule information resulted into a small decrease in prediction error. Further inclusion of X -variables did not benefit the predictions and tends to indicate overfitting. For both BD and TD, the models fit the data well, but TD predictions are less good, indicating an improved correlation between the collected granule information and the free bulk density. These results are consistent with the observations made in case study A.

Next to the valid prediction of batch density from the data collected during the spraying phase, the reliable estimation of the optimal drying temperature resulting in the required density was assessed. This was initially examined by calculating the drying temperatures using the PLS predicted BD and TD values of the four test batches (for the 5 PLS models), in combination with Eq. 6.5 and 6.6, respectively. The drying phases of the four batches were experimentally completed, which allowed the comparison between the predicted and the applied drying temperature (Table 6.3). The correctness in temperature prediction based on predicted BD was comparable to the results in case study A. The computed drying temperatures based on predicted TD however displayed a larger bias, probably due to the notable higher TD prediction error (Figure 6.8).

Table 6.3. Comparison of the experimentally applied drying temperature with the estimated optimum drying temperature for 4 test batches (case study B) using the process control methodology.

Estimated drying temperature based on predicted bulk density (°C)						
Batch	Used T_{drying} (°C)	M1	M2	M3	M4	M5
T1	50	52	52	51	53	54
T5a	70	67	68	62	64	63
T5b	70	69	71	67	72	71
T8	70	73	72	68	70	68
Estimated drying temperature based on predicted tapped density (°C)						
Batch	Used T_{drying} (°C)	M1	M2	M3	M4	M5
T1	50	51	49	52	52	54
T5a	70	75	73	69	69	68
T5b	70	78	81	80	78	79
T8	70	77	79	74	73	71

In case studies A and B, the ability of the developed PLS models to predict the density of future batches was evaluated using test batches not included in the calibration set. Hence, a primary selection of the X -variables correlating with the batch density was made. Comparing the predicted drying temperature (from implementing the PLS predicted density in the DoE models) with the experimentally applied temperature allowed a first assessment of the suitability of the proposed

feed-forward strategy. In a next step, the developed methodology was tested during the granulation of new batches. To predict the batch quality at the end of the spraying period and adjust/correct the granulation progress during drying, **BD** PLS models were combined with the **BD** DoE regression equation.

Batch CS (*control strategy*) was granulated using an inlet air temperature of 30 °C and binder addition rate of 12 g/min during the spraying period. The subsequent drying phase was executed at an inlet air temperature of 50 °C. Throughout the complete granulation process, granule size data and NIR spectra were continuously collected. The acquired granulation information was used to predict the batch bulk density using models M1 to M5. Hence, by use of the two spraying period parameters, the in-line collected product information and the intended use of an inlet air temperature of 50 °C during drying, the bulk density of the completed batch was predicted at the end of the spraying period. Drying of batch CS at an inlet air temperature of 50 °C enabled the comparison between this early-on predicted BD and the experimentally measured value (Table 6.4, batch ID CS). The excellent agreement between the measured BD (after batch production) and the predicted BD (at the end of the spraying period) for models M1 to M3 demonstrated the validity of the developed PLS models. The predicted BD values by models M4 and M5 are also in close agreement with the measured BD, but exhibit a slightly larger deviation compared to M1 – M3 predictions, which is in analogy with Figure 6.8.

Table 6.4. Use of the developed granulation feed-forward control strategy. Comparison of the predicted bulk density (BD) at the end of the spraying period using a drying temperature of 50 °C, with the experimentally measured bulk density applying a drying temperature of 50 °C (batch CS) and 67 °C (batch CS adjusted a and b).

Batch ID	Predicted BD (g/mL)					Measured BD (g/mL)	
	M1	M2	M3	M4	M5	T _{drying} 50 °C	T _{drying} 67 °C
CS	0.5174	0.5136	0.5165	0.5119	0.5102	0.5161	
CS adjusted a	0.5233	0.5185	0.5248	0.5192	0.5197		0.4823
CS adjusted b	0.5173	0.5130	0.5172	0.5058	0.5044		0.4792

Next, the use of the developed BD DoE regression equation to determine the optimal drying temperature was examined. We decided that granulation of batch CS should give a BD of 0.48 g/mL instead of 0.52 g/mL. The adjusted drying temperature resulting in a BD decrease of 0.04 g/mL, was calculated by use of Eq. 6.4 (*vide supra*). Keeping in mind that the values of the process variables and coefficients are expressed according to the DoE scaling (i.e., spraying temperature of -1 and spray rate of -1), the following calculations were performed:

$$adjusted\ x_3 = x_3 + \Delta = x_3 + \left[\frac{-0.04}{\beta_3 + \beta_{13}x_1 + \beta_{23}x_2} \right]$$

$$adjusted\ x_3 = -1 + \left[\frac{-0.04}{-0.0164 + (-0.00258 * -1) + (0.009275 * -1)} \right] = 0.7$$

The experimental drying temperature levels of 50 °C, 60 °C and 70 °C were coded to -1, 0 and 1 according to the DoE (Table 6.1). Hence, conversion of the coded into the uncoded value shows that the pre-set drying temperature of 50 °C should be increased to 67 °C to obtain the desired BD:

$$0.7\ (coded) = 60\ ^\circ C + (10 * 0.7) = 67\ ^\circ C\ (uncoded)$$

Therefore, batch CS was granulated twice more using identical spraying phase settings and a drying temperature of 67 °C (i.e., batch CS adjusted a and b). Table 6.4 displays the predicted bulk density based on the process settings (drying temperature of 50 °C) and the collected granule information at the end of the spraying period. According to the predictions by M1 – M3, this would result for both batches into a BD of 0.52 g/mL as observed for batch CS. However, as we aimed to obtain a BD of 0.48 g/mL, a temperature of 67 °C derived from the BD DoE regression equation was applied during drying. The subsequent experimental BD value measurements of 0.48 g/mL were consistent with the desired density.

These results suggest that the developed BD PLS model allowed a reliable prediction of batch density using granule information collected during the end of the spraying period (M1 – M3). The granule behavior fingerprint during the complete granulation cycle did not improve the predictions. By use of the BD design equation, the granulation process could be adjusted during drying (adjusted drying temperature), hence guiding the process towards the desired density.

6.3.2.3. Development of an NIR method to predict end product moisture content

The developed PLS calibration model for end product moisture content prediction (described in 6.2.6.1) exhibited an RMSEE and RMSEP of 0.51% and 0.47%, respectively. Optimum moisture content predictions were obtained using two PLS factors. In the selected predictive model, 94% of the spectral variance was correlated with 87% of the water variation. The calibration model was applied to the in-line collected NIR spectra of the 11 design batches. The moisture content predicted during the final minute of drying was compared to the reference moisture content determined by Karl Fischer titration (Table 6.5). The in-line predictions were attended with an RMSEP of 0.51%, comparable to the error of the calibration model. Hence, although the calibration model was developed by use of statically recorded NIR spectra, the model was also applicable to dynamically collected spectra.

In addition to the in-line collected NIR spectra, 20 at-line NIR spectra were recorded per design batch after granulation. At-line moisture content predictions resulted in an RMSEP of 0.43%. Similar in-line

and at-line prediction errors suggest that the continuous flow of particles during in-line NIR spectra collection did not reduce the predictability of the NIR measurements. It also implies that the moisture predictions were not affected by the build-up of material on the probe using these granulation process conditions. Since no cleaning device was used, the NIR window was probably continuously cleaned by the product itself during fluidization.

Table 6.5. Moisture content (MC) and standard deviation, determined using Karl Fischer (KF) and predicted by the near infrared PLS calibration models, for the design granulations performed in case study B.

Case study B (conventional NIR probe)			
DoE Batch	KF MC (%)	in-line NIR (%)	at-line NIR (%)
1	6.21 ± 0.23	7.69 ± 0.00	7.23 ± 0.12
2	7.13 ± 0.18	7.05 ± 0.02	7.19 ± 0.04
3	7.28 ± 0.02	7.01 ± 0.04	7.22 ± 0.07
4	6.87 ± 0.07	6.88 ± 0.01	6.81 ± 0.03
5	7.01 ± 0.35	7.33 ± 0.02	7.36 ± 0.06
6	7.69 ± 0.12	7.46 ± 0.04	7.31 ± 0.06
7	7.21 ± 0.22	7.40 ± 0.04	7.25 ± 0.10
8	7.23 ± 0.08	7.55 ± 0.03	6.51 ± 0.04
9	6.72 ± 0.21	7.19 ± 0.02	7.13 ± 0.04
10	7.38 ± 0.06	7.03 ± 0.08	7.56 ± 0.05
11	7.17 ± 0.08	7.06 ± 0.00	7.15 ± 0.04

6.3.3. Case study C: in-line FBRM and in-line Lighthouse NIR spectroscopy

6.3.3.1. Development of the granulation feed-forward control strategy

Similar to case studies A and B, bulk and tapped densities were determined and used to develop a BD and TD regression model. Results showed that the density was not significantly affected by the applied drying temperature, hence the regression models in case study C did not correspond to the models developed in the previous case studies. This most likely originated from the way the process analyzers were implemented into the process environment.

The height and depth of the FBRM probe were identical to, respectively smaller than, the SFV probe positioning, which suggests that the FBRM probe did not disturb the granulation process. The NIR probe in case study B and the NIR LHP were located in close proximity to the bottom of the fluid bed granulator, ensuring a measurement position with continuous dynamically flowing material in front of the probe windows. However, this also introduced the danger of modifying the airflow pattern in

the granulator and consequently the agglomeration process. Especially in case study C, where the NIR LHP had to be inserted with a greater depth due to the probe design. The measurement windows are not positioned at the probe tip (as for the NIR probe in case study B), but at a distance of 3.75 cm.

Figure 6.9 displays the off-line sieve analysis results of batches 2, 1 and 7 granulated in case studies A and C to show the effect of implementing the NIR LHP. Batch 2 was granulated using a spraying temperature of 50 °C and spray rate of 12 g/min (Table 6.1). The perfect agreement between batch 2 sieve distributions for case studies A and C proved that the NIR LHP did not influence the agglomeration process under low-moisture spraying phase conditions. However, the particle size distributions of batch 1 and particularly batch 7 (granulated at an inlet air temperature of 30 °C and spray rate of 12, respectively 20 g/min) shifted to larger sizes in case study C. Hence, the influence of the NIR LHP on the granulation process was more pronounced using medium- and high-moisture granulation conditions. The probe significantly disturbed the airflow pattern and consequently the simultaneous process of heat and mass transfer during granulations with a low spraying temperature and/or a fast spray rate. Therefore, the granulation liquid was not efficiently evaporated and overwetted granules were produced, which were less affected by attrition during drying. Hence, the applied drying temperature range in case study C did not influence the granule size of these batches which led to the insignificance of the drying temperature coefficient in the resulting TD and BD regression models.

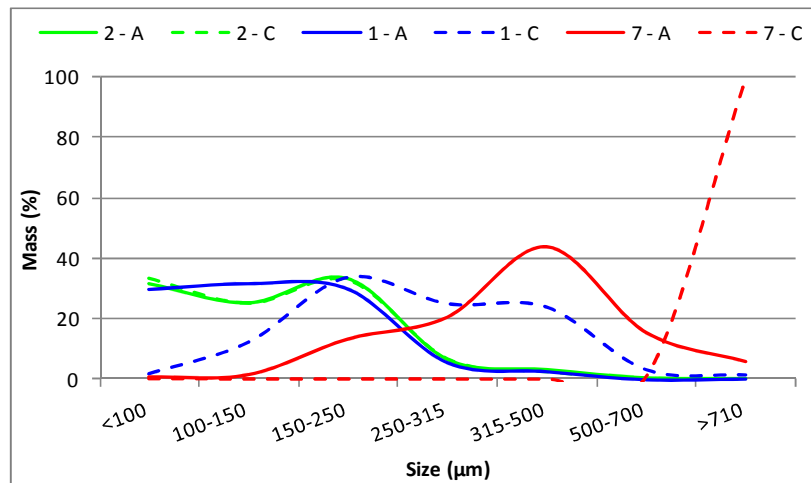


Figure 6.9. Sieve distributions of batches 2, 1 and 7 granulated in case study A (solid line) and case study C (dashed line).

Although the information provided by the in-line FBRM and NIR LHP described the different stages of granulation and allowed to monitor the process, the NIR LHP should not be used under these experimental conditions. For the NIR probe implemented in case study B, the same conclusions may

not be drawn. The smaller depth with which the NIR probe was inserted in the granulator eliminated the risk of airflow disturbance.

6.3.3.2. Development of an NIR method to predict end product moisture content

The developed PLS calibration model (described in 6.2.6.2) correlated 97% of the spectral variance with 98% of the water variation. The close fitting between NIR spectra and moisture content and the excellent predictability was reflected by an RMSEE and RMSEP of 0.23% and 0.20%, respectively. The calibration model was applied to the in-line collected NIR spectra of the 11 design granulations. A prediction error of 1.03% was obtained by comparing the in-line predicted moisture content during the final minute of drying, with the reference moisture content determined by Karl Fischer (Table 6.6). The large error resulted from the incorrect moisture content prediction of batch 7. This batch exhibited a moisture level of 12.82%, which was not included in the range of the calibration model. Recalculation of the prediction error with exclusion of batch 7 resulted into an RMSEP of 0.29%.

Although batch 7 was dried until the pre-defined product and outlet air temperature (similar for all batches) was reached, an unexpectedly high moisture content was obtained. This was most likely caused by the disturbed airflow pattern observed for batches processed under high-moisture granulation conditions in case study C (6.3.3.1, Figure 6.9). The improper fluidization induced the inhomogeneous drying of the granules.

Table 6.6. Moisture content (MC) and standard deviation, determined using Karl Fischer (KF) and predicted by the near infrared PLS calibration models, for the design granulations performed in case study C.

Case study C (Lighthouse NIR probe)		
DoE Batch	KF MC (%)	in-line NIR (%)
1	7.25 ± 0.26	7.44 ± 0.01
2	7.00 ± 0.07	7.36 ± 0.04
3	7.00 ± 0.05	7.28 ± 0.01
4	7.57 ± 0.06	7.77 ± 0.04
5	7.40 ± 0.10	7.84 ± 0.10
6	7.66 ± 0.13	7.81 ± 0.03
7	12.82 ± 0.44	9.54 ± 0.19
8	7.38 ± 0.11	7.03 ± 0.09
9	7.12 ± 0.13	7.03 ± 0.03
10	7.07 ± 0.08	7.47 ± 0.08
11	7.29 ± 0.02	7.57 ± 0.05

Further study is necessary to examine the use of the NIR LHP in varying experimental conditions, but the low calibration and prediction errors might suggest the supremacy of the NIR LHP to the conventional design with regard to moisture content prediction. Apart from batch 7, the NIR LHP predictions showed excellent agreement with the reference values and might therefore be a valid alternative to the off-line Karl Fischer moisture content determinations.

6.4. CONCLUSIONS

Chapter 6 describes the development a fluid bed granulation control strategy based on real-time collected process and product information. The feed-forward control strategy uses granulation information collected during the spraying phase to determine the optimal drying phase temperature, hence ensuring end product density.

The finalized control strategy (*case study B*) applied an in-line SFV and NIR probe to continuously collect granule size and moisture data. The developed BD PLS model enabled a good prediction of batch BD by use of the granule size distribution and NIR data collected at the end of the spraying period. Addition of granule product information collected during the complete granulation cycle did not improve the predictions. By applying the BD DoE regression equation information, the granulation process was modified during the drying period to meet the quality requirements. In addition, the SFV measurements and NIR data allowed the clear distinction between the three different stages of a granulation process. Through the development of a NIR moisture calibration model, adequate in-line prediction of batch end product moisture levels was achieved.

Hence, the results showed that by combining particle size (SFV) and moisture (NIR) trajectories, real-time monitoring of the granulation progress was accomplished. The real-time measurement of end product particle size and prediction of its moisture content enabled in-line granule quality analysis. In addition, the adjustment of granulation progress during drying to meet the desired bulk density requirements showed that full control of the granulation process is possible by use of SFV and NIR spectroscopy. Implementation of the (automated) control strategy should result into the production of high quality batches at lower overall costs.

REFERENCES

- [1] D.E. Wurster, *Journal of the American Pharmaceutical Association*, 48 (1959) 451-454.
- [2] D.E. Wurster, *Journal of the American Pharmaceutical Association*, 49 (1960) 82-84.
- [3] Food and Drug Administration, *Guidance for Industry; PAT - A framework for innovative pharmaceutical development, manufacturing and quality assurance*, (2004)
- [4] D.M. Parikh, J.A. Bonck, M. Mogavero, in: D.M. Parikh (Ed.), *Handbook of Pharmaceutical Granulation Technology*, Marcel Dekker Inc., New York, 1997, p. 227-302.
- [5] A. Burggraeve, T. Van Den Kerkhof, M. Hellings, J.P. Remon, C. Vervaet, T. De Beer, *European Journal of Pharmaceutics and Biopharmaceutics*, 76 (2010) 138-146.
- [6] A. Burggraeve, T. Van den Kerkhof, M. Hellings, J.P. Remon, C. Vervaet, T. De Beer, *European Journal of Pharmaceutical Sciences*, 42 (2011) 584-592.
- [7] C. Fischer, M. Peglow, E. Tsotsas, *Chemical Engineering Science*, 66 (2011) 2842-2852.
- [8] A. Hartung, M. Knoell, U. Schmidt, P. Langguth, *Drug Development and Industrial Pharmacy*, 37 (2011) 274-280.
- [9] J. Huang, C. Goolcharran, J. Utz, P. Hernandez-Abad, K. Ghosh, A. Nagi, *Journal of Pharmaceutical Innovation*, 5 (2010) 58-68.
- [10] T. Närvänen, 19th Helsinki Drug Research, Helsinki, FINLAND, 2008, p. S12-S12.
- [11] T. Närvänen, T. Lipsanen, O. Antikainen, H. Räikkönen, J. Heinämäki, J. Yliruusi, *Journal of Pharmaceutical Sciences*, 98 (2009) 1110-1117.
- [12] T. Närvänen, T. Lipsanen, O. Antikainen, H. Räikkönen, J. Yliruusi, *International Journal of Pharmaceutics*, 357 (2008) 132-138.
- [13] D. Petrak, S. Dietrich, G. Eckardt, M. Koehler, *Advanced Powder Technology*, 22 (2011) 203-208.
- [14] S. Schmidt-Lehr, H.U. Moritz, K.C. Jurgens, *Pharmazeutische Industrie*, 69 (2007) 478-484.
- [15] X.H. Hu, J.C. Cunningham, D. Winstead, *International Journal of Pharmaceutics*, 347 (2008) 54-61.
- [16] J. Huang, G. Kaul, J. Utz, P.W. Hernandez, V., D. Bradley, A. Nagi, D. O'Grady, *Journal of Pharmaceutical Sciences*, 99 (2010) 3205-3212.
- [17] A. Tok, X.P. Goh, W. Ng, R. Tan, *Aaps Pharmscitech*, 9 (2008) 1083-1091.
- [18] D. Petrak, *Particle & Particle Systems Characterization*, 19 (2002) 391-400.
- [19] D. Petrak, H. Rauh, *Particulate Science and Technology*, 24 (2006) 381-394.
- [20] N. Kail, W. Marquardt, H. Briesen, *Industrial & Engineering Chemistry Research*, 48 (2009) 2936-2946.

- [21] A. Ruf, J. Worlitschek, M. Mazzotti, *Particle & Particle Systems Characterization*, 17 (2000) 167-179.
- [22] M. Blanco, J. Coello, H. Iturriaga, S. Maspoch, C. de la Pezuela, *Analyst*, 123 (1998) 135R-150R.
- [23] Y. Roggo, P. Chalus, L. Maurer, C. Lema-Martinez, A. Edmond, N. Jent, *Journal of Pharmaceutical and Biomedical Analysis*, 44 (2007) 683-700.
- [24] F.J.S. Nieuwmeyer, M. Damen, A. Gerich, F. Rusmini, K.M. van der Voort, H. Vromans, *Pharmaceutical Research*, 24 (2007) 1854-1861.
- [25] T. De Beer, A. Burggraeve, M. Fonteyne, L. Saerens, J.P. Remon, C. Vervaet, *International Journal of Pharmaceutics*, 417 (2011) 32-47.
- [26] M. Alcala, M. Blanco, M. Bautista, J.M. Gonzalez, *Journal of Pharmaceutical Sciences*, 99 (2010) 336-345.
- [27] R.L. Green, G. Thurau, N.C. Pixley, A. Mateos, R.A. Reed, J.P. Higgins, *Analytical Chemistry*, 77 (2005) 4515-4522.
- [28] J.T.T. Leskinen, M.A.H. Okkonen, M.M. Toiviainen, S. Poutiainen, M. Tenhunen, P. Teppola, R. Lappalainen, J. Ketolainen, K. Jarvinen, *Chemical Engineering Journal*, 164 (2010) 268-274.
- [29] W.P. Findlay, G.R. Peck, K.R. Morris, *Journal of Pharmaceutical Sciences*, 94 (2005) 604-612.
- [30] P. Frake, D. Greenhalgh, S.M. Grierson, J.M. Hempenstall, D.R. Rudd, *International Journal of Pharmaceutics*, 151 (1997) 75-80.
- [31] S.G. Goebel, K.J. Steffens, *Pharmazeutische Industrie*, 60 (1998) 889-895.
- [32] A. Peinado, J. Hammond, A. Scott, *Journal of Pharmaceutical and Biomedical Analysis*, 54 (2011) 13-20.
- [33] J. Rantanen, O. Antikainen, J.P. Mannermaa, J. Yliruusi, *Pharmaceutical Development and Technology*, 5 (2000) 209-217.
- [34] J. Rantanen, S. Lehtola, P. Ramet, J.P. Mannermaa, J. Yliruusi, *Powder Technology*, 99 (1998) 163-170.
- [35] J. Rantanen, E. Rasanen, O. Antikainen, J.P. Mannermaa, J. Yliruusi, *Chemometrics and Intelligent Laboratory Systems*, 56 (2001) 51-58.
- [36] J. Rantanen, E. Rasanen, J. Tenhunen, M. Kansakoski, J.P. Mannermaa, J. Yliruusi, *European Journal of Pharmaceutics and Biopharmaceutics*, 50 (2000) 271-276.
- [37] T. Kourti, *Journal of Chemometrics*, 17 (2003) 93-109.
- [38] J. Rantanen, J. Yliruusi, *Pharmacy and Pharmacology Communications*, 4 (1998) 73-75.
- [39] R.J. Barnes, M.S. Dhanoa, S.J. Lister, *Applied Spectroscopy*, 43 (1989) 772-777.
- [40] I.S. Helland, T. Naes, T. Isaksson, *Chemometrics and Intelligent Laboratory Systems*, 29 (1995) 233-241.

CHAPTER 7

REAL-TIME IMAGE-BASED INVESTIGATION OF SPHERONIZATION AND DRYING PHENOMENA USING DIFFERENT PELLET FORMULATIONS

Parts of this chapter are published in:

A. Burggraeve, N. Sandler, J. Heinämäki, H. Räikkönen, J.P. Remon, C. Vervaet, T. De Beer, J. Yliruusi, Real-time image-based investigation of spheronization and drying phenomena using different pellet formulations, *European Journal of Pharmaceutical Sciences*, 44 (2011) 635-642.

ABSTRACT

Chapter 7 describes the real-time application of photometric stereo imaging during the final steps of the extrusion-spheronization process, being spheronization and drying. In addition to the pellet size distribution of undispersed (wet) samples, the imaging technique captures visual information on pellet shape and surface brightness.

Pellet samples were taken at 20 time points during *spheronization* and were imaged at-line (during spheronization) and off-line (after spheronization). Particle size distributions and visual image information were both used to characterize the spheronization behavior of different formulations. Next, particle size distributions and surface brightness values calculated from the at-line obtained images during *fluid bed drying* of pellets were analyzed. The particle size distribution and brightness value changes occurring during pellet drying were explained both by the reduction in residual moisture content and drug solid-state transition.

Due to the rapidness of the technique with regard to sample preparation, sample measurement and the acquisition of results in combination with the possibility to measure undispersed (wet) samples, valuable information on spheronization and drying characteristics of different formulations was obtained in real-time.

CHAPTER 7

REAL-TIME IMAGE-BASED INVESTIGATION OF SPHERONIZATION AND DRYING PHENOMENA USING DIFFERENT PELLET FORMULATIONS

7.1. INTRODUCTION

Extrusion-spheronization (ES) is a frequently used agglomeration process in the pharmaceutical industry to manufacture spherical solid units or pellets with a narrow size and shape distribution. It is a multi-step process consisting of four consecutive stages: dry blending, preparation of the wet mass (granulation), shaping of the wet mass into cylinders (extrusion) and rounding of the cylinders into spheres (spheronization) [1]. Afterwards, fluid bed drying is usually applied to effectively remove water (or solvent) from the wet pellets. Pellets produced by ES offer several technological advantages (e.g., optimal packing and flow properties, ideal shape for coating, low friability) and therapeutic advantages (e.g., less irritation of the gastro-intestinal tract and a lowered risk of side effects due to dose dumping) compared to conventional drug delivery systems.

The influence of process and formulation variables upon the quality (e.g., size, shape, drug release rate) of produced pellets has extensively been investigated [2-11]. Due to the large amount of liquid in the granulated mass, the interaction of API with water can induce phase transformations altering the pharmaceutical and biopharmaceutical performance of the drug. Hence, research on *real-time* monitoring of ES has mainly focused on the detection of process-induced transformations of the API throughout the different ES process steps. Sandler et al. [12] investigated the phase transitions in nitrofurantoin and theophylline formulations during pelletization. An at-line PAT approach consisting of Raman spectroscopy, near infrared spectroscopy and X-ray powder diffraction was used to increase the understanding of the solid-state behavior of the APIs during pelletization. More recently, Römer et al. [13] applied at-line NIR spectroscopy and XRPD to better understand process-

induced transformations of erythromycin dihydrate during pellet manufacturing (ES and oven tray drying). The same group reported on the use of in-line NIR spectroscopy to monitor phase transformations of erythromycin dihydrate pellets during a miniaturized fluid bed drying process [14].

The amount of granulation liquid also influences the extrusion and spheronization behavior of the granulated mass. Extrudates must possess an optimal level of strength, brittleness and plasticity to obtain pellets with a desired size and shape. The most applied techniques to determine pellet size distribution include sieving, laser diffraction and image analysis. These methods can be time-consuming (sample preparation and analysis) and require large amounts of sample. Moreover, the cohesiveness of wet materials often impedes the measurement. In this study, particle size and shape information were obtained in *real-time* by applying a photometric stereo imaging technique (FlashSizer 3D, FS3D) [15]. The tool consists of two white light sources, positioned 180° from each other in a horizontal plane. By illumination of the sample surface, two images are captured and are reconstructed to a 3D image from which the particle size can be calculated. In addition to the particle size distribution, the photometric approach also provides information on particle shape and particle surface roughness and brightness. Different roughness or brightness parameters, based on the change in grey scale values of the surface images can be computed. The FS3D is a very fast technique with regard to sample preparation, sample measurement and the acquisition of results. Moreover, the cohesiveness of samples is not problematic as measurements do not require sample dispersion.

Chapter 7 describes the application of photometric stereo imaging during the final steps of the ES process, being spheronization and drying. Samples were taken from the spheronizing mass at different time points and imaged at-line (i.e., during spheronization) and off-line (i.e., after spheronization) with the instrument. Visual image information and particle size distributions were both used to characterize the spheronization behavior of different formulations. Next, particle size distributions and surface brightness values calculated from the at-line obtained images during fluid bed drying of pellets were analyzed. Residual moisture content and solid-state information were used to explain the particle size distribution and brightness value changes occurring during pellet drying.

Taking images during spheronization has been reported previously by Fielden et al. [16, 17] using high speed photography. They present images of the spheronizing mass, taken from a distance, at 1 and 5 min of spheronization. Our results are based on images taken more frequently during the spheronization process (i.e., during the first 5 min, samples were taken every 20 s from the pellet bed. Subsequently, pellets were obtained every minute until a 10 min spheronization time was

reached). The FS3D images provide a clear view of the spheronized mass in which the dimensions of individual pellets can be distinguished. This is not the case for the images shown in the work by Fielden et al. Moreover, the photometric approach allowed to derive size information directly from the obtained images, without the need to disperse the wet sample. In the work presented by Fielden et al., drying was performed prior to the determination of size and shape via sieving and image analysis.

7.2. MATERIALS AND METHODS

7.2.1. Materials

The pellet formulation consisted of 50% (w/w) anhydrous theophylline (TP, BASF Aktiengesellschaft, Ludwigshafen, Germany) and 50% (w/w) microcrystalline cellulose (MCC, Avicel PH101, FMC Biopolymer, Cork, Ireland). Purified water was added as a granulation liquid.

7.2.2. Methods

7.2.2.1. Pelletization and drying

Pellets were manufactured using the continuous Nica pelletizing system (Nica System AB, Mölndal, Sweden) consisting of three units: a mixer/granulator, an extruder and a spheronizer.

First, anhydrous TP and MCC were weighed and dry-mixed in a double cone mixer during 10 min. The blended powder mass (200 g) was added to the granulator (Nica M6L), mixing the powder blend and granulation liquid instantaneously. The powder feed rate was 35 rpm (1148 g/min) and different liquid addition rates were used (*vide infra*). The radial screen extruder (Nica E140) shaped the granules into cylinders by rotation of the feeder and agitator in opposite directions. Feeder and agitator speed were set to 45 rpm and 28 rpm, respectively. A screen thickness of 1.2 mm was employed and the granules were forced through dies with a 1 mm diameter. At the base of the spheronizer (Nica S320), a friction plate (diameter of 32 cm) with crosshatched pattern was inserted. The spheronizer friction plate rotated at 900 rpm during a total residence time of 10 min.

Pellets with three levels of moisturizing liquid were prepared for the **spheronization study**. Liquid addition rates of 750, 870 and 990 g/min resulted into pellets with a moisture level of 40% (w/w) **batch I**; 43% (w/w) **batch II**; and 46% (w/w) **batch III** on the basis of the wet mass. Batches I-III were each manufactured three times (total of nine batches) by the continuous ES technique (Table 7.1).

Pellets with a moisture level of 41% (w/w) (**batch A**) and 45% (w/w) (**batch B**) were prepared for the **fluid bed drying experiments** (Strea-1, Aeromatic-Fielder AG, Switzerland). A liquid addition rate of 810 g/min (batch A) and 930 g/min (batch B), respectively was therefore used during granulation. Extrudates were spheronized during a total process time of 5 min. Other granulation, extrusion and spheronization settings were identical to those stated above. Drying was performed using inlet air temperatures of 50 °C and 59 °C (Table 7.1).

Table 7.1. Overview of performed experiments.

	Batch	Water (%w/w)	# Batches	Drying T (°C)	Sampling during spheronization	Sampling during fluid bed drying	Measurement
Spheronization	I	40	3	-	0, 20, 40 s, ...	-	
	II	43	3		5, 6 min, ...		At-line FS3D (1x) Off-line FS3D (5x)
	III	46	3		10 min		
Fluid bed drying	A	41	2	50	-	Every 20 min	At-line FS3D
				59			At-line Raman spectroscopy
	B	45	2	50 59			Off-line moisture analysis

7.2.2.2. Sampling

The extrudates of formulations I-III were spheronized for a total process time of 10 min. During the first 5 min, samples (4 g) were taken every 20 s from the pellet bed while the spheronizer plate was running at 900 rpm. Subsequently, pellets were obtained every minute until a 10 min spheronization time was reached (i.e., 20 samples in total per batch). The samples were imaged at-line (i.e., during spheronization, one measurement) and off-line (i.e., after spheronization, five measurements).

Following spheronization of formulations A and B, the wet pellets were fluid bed dried at 50 °C and 59 °C (Table 7.1). After removal of free surface water (corresponding to a product temperature of approximately 50 °C), samples were taken from the pellet bed every 20 min and measured at-line with photometric stereo imaging and Raman spectroscopy, and off-line via loss-on-drying. Drying continued until no significant changes in residual moisture content were measured.

7.2.2.3. Photometric stereo imaging

The imaging unit (FlashSizer 3D, Intelligent Pharmaceuticals Ltd., Finland) consists of a monochrome CCD camera connected to a metal cuvette with a glass window and a computer. A variant of photometric stereo [18] with two white light sources, placed 180° from each other in a horizontal plane, was used. All measured samples were filled into a petridish (layer thickness 5 mm) and positioned on top of the imaging instrument's glass window. Two digital images were captured during each measurement and recombined to extract particle size distribution information.

The grey scale values of the digital images of sample surfaces correspond to the brightness of the surfaces, and are characterized by a number in the range from 0 to 255 where 0 is totally black and 255 is completely white. The pellet surface brightness index is then calculated and is based on differences in these grey scale values. The calculations are derived from roughness measurements

and accordingly different parameters can be calculated in a similar way using the grey scale profiles. In this study, the arithmetic average of the brightness profile (Ba) of the digital images' grey scale values was used. The average Ba parameter is calculated from the height data according to Eq. 7.1:

$$Ba = \sum_{n=1}^N \frac{|Z_n - \bar{Z}|}{N} \quad (7.1)$$

where Z_n is the individual height (brightness) value of one measurement point and \bar{Z} the mean value of all the height data points. N is the number of measurement points. Ba measures the average brightness of the profile points to the average line.

7.2.2.4. Raman spectroscopy

Pellets sampled during fluid bed drying were measured at-line using Raman spectroscopy. Three Raman spectra of each sample were collected with a Raman Rxn 1 spectrometer (Kaiser Optical Systems, Ann Arbor, MI, USA), equipped with an air-cooled CCD detector and a fiber-optically coupled P^hAT probe head. The laser wavelength was the 785 nm line from a 785 nm Invictus NIR diode laser. The spectra were recorded over the 0 – 1900 cm⁻¹ range with a resolution of 4 cm⁻¹ and an exposure time of 5 s. Data collection and analysis were performed with the HoloGRAMSTM data collection software, the HoloREACTTM reaction analysis and profiling software, and the Matlab software (version 2007b). Spectra were preprocessed by normalization and analyzed using multivariate curve resolution (MCR).

7.2.2.5. Moisture analysis

Pellet samples taken during fluid bed drying were measured off-line with an infrared dryer (Sartorius MA100, Sartorius, Göttingen, Germany). Pellets were heated to a temperature of 105 °C and dried until the weight loss rate was 0.1% in 50 s. Average moisture levels were calculated based on three measurements per sample.

7.3. RESULTS AND DISCUSSION

7.3.1. Photometric stereo imaging during spheronization

The FS3D imaging equipment expresses the particle size distribution of a measured sample as sieve fractions and on the basis of this distribution computes D_{10} , D_{50} and D_{90} percentiles. Figure 7.1 displays the particle size distributions of batches I-III measured at-line, after 10 min of spheronization. With increasing amount of granulation liquid, the distribution shifted towards larger sizes. The use of MCC as an extrusion and spheronization aid, even in small quantities, requires a minimum presence of water as granulating fluid [11]. Below the required moisture level of the granulated mass, the plasticity of the extrudates is insufficient resulting in a larger fraction of fines during spheronization. Above the specific moisture range, extrudates are soft and easy to deform, resulting into large and round shaped particles. Hence, the high yield of pellets sized $< 500 \mu\text{m}$ for batch I indicated that the amount of granulation liquid was close to this lower limit. The moisture level of batch III probably corresponded to the upper level of the specific water content range as the batch yielded a large fraction of oversized pellets (size $> 1500 \mu\text{m}$).

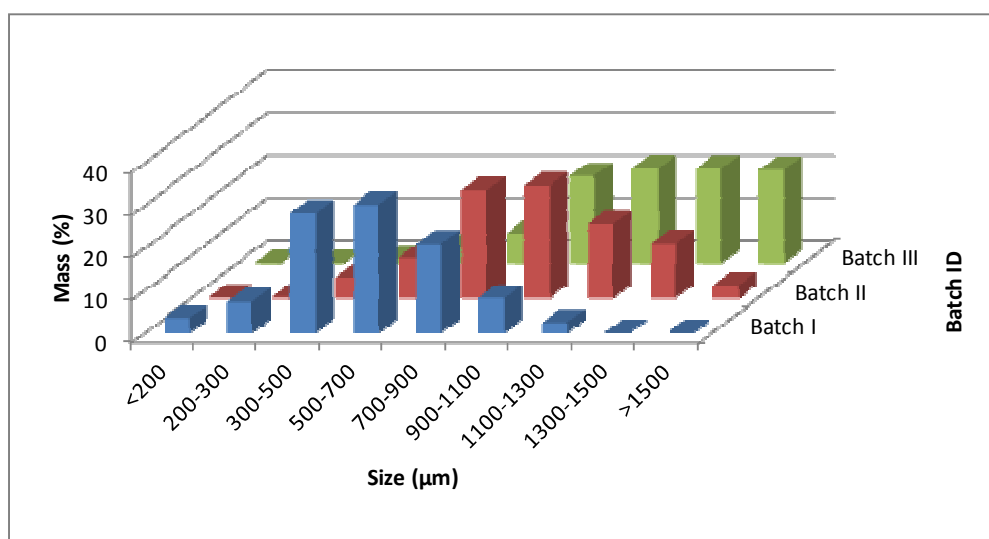


Figure 7.1. Particle size distributions of batches I (40% w/w), II (43% w/w) and III (46% w/w) measured after spheronization.

Batches I-III were each manufactured in threefold to compare batch-to-batch reproducibility. Figure 7.2 displays the corresponding average D_{10} , D_{50} and D_{90} percentiles and standard deviations for the three replicates per batch. The particle size variation between the replicates decreased with increasing amount of granulating liquid. The decrease in standard deviation was more pronounced for the smallest and median sized particles (D_{10} and D_{50}). At the low liquid content of batch I, extrudates were brittle and shattered upon spheronization creating a large quantity of fines. Hence,

particles of various sizes were spheronized causing the increased size variability between the replicates of batch I.

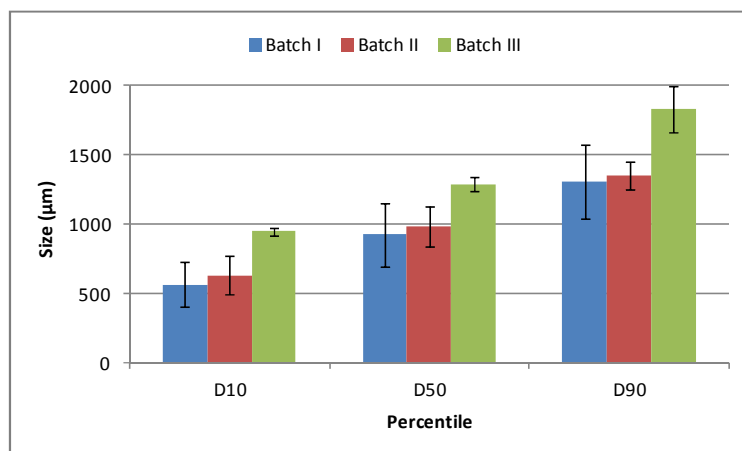


Figure 7.2. Average D10, D50 and D90 percentiles of batches I (40% w/w), II (43% w/w) and III (46% w/w) measured after spheronization. Averages and standard deviations are based on the measurement of three replicate batches.

Besides at-line FlashSizer imaging, five off-line FS3D measurements of each sample were performed. Figure 7.3a and b displays the at-line and off-line size percentiles for batches I and III, respectively, at different time points during the spheronization process. For batch I, most at-line determined particle sizes lay within the standard deviation interval of the average off-line sizes. Hence, the good correspondence between at-line and off-line sizes for batch I indicates that the single image captured during spheronization provides equal particle size distribution information as the off-line (reference) images. In addition to the between-replicate-batch variation observed in Figure 7.2, a large within-batch variation for the lowest water amount is visible in Figure 7.3a. The large standard deviations at each time point depict the size differences between the five off-line measurements.

For the increased water level experiments (batch III, Figure 7.3b), all five off-line FS3D measurements corresponded to each other resulting in smaller standard deviations. Figure 7.3b also shows that during the initial stages of spheronization of batch III, the at-line determined sizes were smaller than the average off-line particle sizes. As more moisture could migrate to the surface of the pellets during spheronization, the obtained images were slightly blurred and displayed a lower contrast at the edges of the particles. This affected the particle size calculation and led to smaller, somewhat underestimated at-line sizes compared to the results of the off-line measured samples, where the moisture is partially reabsorbed by the MCC core of the pellets.

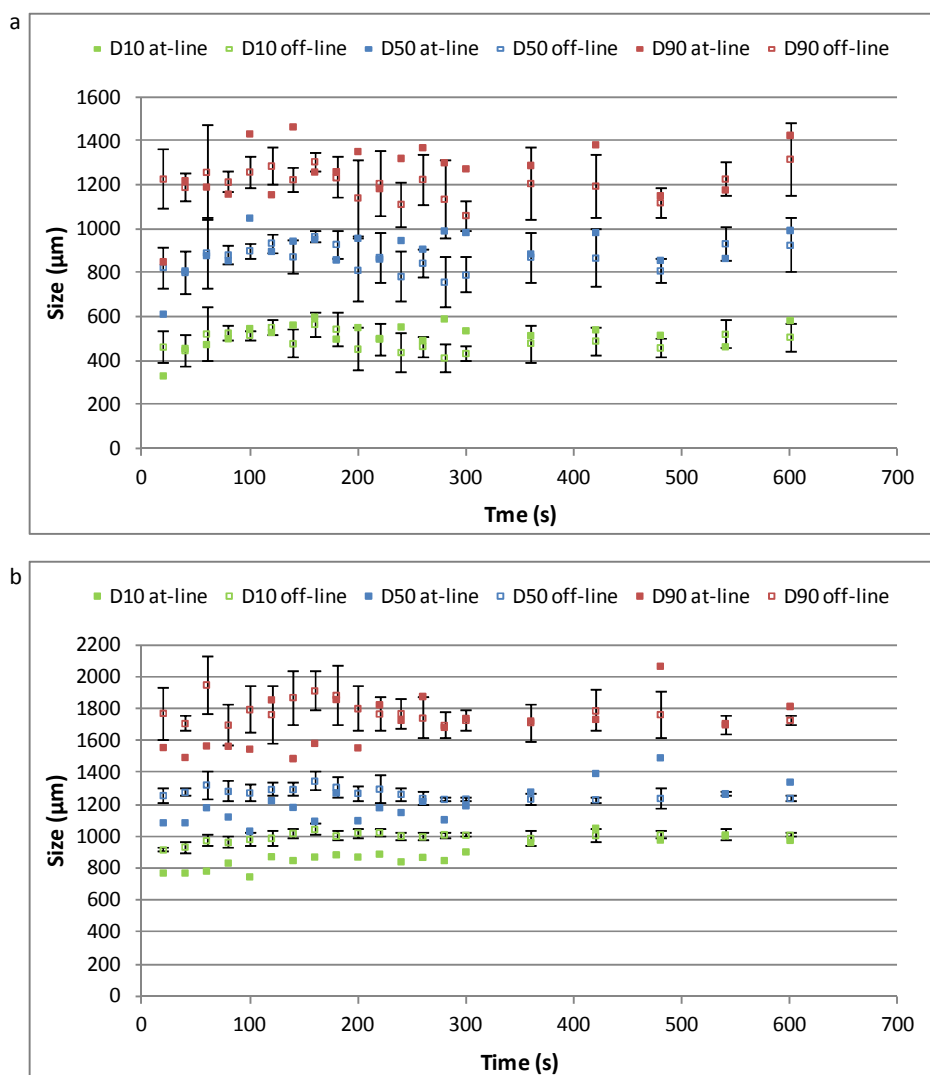


Figure 7.3. At-line and average off-line (with standard deviation) *D10*, *D50* and *D90* percentiles based on FS3D images of batches I (40% w/w) (a) and III (46% w/w) (b) in function of spheronization time.

Next to the numerical values for the particle size distribution, the imaging technique also provides visual information about the samples. By comparing the images collected at 20 different time points during spheronization, a visual record of the evolution of the granule shape in function of time was obtained. In Figure 7.4, the at-line obtained images for batches I-III after 0, 1, 5 and 10 min of spheronization are shown. The amount of granulation liquid clearly influenced the surface texture and length of the extrudates (sampling time point 0). The batch I extrudates were short, brittle and rough. The higher liquid amount in batches II and III yielded longer extrudates with smoother surfaces. After 1 min of spheronization, most wet granules of batches I and II had an irregular shape. Frictional forces during the remainder of the spheronization period resulted in spherical particles at the end of the process. The water present in the extruded mass of batch III provided the necessary plasticizing and lubricating properties to produce spheroids after 1 min of spheronization. Additional spheronization caused further smoothing of spheroid surfaces. By comparing the FS3D images for

the three batches, it is clear that the deformation rate increased by increasing the amount of granulation liquid. The mixture of small and larger sized pellets shown during spheronization of batch I (images in row 1 of Figure 7.4) explain the large standard deviations plotted in Figure 7.3a. The small standard deviations of batch III resulted from the uniform size distributions shown in the images in row 3 of Figure 7.4.

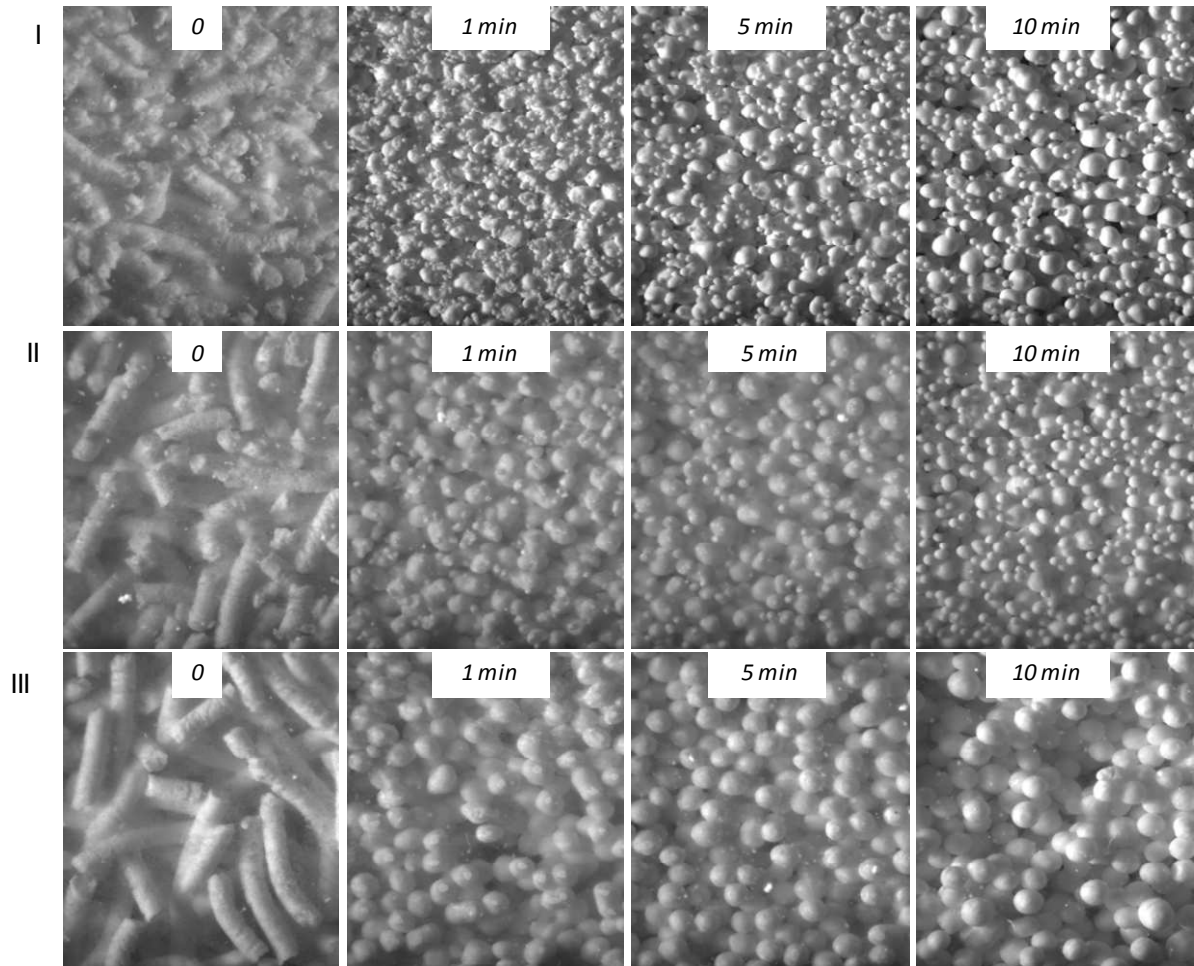


Figure 7.4. At-line obtained FS3D images of batches I (40% w/w), II (43% w/w) and III (46% w/w) after 0, 1, 5 and 10 min spheronization.

Recently, Koester and Thommes [19] reported an extension to the traditional pelletization mechanisms suggested by Rowe [20] and Baert and Remon [21]. Their study showed that next to the plastic deformation of the initially fractured extrudates, material transfer between the pellet particles should also be considered in the spheronization mechanism (Chapter 2). The particle size distribution profile during spheronization of batch I (Figure 7.5a) demonstrates that in the beginning of the process, the decrease in fines (size < 500 μm) was accompanied by an increase of pellets in the size fraction 500 – 1500 μm . Analysis of the corresponding FS3D images showed the loss of fine fragments during the initial 100 s of spheronization. In the images corresponding to the next stages of spheronization, small defects on the surfaces of pellets were observed. The areas encircled in

Figure 7.5b-d exemplify this phenomenon. After approximately 480 s of plastic deformation during processing in the spheronizer, completely smooth surfaces were obtained (Figure 7.5e). Hence, combining size and visual information suggests the adhesion of fine particles to larger sized pellets as reported by Koester and Thommes. After 100 s the amount of fines stayed constant during the remainder of the spheronization process. Due to the low amount of granulation liquid, further agglomeration of these small particles to the pellet surface of larger granules was not possible.

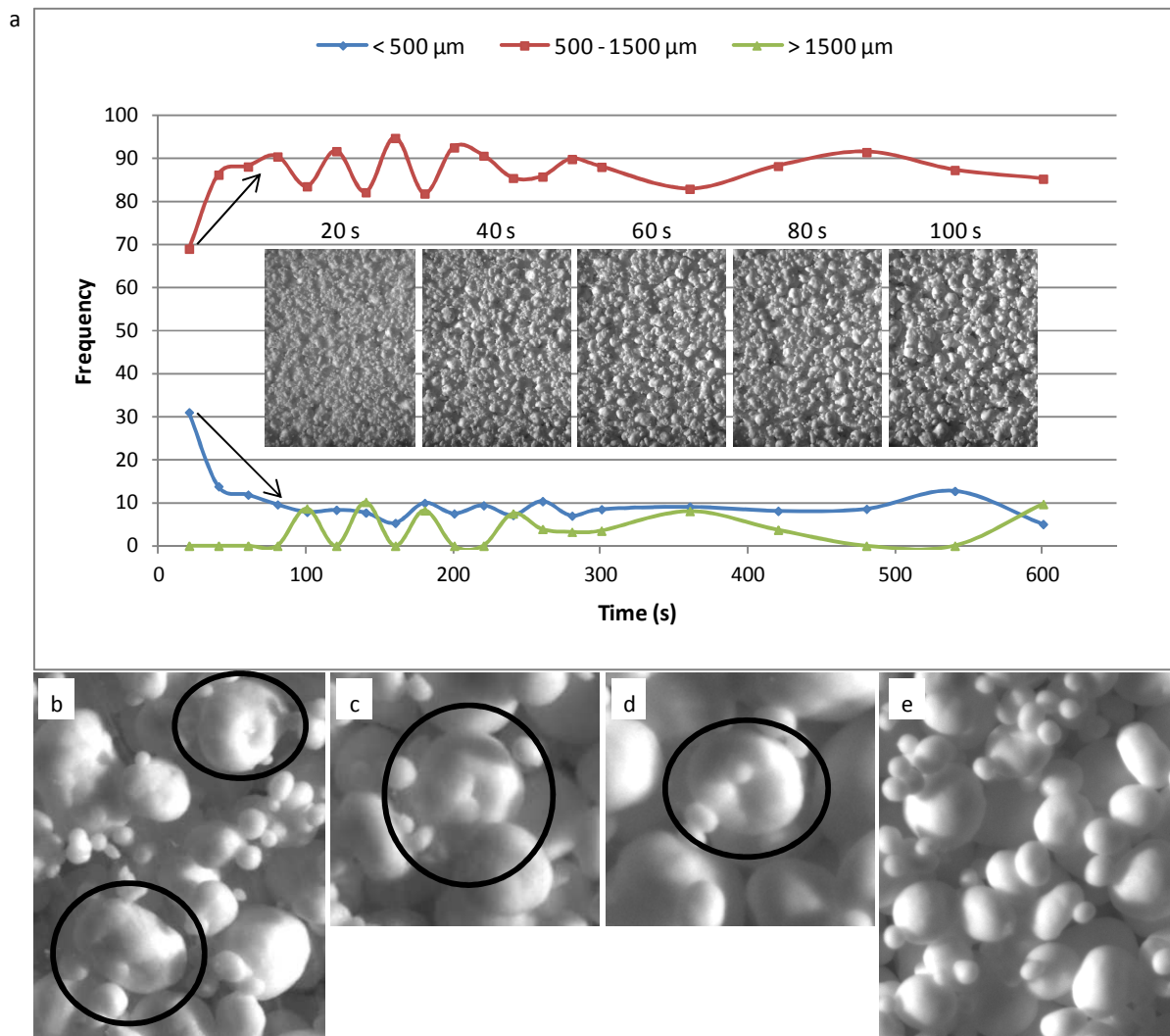


Figure 7.5. FS3D particle size distribution profile and images during spheronization of batch I (40% w/w). The images obtained after 160 s (b), 220 s (c), 260 s (d) and 480 s (e) are displayed.

7.3.2. Photometric stereo imaging during pellet fluid bed drying

A spheronization process is always followed by a drying step to complete the formation of the pellet matrix structure. Drying affects pellet characteristics such as size, density and tensile strength. At the same time, micro-structural properties change due to the densification of pellets, and solid-state transformations may occur which both influence the drug release rate.

7.3.2.1. Particle size distribution

FS3D measurements

Figures 7.6a and 7.7a display the D_{10} , D_{50} and D_{90} trajectories during fluid bed drying of batches A and B, respectively. The particle size distribution profiles for both batches are shown during drying at two inlet air temperature levels (50 °C and 59 °C). For both formulations, a decrease in particle size distribution during the initial drying minutes (i.e., between the first and second measured sample) was observed. The shrinkage of pellet size was most prominent for the D_{90} percentile. Throughout the further drying process, no relevant size changes occurred. For both batches, the size of the pellets measured at the second sampling time point was similar for the two inlet air temperatures (50 °C and 59 °C). Hence, the size shrinkage did not depend on the drying temperature in this temperature interval. Due to the lack of size data between the first and second time point, no information was available on the rate of pellet shrinkage at the two temperature levels.

Moisture analysis

Figures 7.6b and 7.7b display the corresponding decrease in residual moisture content during fluid bed drying of batches A and B, at the two drying temperature levels. The total moisture content of batch B at sampling time point 1 was approximately 3.4% (w/w) higher than the water content of batch A. A large drop in water content was observed between the first and second measured sample. Although the difference in granulation liquid between batches A and B clearly influenced the plasticity of the wet mass and the size of the pellets, similar moisture levels were obtained at sampling time point 2. From time point 2 onwards, the moisture content profiles of the two batches at the same temperature level did not distinctively differ. Both formulations demonstrated that the granulation liquid was removed faster when a higher drying temperature was applied. When dried for an extensive time period (more than two times longer), the 50 °C-dried batches reached the same residual moisture level as the 59 °C-dried batches.

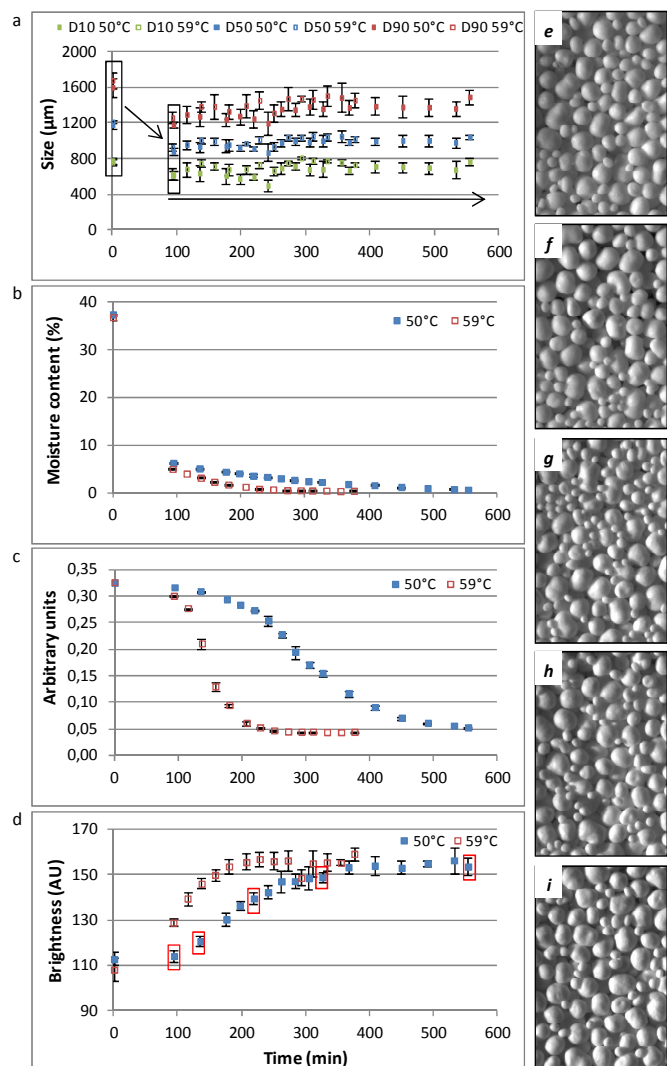


Figure 7.6. Data obtained during fluid bed drying of batch A (41% w/w) at 50 °C and 59 °C. *D*10, *D*50 and *D*90 profiles (a), moisture content (b), MCR estimated concentration profile (c) and brightness (d). FS3D images at sampling time points 2 (e), 3 (f), 6 (g), 11 (h) and 17 (i). The brightness values at these time points are indicated by red rectangles in 7.6d.

Raman spectroscopy

Theophylline is known to exist in both the (stable and metastable) anhydrous and hydrous crystalline form. The monohydrous crystallite is a channel hydrate characterized by a crystal structure in which every water molecule is located next to other water molecules along an axis of the lattice. It has been reported that theophylline undergoes polymorphic changes during wet granulation [22] and during subsequent drying [23]. Transitions between these solid forms depend on kinetic and thermodynamic factors. Raman spectroscopy is sensitive to alterations in intra- and intermolecular

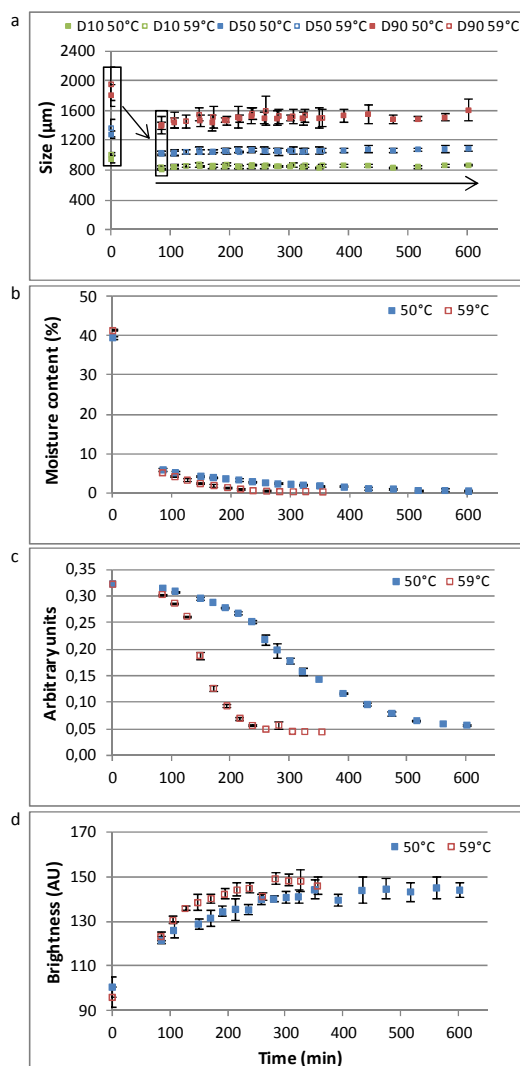


Figure 7.7. Data obtained during fluid bed drying of batch B (45% w/w) at 50 °C and 59 °C. *D*10, *D*50 and *D*90 profiles (a), moisture content (b), MCR estimated concentration profile (c) and brightness (d).

bonding and hence solid-state transformations. Unlike NIR spectroscopy, it does not provide information on the presence of free water molecules as water is a weak Raman scatterer. Figure 7.8 displays the Raman spectra (1500 – 1800 cm^{-1}) of batch A pellets, captured during fluid bed drying using an inlet air temperature of 50 °C. Differences between the spectra correspond to the TP monohydrate to anhydrate transformation. The 1688 cm^{-1} Raman band of TP monohydrate was splitted into two bands in the TP anhydrate spectrum (1666 cm^{-1} and 1707 cm^{-1} , respectively).

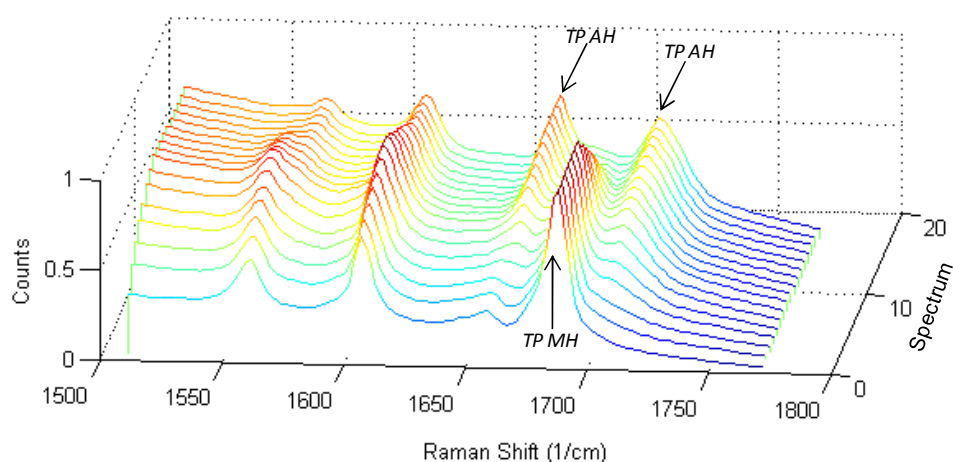


Figure 7.8. Raman spectra (1500 – 1800 cm^{-1}) of batch A (41% w/w) pellets collected during fluid bed drying using an inlet air temperature of 50 °C. (TP AH = theophylline anhydrate, TP MH = theophylline monohydrate)

Multivariate curve resolution was performed on the 1500 – 1800 cm^{-1} spectral region of all Raman spectra of batch A and B pellets, collected at-line during drying at 50 °C and 59 °C. By decomposition of this data matrix, the true underlying sources responsible for the spectral variation were identified. The two resolved underlying factors contributing to the spectral variation corresponded to the pure spectra of theophylline anhydrate and monohydrate, respectively. The estimated concentration profiles shown in Figures 7.6c and 7.7c display the contributions of the second factor (i.e., TP monohydrate) to the Raman spectra collected during fluid bed drying of batches A and B. At sampling time point 1, all batches showed a maximum contribution of component 2, corresponding to a complete TP monohydrate state. The large drop in moisture content observed for all batches between time points 1 and 2 in Figures 7.6b and 7.7b, corresponded to a small estimated concentration decrease in Figures 7.6c and 7.7c. This demonstrates that only the evaporation of free water occurred between sampling time points 1 and 2. The similar MCR weights of the first 2 time points indicate that almost no dehydration via the TP monohydrate water channels had occurred before time point 2. From time point 2 onwards, the contribution decrease corresponds to the solid-state transformation from monohydrate TP to anhydrous TP. The dehydration of monohydrate water molecules continued until no more water could be removed from the structure (no change in contribution at the end of drying). A clear difference between the contribution

trajectories of experiments performed at different drying temperatures was noticed. The dehydration rate increased at a higher temperature. After an extended drying period, the same level of anhydrate was reached for the batches dried at the lowest temperature. As previously observed for the residual moisture content trajectories, the amount of granulation liquid did not distinctively differentiate the dehydration profiles of the two batches at the same temperature level. Airaksinen et al. [23] reported on the presence of an anhydrous metastable form during the fluid bed drying of theophylline granules. The characteristic peak of metastable anhydrous theophylline was not detected during drying of the pellets.

Combining particle size distribution information from FS3D measurements (Figures 7.6a and 7.7a) with moisture content (Figures 7.6b and 7.7b) and solid-state trajectories (Figures 7.6c and 7.7c) showed that the size shrinkage during the initial drying was caused by the evaporation of free water. The dehydration of TP monohydrate to TP anhydrate did not influence the pellet size distribution.

7.3.2.2. Surface brightness and visualization

Next to the particle size distribution, the FS3D tool also provided information on surface reflective properties. Based on the change in grey scale values in the surface images, several brightness parameters were calculated. In this study, the arithmetic average of the brightness profile (Ba) was used to describe the surface of dried pellets. Figures 7.6d and 7.7d represent the at-line measured Ba profiles (expressed as arbitrary units based on variations in pixel grey scale) of batches A and B, respectively, during fluid bed drying at two temperature levels. Both plots demonstrate a gradual increase in surface Ba values during drying until a maximum (plateau) was reached. The rate of increase was dependent of the applied drying temperature. The maximum value was reached faster when a higher drying temperature was used. The moisture level profiles (Figures 7.6b and 7.7b) showed that at sampling time point 1 the pellets were at the highest water state. This corresponded to a minimum brightness value in Figures 7.6d and 7.7d. Combining moisture content and solid-state information with brightness profiles learned that the evaporation of free water and the successive polymorph transformation was accompanied by an increase in surface reflective properties and therefore Ba values. Maximum values were reached when the TP monohydrate to anhydrate conversion was completed. A ranking of the FS3D images, on the basis of which brightness values were calculated, explained the increasing Ba numbers. Moving from Figure 7.6e towards 7.6i, a grey scale gradient appears. As long as water was removed from the pellet matrix, light reflection changed. The presence of surface water and a monohydrate state caused a different reflection of the light compared to a completely anhydrous system.

7.4. CONCLUSIONS

In Chapter 7, the at-line use of photometric stereo imaging during spheronization and fluid bed drying was described. Data showed that one single at-line measurement provided equal pellet size information as the average of five off-line measurements. Based on the captured images and computed particle size distributions, the necessary information was provided to characterize the spheronization behavior of different formulations. The comparison of images obtained at different time points during spheronization, allowed a visual record of the change in granule shape and size. During pellet fluid bed drying, the FS3D technique measured an initial decrease of pellet size and increase of surface brightness. Comparing size, brightness, moisture content and solid-state trajectories showed that the size shrinkage was due to the evaporation of free water. The increase of surface Ba values resulted from both the removal of free and crystal water.

Due to the rapidity of the technique and the possibility to measure undispersed wet samples, valuable information about spheronization and drying features of different formulations was obtained in real-time. Hence, insight into the spheronization and drying step is provided, which allows the fast and effective development of a pelletization process. Particle size (distribution), density, sphericity, flowability, porosity, surface roughness, friability and drug release are the important physical properties of pellets prepared via extrusion-spheronization [24]. This study showed that several of these properties can be obtained in real-time by a single measurement.

REFERENCES

- [1] A. Reynolds, *Manufacturing Chemist and Aerosol News*, 41 (1970) 40-43.
- [2] A.B.B. Bashaiwoldu, F. Podczek, M. Newton, *European Journal of Pharmaceutical Sciences*, 21 (2004) 119-129.
- [3] L. Hasznos, I. Langer, M. Gyarmathy, *Drug Development and Industrial Pharmacy*, 18 (1992) 409-437.
- [4] L. Hellén, J. Yliruusi, *International Journal of Pharmaceutics*, 96 (1993) 217-223.
- [5] L. Hellén, J. Yliruusi, E. Kristoffersson, *International Journal of Pharmaceutics*, 96 (1993) 205-216.
- [6] L. Hellén, J. Yliruusi, P. Merkkü, E. Kristoffersson, *International Journal of Pharmaceutics*, 96 (1993) 197-204.
- [7] J.M. Newton, S.R. Chapman, R.C. Rowe, *International Journal of Pharmaceutics*, 120 (1995) 101-109.
- [8] D. Sonaglio, B. Bataille, C. Ortigosa, M. Jacob, *International Journal of Pharmaceutics*, 115 (1995) 53-60.
- [9] J.J. Sousa, A. Sousa, F. Podczek, J.M. Newton, *International Journal of Pharmaceutics*, 144 (1996) 159-169.
- [10] C. Vervaet, J.P. Remon, *International Journal of Pharmaceutics*, 133 (1996) 29-37.
- [11] L.S.C. Wan, P.W.S. Heng, C.V. Liew, *International Journal of Pharmaceutics*, 96 (1993) 59-65.
- [12] N. Sandler, J. Rantanen, J. Heinämäki, M. Römer, M. Marvola, J. Yliruusi, *Aaps Pharmscitech*, 6 (2005) E174-E183.
- [13] M. Römer, J. Heinämäki, I. Miroshnyk, N. Sandler, J. Rantanen, J. Yliruusi, *European Journal of Pharmaceutics and Biopharmaceutics*, 67 (2007) 246-252.
- [14] M. Römer, J. Heinämäki, I. Miroshnyk, N. Kivikero, N. Sandler, J. Rantanen, J. Yliruusi, *Journal of Pharmaceutical Sciences*, 97 (2008) 4020-4029.
- [15] N. Sandler, *International Journal of Pharmaceutics*, 417 (2011) 227-234.
- [16] K.E. Fielden, J.M. Newton, R.C. Rowe, *International Journal of Pharmaceutics*, 97 (1993) 79-92.
- [17] K.E. Fielden, J.M. Newton, R.C. Rowe, *International Journal of Pharmaceutics*, 81 (1992) 205-224.
- [18] R.J. Woodham, *Optical Engineering*, 19 (1980) 139-144.
- [19] M. Koester, M. Thommes, *Aaps Pharmscitech*, 11 (2010) 1549-1551.
- [20] R.C. Rowe, *Pharmacy International*, 6 (1985) 119-123.
- [21] L. Baert, J.P. Remon, *International Journal of Pharmaceutics*, 95 (1993) 135-141.

- [22] E. Räsänen, J. Rantanen, A. Jørgensen, M. Karjalainen, T. Paakkari, J. Yliruusi, *Journal of Pharmaceutical Sciences*, 90 (2001) 389-396.
- [23] S. Airaksinen, M. Karjalainen, E. Räsänen, J. Rantanen, J. Yliruusi, *International Journal of Pharmaceutics*, 276 (2004) 129-141.
- [24] N.R. Trivedi, M.G. Rajan, J.R. Johnson, A.J. Shukla, *Critical Reviews in Therapeutic Drug Carrier Systems*, 24 (2007) 1-40.

SUMMARY & GENERAL CONCLUSIONS

SUMMARY & GENERAL CONCLUSIONS

The traditionally applied granulation control and endpoint determination tools in the pharmaceutical industry do not ensure the consistent production of granules with the desired quality characteristics. Therefore in this thesis, the application of novel process analyzers for fluid bed granulation and extrusion-spheronization, capturing direct granule product information, was evaluated (**Chapter 1**).

In **Chapter 2**, the characteristics of these two wet granulation techniques were outlined, which showed that both processes are complex as the quality of the produced granules and pellets is determined by various interrelated process and formulation variables. Traditionally, process parameters are measured to assess the state of the process and detect its endpoint. However, these are considered indirect measurements as the parameter values are correlated with the granule properties. At times, these methods are inadequate since they do not account for changes in feed material properties or external disturbances. Limited relevant product information is mainly obtained after processing, making process control difficult which can lead to batch losses.

The use of innovative and efficient technologies in the pharmaceutical manufacturing processes, improving process performance and product quality, is encouraged by the regulatory authorities. As described in **Chapter 3**, a shift from traditional off-line quality analyses to real-time quality assurance by implementing a combination of PAT tools and principles is promoted. By direct monitoring of the critical granule characteristics, an in-depth understanding of the granulation process can be achieved. In addition, combining the real-time collected granule product information with appropriate data processing techniques and chemometrics enables the development of adequate process control and endpoint determination tools to consistently produce granules with the desired quality. Literature shows that a variety of real-time analytical process sensors have been applied in fluid bed granulation and extrusion-spheronization, to improve the understanding and control of the processes. Each technique has its advantages and drawbacks, but a common, main challenge usually lies in the appropriate interfacing of the measurement sensor with the process stream, enabling representative data collection. In addition, the development of a control strategy using the in-line collected product data is not straightforward.

The feasibility of spatial filter velocimetry as a potential PAT tool for the in-line particle size monitoring of a fluidized bed granulation process was critically examined in **Chapter 4**. In first

instance, the practical aspects with regard to the probe's implementation were considered. The SFV probe was located approximately 5 cm from the sidewall of the granulator, to prevent fouling of the measurement zone by the moist mass and to ensure that the probe did not interfere with the agglomeration process. In addition, particles passed through an aperture with 4 mm diameter and a pressurized air connection was used to keep the measurement windows clean and disperse the product mass. A design of experiments was performed, examining the influence of several process and formulation variables on the average granule size, measured in-line with SFV. Real-time SFV and off-line laser diffraction data showed an identical trend in measured D_{50} values among the various batches. The consistent discrepancy in absolute size value between the two sizing techniques was explained by the laser diffraction measurement method. Analysis of the experimental design indicated that two variables had a significant positive effect upon the granule size, i.e., the HPMC concentration and the inlet air temperature during drying. An explanation and better understanding of the (in)significance of the studied variables upon granulation was provided by the SFV granule size trajectories during processing. In-line particle size data were also related to off-line-measured end granule properties (i.e., tapped density and Hausner ratio), using univariate, multivariate and multiway models, enabling the early estimation of these end product properties immediately after processing. Although the multivariate PLS tapped density and the multiway N-PLS Hausner ratio model had acceptable R^2 and RMSEE values, the assessment of end granule properties based on SFV data requires further testing of model performance on an independent test set.

Once it was demonstrated that spatial filter velocimetry enables the direct, fast and non-destructive size determination during fluid bed granulation, the technique was used for the multivariate statistical modeling and control of the process (**Chapter 5**). The presented approach used in-line granule size measurements and granule product temperature registrations of ten reference batches (with identical process settings) to develop a reference PLS model. By rearranging the scores of each PLS component, score control charts were established in which the characteristic trajectory of a reference batch, with upper and lower control limits, is displayed. The use of these score control charts during the granulation of four new test batches showed that the developed reference model was sensitive to small process deviations and allowed early fault detection. In that way, the reprocessing and/or loss of batches is reduced.

The use of all real-time collected granulation information after batch completion allowed to estimate batch density and flowability at an early stage.

Chapter 6 describes the results of three case studies conducted consecutively, in order to develop a process control strategy for a fluid bed granulation process. Real-time granule size distribution information was provided via the implementation of an SFV probe directly into the process

environment in case studies A and B, while in case study C an FBRM probe was (identically) installed in the granulator. Simultaneously, NIR spectra were collected at-line (case study A) and in-line (case studies B and C). The in-line NIR probe was inserted in the granulator at the base of the granulator's front window. A conventionally designed diffuse reflectance and Lighthouse NIR probe were used in case studies B and C, respectively. The rapid data collection offered by these PAT tools enables real-time granulation analysis to control the manufacturing process.

The continuously in-line captured granule size (SFV) and moisture (NIR) trajectories in case study B, enabled the clear distinction between the three stages of a granulation process (mixing, spraying and drying). Comparison with traditionally used product and exhaust air temperature control charts, showed the advantages of implementing an advanced PAT system. Through the development of an NIR moisture calibration model, adequate in-line prediction of batch end product residual moisture level was achieved. Hence, combined with the in-line SFV measurements, end product residual moisture and size (critical granule attributes) were determined in real-time. A feed-forward process control method was developed, where in-line collected granulation information during the process spraying phase was used to determine the optimum drying temperature of the consecutive drying phase, guiding the process towards the desired end product bulk density. Via real-time collection of process (i.e., spraying temperature and spray rate) and product (i.e., granule size distribution and moisture) parameters during the spraying period, the batch density is predicted early-on, i.e., at the end of the spraying cycle. When the predicted density does not meet the desired value, the control method proposes the use of an adjusted drying temperature leading to the desired granule density at the end of the granulation process. Results showed that the bulk density PLS model, based on the SFV and NIR data collected at the end of the spraying period, enabled a good prediction of batch bulk density. The addition of granule product information collected during the complete granulation cycle did not improve the predictions. The granulation process of two new batches was successfully modified during the drying period, meeting the quality requirements, by applying the bulk density DoE regression equation information. Implementation of the automated control strategy should result into the production of high quality batches at lower overall costs.

The information provided by the in-line FBRM and NIR Lighthouse probe in case study C allowed to monitor the different stages of the granulation process, but the NIR LHP affected the agglomeration process under medium- and high-moisture granulation conditions. Due to the location of the NIR measurement windows, the probe was inserted with a greater depth compared to the NIR probe used in case study B (measurement window at probe tip). This disturbed the airflow pattern, and therefore the simultaneous process of heat and moisture transfer during granulation. Nevertheless, the developed NIR moisture calibration model exhibited low calibration and prediction errors, which

might suggest the supremacy of the NIR LHP to the conventional design with regard to moisture content prediction.

Chapter 7 describes the application of a real-time photometric stereo imaging method during the final steps of the extrusion-spheronization process, namely spheronization and drying. The at-line collected images during the spheronization and drying of different pellet formulations contained information related to the pellet size distribution, shape and surface brightness. Results showed that by use of the captured images and computed particle size distributions, the necessary information was provided to characterize the spheronization behavior of different formulations. By comparing the images obtained at different time points during spheronization, a visual record of the change in granule shape and size was displayed. During pellet fluid bed drying, the imaging technique measured an initial decrease of pellet size and increase of surface brightness. Comparing size, brightness, moisture content (determined with an infrared dryer) and solid-state (determined with Raman spectroscopy) trajectories learned that the size shrinkage was due to the evaporation of free water. The increase of surface brightness values resulted from both the removal of free and crystal water.

Due to the rapidity of the technique and the possibility to measure undispersed wet samples, valuable information about spheronization and drying features of different formulations was obtained in real-time. Hence, insight into the formulations' spheronization and drying characteristics was provided, showing the potential of the technique as a fast and non-destructive research tool in the development and optimization of an extrusion-spheronization process.

FUTURE PERSPECTIVES

FUTURE PERSPECTIVES

The results in this thesis show that by implementing an SFV probe and/or NIR probe into a fluid bed granulator, an improved granulation understanding, control and endpoint detection (compared to traditionally used process parameter measurements) are obtained. The in-line collected granule size (SFV) and moisture (NIR) trajectories enable the clear distinction between the three granulation process phases and granulation endpoint is defined by these real-time measured granule properties.

All experimental data was retrieved from granulations performed on a laboratory-scale fluid bed granulator (GPCG 1). Hence, the applicability of the developed monitoring and control methods should be evaluated for larger and commercial-scale granulators. Can an identical experimental setup be used in the larger scale granulator, or do some adaptations have to be made? Are the process analyzers able to sample appropriately, hence measuring the required data and information? How does the process analyzer perform in function of granulation time? Does fouling of the process analyzers occur, when granulating larger amounts of powder, for longer periods of time, using other formulations (containing more sticky materials)? Once these questions are answered, the introduced PAT tools and methods can be successfully applied both in process development and full commercial scale production.

The results in Chapter 6 suggest that the proposed control strategy is able to monitor the granule size and moisture throughout the process, to determine end granule characteristics in real-time and to ensure the desired bulk density at the end of processing. However, the full use of the control strategy requires further research on the automation of the feed-forward control methodology and the performance of the process control method on a longer term. The granule properties measured with the different process analyzers need to be aligned and combined with the data from the granulator process sensors and developed models. Warnings should be automatically generated when the product quality tends to fail the requirements and corrective actions, leading the process to its desired state should be suggested.

The process analyzers that were examined in this work provide real-time granule *size* and *moisture* information during fluid bed granulation. In addition, the granule *shape* may be another important (critical) granule characteristic that needs to be evaluated. Monitoring the evolution of the particle shape during fluid bed granulation may support the understanding and development of lab-based

(and/or pilot-scale) processes. The visual information captured in the images may provide knowledge on the different granule growth phenomena and the further processability of the granules with respect to their tableting behavior. The implementation of real-time imaging tools, providing the desired granule shape information, is however challenged by the inherent features of the granulation process. The highly dynamic behavior of the powders and fouling of the measurement zone impedes the tools' application.

Real-time monitoring and endpoint determination of the granule *solid-state* by use of spectroscopic techniques (e.g., Raman and NIR spectroscopy) may also be desired, but this is highly dependent of the granule formulation and therefore not applicable to all granulation processes. As with any other process analyzer, the location and fouling of the sensor are the first issues that need to be addressed.

The control methodologies described in Chapters 5 and 6 ensure that the desired granule properties are met at the end of processing. As granulation and tableting are closely related process steps in the production of solid dosage forms, the adjustment of process variables during manufacturing (to achieve the granule quality requirements) should also take the quality characteristics of tablets into account. Therefore, future work may focus on the development of an integrated control strategy, guaranteeing optimal granulation and tableting leading to in-spec tablets.

SAMENVATTING & ALGEMEEN BESLUIT

SAMENVATTING & ALGEMEEN BESLUIT

De methodes die traditioneel gebruikt worden om een farmaceutisch granulatieproces te controleren, leiden niet steeds tot de productie van granulaten met de gewenste kwaliteit. In deze thesis werd bijgevolg het gebruik van innovatieve processensoren tijdens wervelbedgranulatie en extrusie-sferonizatie geëvalueerd (**Hoofdstuk 1**). Door middel van deze analytische technieken kunnen de granulaateigenschappen rechtstreeks, tijdens het productieproces gemeten worden.

In **Hoofdstuk 2** werden de kenmerken van wervelbedgranulatie en extrusie-sferonizatie beschreven, wat toonde dat beide processen complex zijn doordat de kwaliteit van de granulaten beïnvloed wordt door verscheidene, intergerelateerde proces- en formulatievariabelen. Het verloop en eindpunt van een granulatieproces wordt gebruikelijk bepaald door het meten van procesparameters, waarbij de parameterwaarden gecorreleerd worden met de granulaateigenschappen. Deze indirecte metingen zijn echter vaak ontoereikend, bijvoorbeeld wanneer variaties optreden in de eigenschappen van de startpoeders of tengevolge van externe verstoringen. Beperkte granulaatinformatie wordt hoofdzakelijk bekomen na het productieproces door een aantal stalen van het eindproduct te analyseren in een (extern) labo. Hierdoor wordt procescontrole moeilijk en kan batchverlies optreden.

Het gebruik van innovatieve en efficiënte technologieën in farmaceutische productieprocessen, die de proces- en productkwaliteit verbeteren, wordt aangemoedigd door de regelgevende instanties. Door het implementeren van PAT technieken en principes wenst men tijdrovende off-line kwaliteitsanalyses (gedeeltelijk) te vervangen door het in-line opvolgen van de producteigenschappen, en hierbij de productkwaliteit constant te garanderen (zie **Hoofdstuk 3**). Door het rechtstreeks opvolgen van de kritische granulaateigenschappen, kan het granulatieproces beter begrepen worden. Combineren van de real-time gemeten granulaateigenschappen met bepaalde analysetechnieken en chemometrie, leidt tot een efficiëntere procescontrole en correcte eindpuntbepaling, waarbij de productie van granulaten met de gewenste kwaliteitseigenschappen verzekerd is. Literatuuronderzoek toont aan dat verscheidene real-time analytische processensoren ontwikkeld en gebruikt werden tijdens wervelbedgranulatie en extrusie-sferonizatie. Iedere techniek wordt gekenmerkt door specifieke voor- en nadelen, maar een gemeenschappelijke en belangrijke uitdaging bevindt zich steeds in het correct inbouwen van de sensor, zodat representatieve data verzameld kunnen worden.

Het potentiële gebruik van SFV als een PAT techniek om de deeltjesgroottedistributie in-line op te volgen tijdens wervelbed granulatie werd kritisch nagegaan in **Hoofdstuk 4**. De praktische aspecten, die het inbouwen van de SFV probe teweegbrengt, werden in eerste instantie onderzocht. De probe werd op 5 cm van de zijwand van de granulator geplaatst, zodat agglomeratie niet verhinderd werd en de meetvensters niet vervuild werden door de vochtige granulaatmassa. De granulaten werden doorheen een opening met een diameter van 4 mm gestuurd, waarbij een luchttoevoersysteem de meetvensters proper hield en verstopping van de meetzone voorkwam. Een experimenteel design werd uitgevoerd, waarbij de invloed van enkele proces- en formulatievariabelen op de gemiddelde granulaatgrootte werd onderzocht. Hierbij werd de deeltjesgrootte van de granulaten continu gemeten met de SFV probe. De real-time SFV en off-line laserdiffractie data van de eindgranulaten vertoonden een identieke trend in D_{50} waardes over de verscheidene batches. Het verschil in absolute granulaatgrootte, gemeten met de twee technieken werd verklaard aan de hand van de laserdiffractie meetmethode. Twee variabelen hadden een significant positief effect op de granulaatgrootte, namelijk de HPMC concentratie en de inlaattemperatuur van de lucht tijdens de droogfase. Het (on)belang van de onderzochte design variabelen werd verklaard en beter begrepen op basis van de in-line gemeten granulaatgroottes in functie van de procestijd. De in-line bepaalde deeltjesgroottes werden eveneens gerelateerd aan off-line gemeten kwaliteitseigenschappen van het eindproduct (i.e., dichtheid en Hausner ratio), gebruikmakende van univariate, multivariate en multiway modellen. Dit laat toe deze kwaliteitseigenschappen van het eindproduct onmiddellijk na het beëindigen van het granulatieproces te bepalen. Het multivariaat PLS densiteitmodel en het multiway N-PLS Hausner ratio model vertoonden een aanvaardbare R^2 en RMSEE waarde, maar de toepasbaarheid van deze modellen vereist verder onderzoek bij het gebruik van een onafhankelijke testset.

Nadat aangetoond werd dat de deeltjesgroottedistributie tijdens wervelbedgranulatie constant kan bepaald worden door middel van directe, snelle en niet-destructieve SFV metingen, werd de techniek gebruikt om het proces statistisch te modelleren en controleren (**Hoofdstuk 5**). Hierbij werden de in-line gemeten deeltjesgrootte en producttemperatuur van tien referentiebatches (met identieke proceswaarden) gebruikt om een referentie PLS model op te stellen. De scores van de resulterende PLS componenten werden herschikt, zodat score controlegrafieken opgesteld konden worden waarin het karakteristieke verloop van een referentiebatch (met een boven en onder controlelimiet) weergegeven wordt. Deze score controlegrafieken werden vervolgens gebruikt om het verloop van vier nieuwe testbatches op te volgen. Dit toonde aan dat het opgestelde referentiemodel gevoelig is voor kleine procesveranderingen en deze vroegtijdig detecteert. Hierdoor kan het herwerken en/of afkeuren van een batch vermeden worden.

Op basis van alle real-time gemeten batch informatie, werd de dichtheid en vloeibaarheid van het eindproduct voorspeld. Op deze manier kan de periode tussen procesbeëindiging en verdere granulaatverwerking, waarin granulaatstalen off-line labanalyses ondergaan, gereduceerd worden.

In **Hoofdstuk 6** werd in drie opeenvolgende casestudies een controlestrategie ontwikkeld voor een wervelbedgranulatieproces. Hierbij werd de granulaatgrootte real-time gemeten door middel van een SFV probe in casestudies A en B, en door middel van een FBRM probe in casestudie C. Beide probes werden op identieke wijze in de granulator ingebouwd. At-line (casestudie A) en in-line (casestudies B en C) NIR spectra werden eveneens opgenomen. De in-line NIR probe werd onderaan het venster, aan de voorzijde van de granulator geïnstalleerd. Een standaard diffuse reflectance NIR probe en Lighthouse NIR probe werden gebruikt in casestudies B en C, respectievelijk.

Op basis van de deeltjesgrootte (SFV) en vochtgehalte (NIR) profielen in functie van procestijd, werd een duidelijk onderscheid gemaakt tussen de drie fases van een wervelbedgranulatieproces (mengfase, sproeifase, en droogfase) in casestudie B. Een vergelijking met de huidig gebruikte controlegrafieken bestaande uit de product- en uitlaatemperatuur, toonde de meerwaarde van een PAT systeem. Het residueel vochtgehalte van het eindgranulaat werd voorspeld op basis van een NIR calibratiemodel en de in-line opgenomen NIR spectra. Dit betekent dat gebruikmakende van de in-line NIR en SFV metingen, het vochtgehalte en de deeltjesgrootte van het eindproduct (kritische granaateigenschappen) in real-time gekwantificeerd kunnen worden. Een feed-forward controlestrategie werd eveneens ontwikkeld, waarbij de in-line granulaatinformatie die gemeten werd tijdens de sproeifase gebruikt wordt om de optimale droogtemperatuur te voorspellen, zodat de gewenste bulkdensiteit bekomen wordt. Hierbij wordt de batchdensiteit reeds voorspeld op het einde van de sproeifase, gebruikmakende van real-time geïncollateerde procesparameters (i.e., sproeitemperatuur en sproeisnelheid) en productparameters (i.e., granulaatgrootte en vochtgehalte) tijdens de sproeifase. Indien de voorspelde dichtheid niet overeenstemt met de gewenste waarde wordt een aangepaste droogtemperatuur berekend, die aanleiding geeft tot de gewenste batchdensiteit. De resultaten toonden dat de bulkdensiteit correct voorspeld werd op basis van de SFV en NIR data geïncollateerd op het einde van de sproeifase. Het toevoegen van extra productinformatie afkomstig van de complete sproeifase bevorderde de dichtheidvoorspellingen niet. De droogfase van twee nieuwe granulaatbatches werd gewijzigd, gebruikmakende van de bulkdensiteit DoE regressievergelijking, zodat de gewenste dichtheid bekomen werd.

De informatie verkregen met de in-line FBRM en NIR Lighthouse probe in casestudie C liet eveneens toe de drie fases van een wervelbedgranulatieproces te onderscheiden. De positie van de NIR LHP beïnvloedde echter het agglomeratieproces wanneer gebruik gemaakt werd van middelmatige tot vochtige granulatiecondities. De meetvensters van de NIR LHP zijn enkele centimeters verwijderd

van het uiteinde van de probe. Hierdoor werd de probe dieper in de granulator gepositioneerd in vergelijking met de NIR probe uit casestudie B. Bijgevolg verstoorde de NIR LHP de wervelbedbeweging en de simultane warmte- en vochttransfer tijdens granulatie. Het opgestelde NIR calibratiemodel beschikte over kleine calibratie- en voorspellingsfouten, wat kan wijzen op de superioriteit van de NIR LHP in vergelijking met de standaard NIR probe om het residueel vochtgehalte te voorspellen.

In **Hoofdstuk 7** werd een real-time beeldvormingstechniek gebruikt tijdens de sferonizatie- en droogstap van een extrusie-sferonizatie proces. At-line beelden werden opgenomen tijdens het sferonizeren en het drogen van verscheidene pelletformulaties, en bevatten zowel informatie over de grootte, vorm als reflectie-eigenschappen van de pellets. De opgenomen beelden en de daaruit afgeleide deeltjesgroottedistributies lieten toe het sferonizatiegedrag van verscheidene formulaties te karakteriseren. De verandering in granulaatvorm en -grootte werd visueel weergegeven door middel van de opeenvolgende sferonizatiebeelden. De beelden opgenomen tijdens het drogen van de pellets vertoonden een initiële afname in pelletgrootte en toename in reflectie-eigenschappen. De grootte-, reflectie-, vochtgehalte- en solid-stateprofielen werden met elkaar vergeleken en toonden dat de afname in deeltjesgrootte veroorzaakt werd door de vrijstelling van vrij water. De toename in reflectie-eigenschappen werd veroorzaakt door de verwijdering van zowel vrij als gebonden water.

De beeldvormingstechniek was in staat om snel, overlappende en vochtige partikels te meten waardoor informatie omtrent de sferonizatie- en droogeigenschappen van verscheidene formulaties in real-time bekomen werd. Dit wijst op het potentieel van de techniek als een snelle en niet-destructieve onderzoeksmethode tijdens de ontwikkeling en optimalisatie van een extrusie-sferonizatie proces.

De resultaten in deze doctoraatsthesis tonen dat de implementatie van een SFV probe en/of NIR probe in een wervelbedgranulator, toelaat het granulatieproces beter te begrijpen en controleren. Bovendien kan het proceseindpunt bepaald worden aan de hand van real-time gemeten granulaateigenschappen, wat een duidelijke meerwaarde is ten opzichte van de conventioneel gebruikte procesparameters.

Experimenten werden steeds uitgevoerd in een wervelbedgranulator op laboschaal (GPCG 1). Toekomstig onderzoek zal zich bijgevolg richten op het overbrengen van de verkregen kennis en ontwikkelde methodes naar grootschalige wervelbedgranulatoren. Kunnen de probes op identieke wijze ingebouwd worden, of zijn (kleine) aanpassingen noodzakelijk? Treedt er vervuiling van de meetvensters op, wanneer een grotere hoeveelheid poeder gegraneerd wordt, gedurende een

langere procestijd en gebruikmakende van andere start- en bindmaterialen. Eens deze vragen beantwoord zijn, kunnen de ontwikkelde PAT technieken en methodes succesvol toegepast worden in zowel de ontwikkelingsfase als de commerciële productie van een geneesmiddel.

Gebruikmakende van de controlestrategie ontwikkeld in Hoofdstuk 6, kunnen de grootte en het vochtgehalte van granulaten continu opgevolgd worden en in real-time gekwantificeerd worden (voor het eindproduct). Bovendien kan een granulatieproces bijgestuurd worden in de droogfase om de gewenste bulkdensiteit te garanderen. De praktische toepassing van de controlestrategie vereist echter verder onderzoek naar de automatisering van de feed-forward controlemethodologie. De data, die de analytische processensors en de wervelbedgranulator collecteren tijdens een proces, dienen gealigneerd en gecombineerd te worden met de opgestelde modellen. De nodige programma's dienen ontwikkeld te worden zodat (i) waarschuwingen automatisch gegenereerd worden wanneer de granulaatkwaliteit dreigt af te wijken van de gewenste waarde en (ii) gepaste acties ondernomen worden om opnieuw te voldoen aan de vereiste kwaliteit.

CURRICULUM VITAE

ANNELEEN BURGGRAEVE

PERSONAL INFORMATION

SURNAME: Burggraeve
FIRST NAMES: Anneleen, Maria, Georgette
PRIVATE ADDRESS: Spelemanstraat 45
8301 Knokke-Heist
DATE OF BIRTH: November 4th, 1985
NATIONALITY: Belgian
MARITAL STATUS: unwed
EMAIL: anneleen.burggraeve@ugent.be

LANGUAGE SKILLS

NATIVE LANGUAGE: Dutch
OTHER LANGUAGES: English
French
(German)

EDUCATION

2007 – present: Doctoral studies in Pharmaceutical Process Analytical Technology
Ghent University
2003 – 2007: Master in Chemistry, graduated cum laude
Ghent University
1997 – 2003: Higher general secondary education
Degree Sciences – Mathematics
Sint-Jozefsyceum, Knokke

RESEARCH EXPERIENCE

- 2007 – present:** PhD research
Laboratory of Pharmaceutical Process Analytical Technology
Promoter: Prof. Dr. T. De Beer
Title: Development of process analytical and control methodologies for pharmaceutical wet granulation processes
- April 2010 – June 2010:** 3 months research visit at the Division of Pharmaceutical Technology - University of Helsinki (Finland) as part of the PhD research project
Supervisor: Jouko Yliruusi, Jyrki Heinämäki, Niklas Sandler
- 2006 – 2007:** Master thesis
Department of Analytical Chemistry
Promoter: Prof. Dr. P. Vandenabeele
Title: Kwantitatieve analyse van de actieve bestanddelen in geneesmiddelen met Ramanspectroscopie

PUBLICATIONS IN PEER REVIEWED JOURNALS

Process analytical tools for monitoring, understanding and control of pharmaceutical fluidized bed granulation: a review

A. Burggraeve, T. Monteyne, J.P. Remon, C. Vervaet, T. De Beer

***European Journal of Pharmaceutics and Biopharmaceutics*, accepted with minor revisions**

Development of a fluid bed granulation process control strategy based on real-time process and product measurements

A. Burggraeve, Y. Vander Heyden, A. Silva, T. Van Den Kerkhof, M. Hellings, J.P. Remon, C. Vervaet, T. De Beer

***Talanta*, (2012) <http://dx.doi.org/10.1016/j.talanta.2012.07.054>**

Prediction of quality attributes of continuously produced granules using complementary PAT tools

M. Fonteyne, S. Soares, J. Vercruyse, E. Peeters, A. Burggraeve, C. Vervaet, J.P. Remon, N. Sandler, T. De Beer

***European Journal of Pharmaceutics and Biopharmaceutics*, (2012)**

<http://dx.doi.org/10.1016/j.ejpb.2012.07.017>

Understanding fluidized-bed granulation using in-line particle-size measurements

A. Burggraeve, T. Van Den Kerkhof, M. Hellings, J.P. Remon, C. Vervaet, T. De Beer

***Pharmaceutical Technology*, 35 (8) (2011) 63-67**

Real-time image-based investigation of spheronization and drying phenomena using different pellet formulations

A. Burggraeve, N. Sandler, J. Heinämäki, J.P. Remon, C. Vervaet, T. De Beer, J. Yliruusi
European journal of Pharmaceutical Sciences, 44 (2011) 635-642

Batch statistical process control of a fluid bed granulation process using in-line spatial filter velocimetry and product temperature measurements

A. Burggraeve, T. Van Den Kerkhof, M. Hellings, J.P. Remon, C. Vervaet, T. De Beer
European journal of Pharmaceutical Sciences, 42 (2011) 584-592

Near infrared and Raman spectroscopy for the in-process monitoring of pharmaceutical production processes

T. De Beer, A. Burggraeve, M. Fonteyne, L. Saerens, J.P. Remon, C. Vervaet
International Journal of Pharmaceutics, 417 (2011) 32-47

Evaluation of in-line spatial filter velocimetry as PAT monitoring tool for particle growth during fluid bed granulation

A. Burggraeve, T. Van Den Kerkhof, M. Hellings, J.P. Remon, C. Vervaet, T. De Beer
European Journal of Pharmaceutics and Biopharmaceutics, 76 (2010) 138-146

Importance of using complementary process analyzers for the process monitoring, analysis and understanding of freeze drying

T.R.M De Beer, M. Wiggernhorn, R. Veillon, C. Debacq, Y. Mayeresse, B. Moreau, A. Burggraeve, T. Quinten, W. Friess, G. Winter, C. Vervaet, J.P. Remon, W.R.G. Baeyens
Analytical Chemistry, 81 (2009) 7639-7649

In-line and real-time process monitoring of a freeze drying process using Raman and NIR spectroscopy as complementary process analytical technology (PAT) tools

T.R.M De Beer, P. Vercruyssen, A. Burggraeve, T. Quinten, J. Ouyang, X. Zhang, C. Vervaet, J.P. Remon, W.R.G. Baeyens
Journal of Pharmaceutical Sciences, 98 (2009) 3430-3446

Raman spectroscopy as a process analytical technology (PAT) tool for the *in-line* monitoring and understanding of a powder blending process

T.R.M. De Beer, C. Bodson, B. Dejaegher, B. Walczak, P. Vercruyssen, A. Burggraeve, A. Lemos, L. Delattre, Y. Vander Heyden, J.P. Remon, C. Vervaet, W.R.G. Baeyens
Journal of Pharmaceutical and Biomedical Analysis, 48 (2008) 772-779

PRESENTATIONS AT CONFERENCES

Oral presentations

Development of a fluid bed granulation control strategy using real-time process and product measurements

A. Burggraeve, Y. Vander Heyden, J.P. Remon, C. Vervaet, T. De Beer
Fifth pan-European QbD & PAT Science Conference, EuPAT5 Continuous innovation in process analytics & control, Ghent (Belgium), 9-10 May 2012

Development of a fluid bed granulation process control method based on in-line process measurements

A. Burggraeve, Y. Vander Heyden, J.P. Remon, C. Vervaet, T. De Beer

5th Pharmaceutical Solid State Research Cluster (PSSRC) symposium, Helsinki (Finland), 26-27 September 2011

Evaluation of FlashSizer 3D imaging during an extrusion-spheronization process

A. Burggraeve, N. Sandler, J. Heinämäki, J.P. Remon, C. Vervaet, T. De Beer, J. Yliruusi

Drug Analysis 2010, Antwerp (Belgium), 21-24 September 2010

FlashSizer 3D imaging as PAT tool during the production of pellets via extrusion-spheronization and fluid bed drying

A. Burggraeve, N. Sandler, J. Heinämäki, J.P. Remon, C. Vervaet, T. De Beer, J. Yliruusi

4th Pharmaceutical Solid State Research Cluster (PSSRC) symposium, Cambridge (UK), 19-21 September 2010

Batch Statistical Process Control (BSPC) of a fluid bed granulation process based on in-line Spatial Filter Velocimetry (SFV) and product temperature measurements

A. Burggraeve, T. Van Den Kerkhof, M. Hellings, J.P. Remon, C. Vervaet, T. De Beer

Fourth pan-European QbD & PAT Science Conference, EuPAT4 Taking PAT to the Next level, Kuopio (Finland), 5-6 May 2010

NIR and Raman spectroscopy as PAT tools to quantify the particle size of spray dried mannitol

A. Burggraeve, T. De Beer, P. Vercruyssen, J.P. Remon, C. Vervaet, W.R.G. Baeyens

Third pan-European QbD & PAT Science Conference, EuPAT3 Scientific Progress Underpinning Innovative Manufacturing Control and Quality by Design, Gothenburg (Sweden), 7-8 October 2008

Poster presentations

Development of a fluid bed granulation process control method based on real-time process measurements

A. Burggraeve, Y. Vander Heyden, C. Vervaet, J.P. Remon, T. De Beer

8th World Meeting on Pharmaceutics, Biopharmaceutics and Pharmaceutical Technology, Istanbul (Turkey), 19th to 22th March 2012

Real-time image-based investigation of the spheronization and fluid bed drying of different pellet formulations

A. Burggraeve, N. Sandler, J. Heinämäki, H. Räikkönen, J.P. Remon, C. Vervaet, J. Yliruusi, T. De Beer

3rd Scientific Afternoon Faculty of Pharmaceutical Sciences, Ghent (Belgium), 26 May 2011

Evaluation of FlashSizer 3D imaging as PAT tool during spheronization and pellet fluid bed drying

A. Burggraeve, N. Sandler, J. Heinämäki, H. Räikkönen, J.P. Remon, C. Vervaet, T. De Beer, J. Yliruusi

2nd European Conference on Process Analytics and Control Technology, Glasgow (UK), 27-29 April 2011

Real-time particle size distribution evaluation during fluid bed granulation

A. Burggraeve, T. Van Den Kerkhof, M. Hellings, J.P. Remon, C. Vervaet, T. De Beer

Electronic Conference on Pharmaceutical Sciences 2011, 1-31 March 2011

Evaluation of FlashSizer 3D imaging during an extrusion-spheronization process

A. Burggraeve, N. Sandler, J. Heinämäki, J.P. Remon, C. Vervaet, T. De Beer, J. Yliruusi
FIP Pharmaceutical Sciences 2010 World Congress in Association with the AAPS Annual Meeting and Exposition, New Orleans, Louisiana (USA), 14-18 November 2010

Evaluation of FlashSizer 3D imaging during an extrusion-spheronization process

A. Burggraeve, N. Sandler, J. Heinämäki, J.P. Remon, C. Vervaet, T. De Beer, J. Yliruusi
PSWC 2010 Congress for students and postdoctoral fellows, New Orleans, Louisiana (USA), 13-14 November 2010

Evaluation of in-line Spatial Filter Velocimetry as PAT monitoring tool for particle growth during fluid bed granulation

A. Burggraeve, T. Van Den Kerkhof, M. Hellings, J.P. Remon, C. Vervaet, T. De Beer
7th World Meeting on Pharmaceutics, Biopharmaceutics and Pharmaceutical Technology, Valletta (Malta), 8-11 March 2010

Raman and near infrared spectroscopy as Process Analytical Technology (PAT) tools during spray drying of pharmaceuticals

A. Burggraeve, T. De Beer, P. Vercruyssen, J-P. Remon, C. Vervaet, W.R.G. Baeyens
1st Scientific Afternoon Faculty of Pharmaceutical Sciences, Ghent (Belgium), 20 May 2009

NIR and Raman spectroscopy as PAT tools for the particle size determination of spray dried mannitol

A. Burggraeve, T. De Beer, P. Vercruyssen, J-P. Remon, C. Vervaet, W.R.G. Baeyens
Workshop 'Hands-on Implementation of Process Analytical Technology (PAT) Systems in Production Processes', A Training and Discussion Meeting for PhD Students, Post Docs, Academics and Scientists from the Pharmaceutical Industry involved in PAT, Ghent (Belgium), 25-26 August 2008

ATTENDED COURSES AND WORKSHOPS

- Course: *Multivariate Curve Resolution*, April 26th 2011, Glasgow (UK)
- Course: *Hyperspectral Chemical Imaging for Process Analytics*, April 26th 2011, Glasgow (UK)
- Course: *Multivariate Data Analysis* by Umetrics AB (Training in Multivariate Technology), 6-7 January 2009, Ghent (Belgium)
- Course: *Design of Experiments "Pharma Applications"* by Umetrics AB (Training in Multivariate Technology), 16-17 December 2008, Ghent (Belgium)
- *2nd Pharmaceutical Solid State Research Cluster (PSSRC) Symposium*, 27 August 2008, Ghent (Belgium)
- *9th Belgian Chemometrics Symposium*, April 11th 2008, Gembloux (Belgium)
- *13^e Forum der Farmaceutische Wetenschappen*, 11-12 October 2007, Spa (Belgium)
- *Workshop on Multivariate Statistical Process Control*, October 5th 2007, Leuven (Belgium)

